EVALUATION OF THE RESPONSE OF I-10/215 INTERCHANGE BRIDGE NEAR SAN BERNARDINO IN THE 1992 LANDERS AND BIG BEAR EARTHQUAKES

by

Gregory L. Fenves and Reginald Desroches

Department of Civil Engineering
University of California
Berkeley, California 94720

Data Utilization Report CSMIP/95-02

California Strong Motion Instrumentation Program

March 1995

This study was conducted at the University of California at Berkeley. The study was jointly supported by the California Department of Conservation and the California Department of Transportation.

California Department of Conservation
Division of Mines and Geology
Office of Strong Motion Studies
801 K Street, MS 13-35
Sacramento, California 95814-3531

DIVISION OF MINES AND GEOLOGY
JAMES F. DAVIS
STATE GEOLOGIST

DISCLAIMER

The content of this report was developed under Contract No. 1093-546 from the Strong Motion Instrumentation Program in the Division of Mines and Geology of the California Department of Conservation. This report has not been edited to the standards of a formal publication. Any opinions, findings, conclusions or recommendations contained in this report are those of the authors, and should not be interpreted as representing the official policies, either expressed or implied, of the State of California.

PREFACE

The California Strong Motion Instrumentation Program (CSMIP) in the Division of Mines and Geology of the California Department of Conservation promotes and facilitates the improvement of seismic codes through the Data Interpretation Project. The objective of the this project is to increase the understanding of earthquake strong ground shaking and its effects on structures through interpretation and analysis studies of CSMIP and other applicable strong motion data. The ultimate goal is to accelerate the process by which lessons learned from earthquake data are incorporated into seismic code provisions and seismic design practices.

The specific objectives of the CSMIP Data Interpretation Project are to:

1. Understand the spatial variation and magnitude dependence of earthquake strong ground motion.

2. Understand the effects of earthquake motions on the response of geologic formations, buildings and lifeline structures.

3. Expedite the incorporation of knowledge of earthquake shaking into revision of seismic codes and practices.

4. Increase awareness within the seismological and earthquake engineering community about the effective usage of strong motion data.

5. Improve instrumentation methods and data processing techniques to maximize the usefulness of SMIP data. Develop data representations to increase the usefulness and the applicability to design engineers.

This report is the twelfth in a series of CSMIP data utilization reports designed to transfer recent research findings on strong-motion data to practicing seismic design professionals and earth scientists. CSMIP extends its appreciation to the members of the Strong Motion Instrumentation Advisory Committee and its subcommittees for their recommendations regarding the Data Interpretation Research Project.

Anthony F. Shakal
CSMIP Program Manager

Moh J. Huang
CSMIP Data Interpretation
Project Manager

ABSTRACT

The response of the Northwest Connector at the I–10/215 Interchange in the 1992 Landers and Big Bear earthquakes was recorded by a strong motion instrumentation network. The Connector is a 2540 ft. curved bridge constructed in 1973 and retrofitted for improved earthquake performance in 1991. Although the peak ground acceleration was approximately 0.10 g at the site for both earthquakes, much less than the level of ground motion expected in a major earthquake, the strong motion data provides important information about the earthquake response of a typical curved freeway bridge. The objectives of this study are to: evaluate the importance of non–uniform support motion on the response of the bridge; determine the vibration properties of the bridge; determine efficacy of typical modeling and dynamic analysis techniques used in the design of bridges to predict the response recorded in the earthquakes; and examine the role of the intermediate hinges on the earthquake response of the bridge.

The input motion was fairly uniform in the two earthquakes. Consequently, the spatial variation of free–field input motion is not important for these cases. The earthquake response of the Connector is predominantly transverse. Bent 8 near the center of the bridge is the most heavily instrumented bent. The maximum transverse deformation of the column was 4.76 in. for Landers (drift=0.86%), and 2.98 in. for Big Bear (drift=0.54%). Pile cap rotation produced 10 to 15 percent of the column displacement in the transverse direction.

The strong motion records show the effects of pounding as evidenced by large acceleration spikes at the five intermediate hinges in the Connector. Using the processed displacement records, Hinge 7 had the largest opening: 1.41 in. for Landers and 1.70 in. for Big Bear. Several of the closing excursions have the high frequency oscillation associated with pounding. Accumulated crushing of the filler material in the hinge may have occurred in the second earthquake. In the transverse direction, the relative hinge displacement is constrained by a shear key. The shear keys were effective in limiting the relative displacement to a maximum of 0.61 in. The maximum relative transverse displacements, however, were greater than the nominal 1/4–inch gap, indicating that the shear keys likely suffered local crushing of filler material.

The most significant finding is the difference in the fundamental mode period of the Connector in the Landers and Big Bear earthquakes. The funda-

mental period lengthened from 1.56 sec in Landers to 1.75 sec in Big Bear. The other noticeable difference between the two earthquakes is that the damping ratio increased in the first and third mode, although it decreased in the second mode. The lengthening of the vibration periods and generally increased damping may indicate that the bridge "softened" in the Landers earthquake. Changes in the pile foundations appear to be the most likely cause, although reduction in stiffness of the steel jacketed columns is a contributing factor in the lengthening of the vibration periods.

Standard three–dimensional "stick models" are used in addition to a nonlinear model of the intermediate hinges. The gross flexural rigidity (EI) for the columns, increased 10 to 15 percent for the steel jackets, are then modified to match the vibration periods of the model with the identified periods of the Connector in the two earthquakes. For the Landers model, the modification factor is 1.05; for the Big Bear earthquake the modification factor is 0.85. The reduction of the column stiffness between the two earthquakes, along with the reduced rotational stiffness for the pile foundations, accounts for the lengthened vibration periods identified from the recorded motion. With these assumptions, the comparison between the model motion and recorded motion is good in many aspects. Although there are some differences, the comparison provides confidence that standard analysis techniques are adequate for design with proper assumptions about column and foundation flexibility. However, the modeling of hinges using gap elements does not provide accurate high frequency response due to pounding of adjacent frames.

The analysis shows that the most heavily loaded column was Bent 9 in the Landers earthquake, with a bending moment that was 73 percent of the ultimate flexural capacity. The nonlinear model showed the restrainers developed a maximum stress of 97 ksi, less than the yield stress. The hinge pounding included in the nonlinear model caused a moderate increase in some column forces compared with the linear tension and compression models which neglect pounding.

APPLICATION TO CODES AND PRACTICE

There is very little strong motion data for long, curved bridges. The response of the Northwest Connector at the I-10/215 Interchange in the 1992 Landers and Big Bear earthquake provides valuable information about the response of this common type of freeway structure.

The response comparison shows that standard modeling techniques, including the nonlinear behavior of the hinges, provides an adequate correlation between the recorded and computed responses. However, the ability of models to represent response accurately depends on realistic estimates of bent and foundation stiffnesses. Although linear tension and compression models typically used in bridge design give an upper bound of forces for many columns, they are not an upper bound for all columns because of hinge pounding. The study shows that the simple nonlinear model of hinges and restrainers is adequate for capturing the hinge behavior in the two earthquakes. An additional aspect is that once a column yields, pounding of adjacent frames may substantially increase the ductility demands of the yielded columns, although inelastic behavior has not been addressed in this study.

The nonlinear hinge models with elastic models for the remainder of the structure have several advantages over the linear models. The nonlinear models provide reasonable estimates of hinge opening and restrainer forces. Furthermore, the nonlinear models can indicate transfer of forces by pounding, and isolation of frames by hinge opening. It is recommended that this type of modeling be considered for the design of bridges where there is particular concern about the performance of hinges and restrainers and the effect of pounding on stiff frames.

ACKNOWLEDGMENTS

The contents of this report were developed under Contract No. 1093–546 from the California Department of Conservation, Division of Mines and Geology, Strong Motion Instrumentation Program. The contract was jointly funded by the California Department of Conservation and the California Department of Transportation. However, these contents do not necessarily represent the policy of these agencies nor endorsement by the State Government.

Dr. Moh Huang and Dr. Robert Darragh from the Strong Motion Instrumentation Program were very helpful in providing information about the Northwest Connector and the strong motion data.

Many engineers with the California Department of Transportation (Caltrans) provided assistance. Patrick Hipley supplied drawings and useful insight into the earthquake response of the Connector. Dr. Ken Jackura was generous in supplying information about the geotechnical investigation related to the seismic retrofit, as did the retrofit designer, Kelly Holden. All of their assistance is greatly appreciated.

This report has been published in substantially similar form by the Earthquake Engineering Research Center, University of California at Berkeley, as Report Number UCB/EERC–94/12.

TABLE OF CONTENTS

TABLE OF CONTENTS (cont'd)

TABLE OF CONTENTS (cont'd)

TABLE OF CONTENTS (cont'd)

Chapter 1

INTRODUCTION

1.1 Background

A common type of freeway bridge in California is the connector. Connectors are elevated, curved bridges at an interchange that allow traffic to move at near full speed from one freeway to another. Interest in the seismic performance of connectors began when the 1971 San Fernando earthquake severely damaged several bridges. As shown in an experimental study conducted nearly twenty years ago (Williams and Godden, 1976), the curved superstructure of a connector can be very effective in resisting seismic loads. The hinges reduce the inherent stiffness of a curved box girder, however, and are susceptible to local damage which may affect the stability of the bridge.

There has been an increased effort to understand the earthquake response and behavior of multiple–span bridges since the 1989 Loma Prieta earthquake demonstrated that existing bridges may not be adequate to protect the public. The partial collapse of two connector bridges at the Interstate 5/Route 14 interchange in the 1994 Northridge earthquake further emphasized the importance of understanding the seismic response of these structures (Moehle, 1994; Priestley, Seible et al., 1994).

The Landers and Big Bear earthquakes, on June 18, 1992, triggered an extensive strong motion instrumentation network at the Northwest Connector, a curved bridge that carries two lanes of traffic from eastbound Interstate 10 to northbound Interstate 215 at an interchange in Colton, California (Darragh, Cao et al., 1993). The Connector is a 2540 ft long, curved, concrete box girder bridge with sixteen spans supported by single column bents and diaphragm abutments.

This report presents a study of the seismic response of the Northwest Connector in the two 1992 earthquakes. The response of the bridge to the 1994 Northridge earthquake is beyond the scope of the current study. This work has been sponsored by the California Division of Mines and Geology (CDMG), Office of Strong Motion Studies, the agency responsible for the instrumentation

network, data collection, and record processing. The study has been conducted in conjunction with the California Department of Transportation (Caltrans), the organization that designed and operates the Connector.

1.2 Objectives of Study

The goal of this study is to use the strong motion data recorded at the Connector during the 1992 Landers and Big Bear earthquakes to improve the understanding of the earthquake response of this common type of freeway bridge. Specifically, the objectives are to

- Determine the vibration characteristics of the bridge.
- Evaluate the importance of non–uniform support motion on the response of the bridge.
- Examine role of the intermediate hinges on the earthquake response of the bridge.
- Determine efficacy of typical modeling and dynamic analysis techniques used in the design of bridges to predict the response recorded in the earthquakes.

The attainment of these objectives will help improve the earthquake–resistant design of freeway structures. The strong motion data collected by CDMG is essential for verifying the earthquake performance of these important lifeline components.

1.3 Previous Studies of Bridges

1.3.1 Studies Utilizing Strong Motion Records

Compared with buildings, few bridges have been instrumented with strong motion accelerometers and there is relatively little strong motion data available. This section summarizes the response studies of multiple–span bridges and viaducts. It does not describe the seismic instrumentation and response studies of long–span suspension and cable–stayed bridges.

An early study examined the response of the Route 156/101 separation in San Juan Batista, California, during the 1979 Coyote Lake earthquake (Wilson, 1984). The six span, steel girder bridge is instrumented with twelve accelerometers to record the response of a single simple–span and its two bents; there is no instrumentation on the abutments or in the free–field. The time–domain identification procedure by Beck (1978) proved successful in identifying

the two lower vibration modes of the bridge. A reasonable comparison of the computed response, using a finite element model of the bridge, with the moderate–amplitude recorded response could only be obtained when the bearings of the simple spans were assumed to resist longitudinal forces.

The Meloland Overcrossing near El Centro, California, is a two–span reinforced concrete box girder bridge with a single column bent and monolithic abutments. In 1978 CDMG installed an array of twenty–six accelerometers on the deck, abutments, and in the free–field. The large amplitude response recorded in the 1979 Imperial Valley earthquake has been the subject of several investigations by Werner (1987; 1993) and Douglas (1984; 1990). The 1987 study by Werner used a system identification technique, named MODE–ID, to determine the vibration properties and pseudo–static displacements of the supports. The results indicated that the abutments and embankments had a major effect on the response of the short bridge. A separate study concentrated on identifying parameters for a detailed model of the abutments and embankments (Wilson and Tan, 1990). The study identified a damping ratio for the embankment alone greater than twenty percent, although the effective damping is substantially less for the complete bridge system.

A recent, extensive study of Meloland (Werner, Crouse et al., 1993) used another identification procedure, MODEL–ID (Katafygiotis, 1991; Beck and Katafygiotis, 1992), to estimate directly the abutment stiffness and damping parameters. The results confirmed that the embankments have large damping ratios. A separate dynamic response analysis provided information about the magnitude of forces in the structure and the foundation piles during the 1979 Imperial Valley earthquake.

Another CDMG instrumented bridge is the Painter Street Overcrossing near Rio Dell, California. It is a skewed two–span reinforced concrete box girder bridge with a two–column central bent; one abutment is monolithic and the other has a seat support. Maroney (1990) interpreted the response of the bridge during six earthquakes between 1980 and 1987. A study based on a detailed nonlinear finite element model of the bridge has been completed at the Lawrence Livermore National Laboratory (McCallen, 1993). In 1992, very strong motion of the bridge was recorded in the Cape Mendocino earthquake sequence, reaching a peak acceleration of 1.2 g in the transverse direction (Darragh, Cao et al., 1993). The response of the bridge system has been studied using a nonlinear finite element model of the embankment and foundations (Sweet and Morrill, 1992). A conclusion from that study is that a nonlinear model of the soil can represent the effects of the abutments on the earthquake response of the superstructure. A recent study of the Painter Street bridge involves using the

recorded response to determine stiffness coefficients for the embankments (Goel and Chopra, 1994).

The Dumbarton bridge, which crosses San Francisco Bay between Menlo Park and Fremont, California, is the longest bridge for which strong motion data is available. In the 1989 Loma Prieta earthquake, strong motion records were obtained from twenty–five accelerometers on the bridge and one free–field instrument. A study by Fenves (1992) obtained spectral estimates of vibration properties and compared the response computed from a model with that recorded in the earthquake. The results showed the sensitivity of the earthquake response to assumptions about the articulations and longitudinal constraints at the hinges. Additional studies have been performed at Lawrence Livermore National Laboratory (McCallen, 1992).

Although not a freeway bridge structure, an elevated section of the Bay Area Rapid Transit (BART) line has been instrumented by CDMG. The records from the 1989 Loma Prieta earthquake have been evaluated in at least one study (Tseng, Yang, et al., 1992).

1.3.2 Experimental Studies

The damage to freeway bridges in the 1971 San Fernando earthquake motivated much of the early research about seismic–resistant bridge design. In one of the most important experimental studies of single bent box girder connectors, Williams and Godden (1976) conducted shaking table tests on models of the South Connector Overcrossing at the Interstate 5/Route 14 interchange, which suffered extensive damage in San Fernando.

The model used in the shaking table investigation was a 1:30 scale model of the eastern portion of the South Connector (Bents 2 to 6), including the frame with one bent that collapsed in the earthquake. The model had well–defined symmetric and antisymmetric vibration modes that correlated fairly well with an analytical model. The measured damping ratios in the vibration modes were two to three percent.

A good correlation with the analytical model, however, required estimating rotational stiffness coefficients for the abutment supports and friction at the hinges. Furthermore, the response was sensitive to the torsional stiffness of the hinges. An extensive set of seismic tests showed how damage is concentrated at the hinges, particularly by vertical lift–off and failure of the transverse shear key. Increasing the torsional stiffness of the hinges was effective in tying the frames together and reducing damage. Longitudinal restrainers were also effective in reducing damage caused by antisymmetric vibration. The study provided many

recommendations for the design of curved connectors, especially related to the hinges, which were incorporated in Caltrans bridge design specifications.

In another study, Gates and Smith (1984), summarized the results from ambient vibration testing of fifty–seven typical California bridges. Bollo and others (1990) performed forced vibration testing and static push testing on a frame of the two–level Cypress Street viaduct, which collapsed in the 1989 Loma Prieta earthquake. Chen (1993) used snap–back testing of a slab–on–girder bridge to investigate various models of transverse response for this common type of bridge in the eastern United States. Recently, Richardson and Douglas (1993) completed field testing of a curved box girder bridge to determine its vibration properties.

1.3.3 Other Applications

An analytical study of the earthquake response of connector bridges was conducted by Imbsen and others (Imbsen, Nutt et al., 1978), as part of a comprehensive study of freeway structures following the 1971 San Fernando earthquake. The parameter study of three curved connector bridges compared the results of linear, response spectrum analysis with nonlinear analysis. The nonlinear modeling included the intermediate hinges.

Several other studies have applied system identification methodology to determining vibration properties and damage parameters for bridges. A recent study used modal analysis to determine the vibration properties of a cable–stayed pedestrian bridge (Gardner–Morse and Huston, 1993). Kim and Ang (1992) computed the statistics of a global damage index for the South Connector Overcrossing. Other system identification application for bridges, not necessarily seismic related, are documented in the literature (Salane and Baldwin, 1990; Hogue, Aktan et al., 1991; Hjelmstad, Wood et al., 1992; Raghavendrachar and Aktan, 1992).

1.4 Organization of Report

Chapter 2 of this report describes the Northwest Connector, site and geological conditions, strong motion instrumentation, and the characteristics of the 1992 earthquakes.

The methodology used for the seismic evaluation of the Connector is described in Chapter 3. After reviewing the equations of motion for a structure subjected to multiple–support excitation, the three major aspects of the methodology are outlined, as follows:

- Analysis of free–field and support motion for the structure (Chapter 4).
- Evaluation of earthquake response and identification of vibration properties (Chapter 5).
- Structural modeling, dynamic analysis and comparison of response (Chapter 6).

Chapter 7 presents conclusions along with recommendations for further study and strong–motion instrumentation of bridges.

Chapter 2

DESCRIPTION OF CONNECTOR AND EARTHQUAKES

2.1 Introduction

The Northwest Connector carries two lanes of traffic from eastbound Interstate 10 to northbound Interstate 215 at a freeway interchange in Colton, California. Figure 2.1 shows a plan of the interchange including the Northwest Connector (Bridge No. 54–823G). The Connector is a 2540 ft long, curved, concrete box girder bridge with sixteen spans supported by single column bents and diaphragm abutments. Figure 2.2 shows a general elevation and plan of the Connector from the Caltrans drawings.

Table 2.1 summarizes the major events in the history of the Connector. Although the design was completed in 1969, construction was delayed by the 1971 San Fernando earthquake. Construction of the interchange was completed in 1973.

While the Interstate 10/215 interchange was under construction, the San Jacinto fault zone was mapped in close proximity to the structures. The geological investigations indicated that the Northwest Connector crosses a major fault in the San Jacinto zone. The California Division of Mines and Geology map of Special Studies Zones shows the northern one–half of the Connector located in the San Jacinto fault zone (CDMG, 1977). The approximate location of the fault in relation to the interchange is indicated in Fig. 2.1.

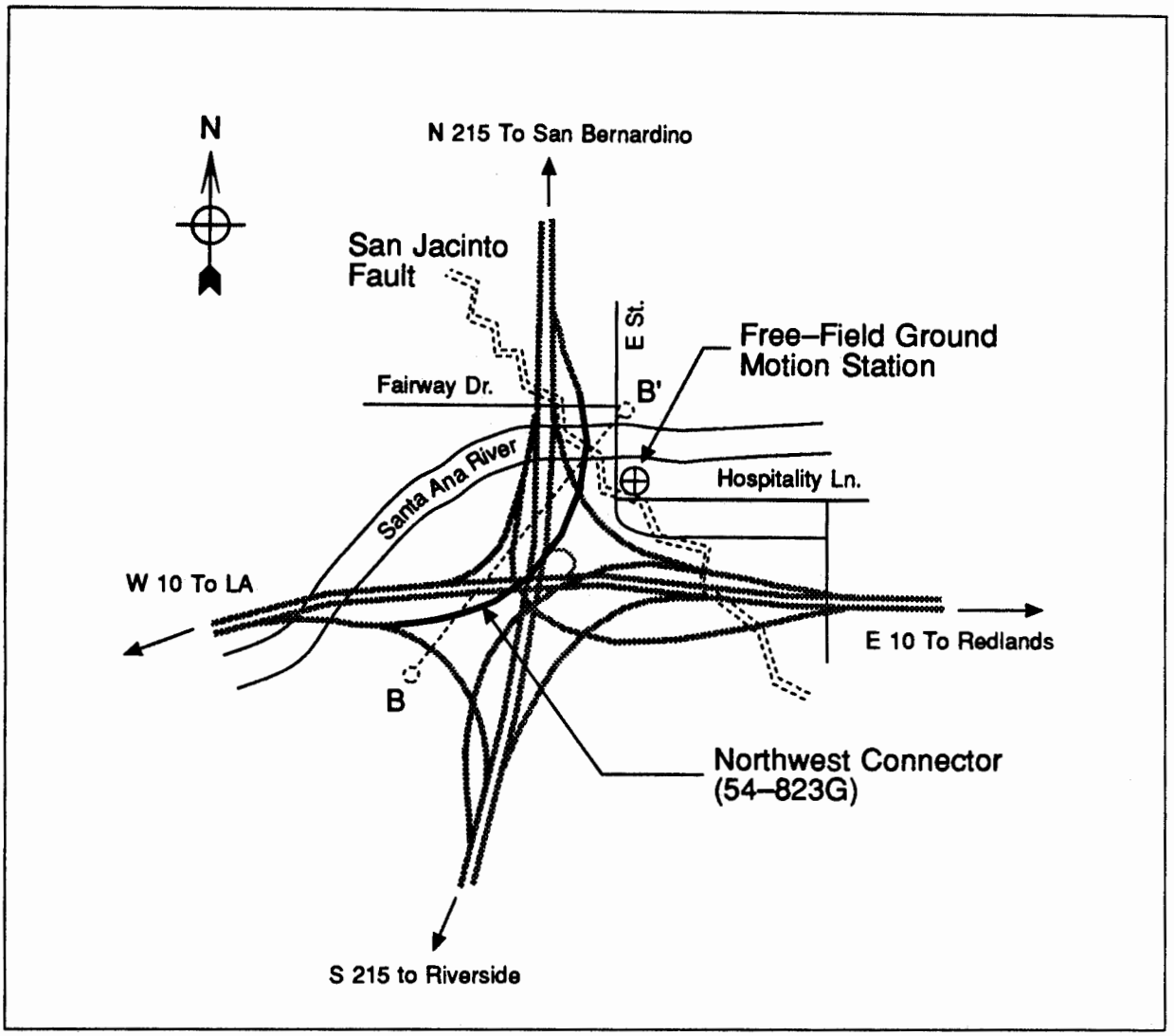

Figure 2.1 Schematic Plan of the Interstate 10/215 Interchange in Colton, California.

The Northwest Connector and the similar Southwest Connector were two of the early bridges retrofitted under Caltrans' Phase II seismic retrofit program. Caltrans selected the bridges for early retrofit because of their importance to the operation of two Interstate routes and their location within the San Jacinto fault zone. Caltrans designed the retrofit in 1990 and construction was completed in early 1992. Near the end of construction, Caltrans and CDMG installed a strong motion instrumentation network on the Northwest Connector. The retrofit and installation of strong motion instrumentation were completed six months before the 1992 earthquakes.

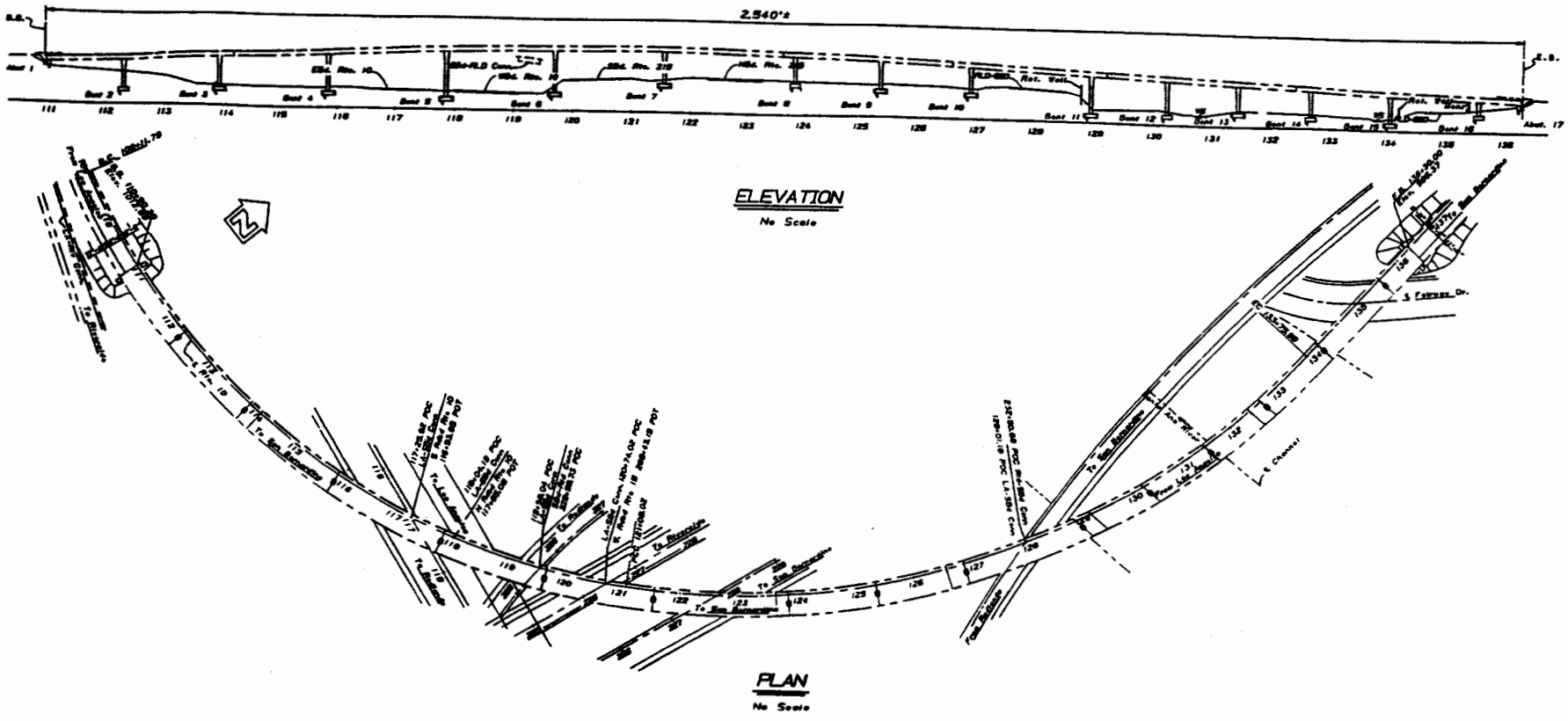

Figure 2.2 General Plan of Northwest Connector (from Caltrans drawings).

Table 2.1. History of Northwest Connector

Date	Event
1969	Design completed
1972	San Jacinto fault zone mapped near the Connector
1973	Construction completed
1987	Expansion joint seals replaced
1990	Seismic retrofit design completed
1991	Seismic retrofit construction completed
Jan. 1992	Strong motion instrumentation installation completed
April 22, 1992	Joshua Tree earthquake
June 28, 1992	Landers and Big Bear earthquakes
Jan. 17, 1994	Northridge earthquake

2.2 Geology and Site Conditions

The Interstate 10/215 interchange is located in the San Bernardino valley near the Santa Ana River basin. The valley consists of alluvial deposits from alluvial fans and river flood plains. The Northwest Connector crosses the northern segment of the San Jacinto fault zone. The fault acts as a barrier against ground water flow, producing a drop in the water table on the southwest side of the fault compared with the northeast side. The sandy soils and high ground water table present a potential for liquefaction during an earthquake. The geology and site conditions are documented in two Caltrans reports which were prepared for the seismic retrofit (Jackura, 1991; Knott and Goldschmidt, 1991).

2.2.1 San Jacinto Fault

The northern segment of the San Jacinto fault zone is an important geological feature of the region and the Connector site. The fault zone, one of the most active in California, consists of a number of individual faults oriented in a northwest–southeast direction from the San Gabriel mountains to the Imperial Valley. In 1972, Sharp (1972) mapped the fault zone in the Valley, identifying the Glen Helen, Loma Linda, and Claremont faults. The latter has generally been considered the San Jacinto fault in the San Bernardino Valley. Earthquakes on the San Jacinto fault near San Bernardino occurred in 1899, 1918

(ML=6.8) and 1923 (ML=6.3) according to Doser (1992). Although there is some controversy about the causative fault for the 1923 earthquake, the epicenter may have been within five miles of the interchange.

Sieh (1973) conducted geological investigations of the Claremont fault in 1972, including trenching at three locations. Based on surface features and inference, the Claremont fault was located through the interchange, which was nearing completion at the time. An aerial photograph, plate 7b in Sieh (1973), shows the trace of the fault crossing the Northwest Connector in a Northwest–Southeast direction at the Santa Ana River channel, directly south of Fairway Drive. The trenching provided evidence that the fault is at most several thousand years old. An analysis of the faulting history indicates three episodes with estimated total horizontal offsets of 1.8 ft, 3.0 ft, and 5.1 ft Each episode may have included several earthquakes. The most recent vertical offset was 2.7 ft to 3.2 ft. The trenching showed evidence of sand boils from the historical episodes, indicating the occurrence of liquefaction.

More recent trenching by Wesnousky and others (Wesnousky, Prentice et al., 1991) within 0.6 mi. southeast of the interchange used the deposits from an ancient stream bed to estimate the minimum average slip rate along the fault as 1.7 to 3.3 mm/year. Based on this estimate and the seventy years since the last moderate earthquake, the authors conclude that the fault is in the later stages of strain accumulation, with a high probability of generating a magnitude 6 to 7 earthquake in the region. A magnitude of 7.5 appears to be the maximum credible event on the fault.

The CDMG map of the special study zone (CDMG, 1977), which does not show the exact plan of the interchange, has the inferred location of the fault crossing under the Connector near Fairway Drive. Again, Fig. 2.1 shows the approximate location of the San Jacinto fault in relation to the Connector.

The Connector is near other important faults. The closest point of the San Andreas fault is 7.5 miles northeast of the interchange. That San Andreas segment has a maximum credible magnitude 8.25. The Cucamonga fault is 12 miles from the Connector; it has a maximum credible magnitude of 7.0.

2.2.2 Geotechnical Conditions

Except for the river channel and flood–control embankments, the site is generally level. The ground elevation ranges from 955 ft in the channel to 1000 ft outside of the channel. The site consists of deep unconsolidated alluvial deposits associated with the Santa Ana river. The alluvial deposits are estimated to be 800 to 900 ft thick near the interchange, but they may be as thick as 1200 ft.

The soil profile along the alignment of the Northwest Connector can be determined from nineteen boreholes drilled in 1968 prior to the original construction, six boreholes drilled in 1989 for the retrofit design, and additional borings for the liquefaction study. The foundation materials consist of slightly compact to dense sand in the upper layer underlain by compact to dense sand, silty sands, and sand and gravel mixtures (Jackura, 1991).

Figure 2.3 shows the profile from the Jackura report (1991), along the line B–B' in Fig. 2.1. Except for fill, the top soil layer generally consists of slightly compact to dense, clean sands and silty sands to an elevation of 930 ft to 945 ft (the thickness varies between 20 to 60 ft). The top layer of clean sands is intermixed with silty sands and occasional fine and coarse gravel at various locations. The top layer of dense sand extends to at least elevation 880 ft.

Consistent with the presence of the river channel and the observation about the effect of the San Jacinto fault on ground water, the water table varies considerably along the bridge, as indicated in Fig 2.3. The ground water elevation changes 35 ft across 400 ft of level ground near the interchange (Knott and Goldschmidt, 1991).

A study concluded that large–scale liquefaction damage of the pile foundations is not expected with existing water table levels, although the approach embankments and river levees may experience damage (Jackura, 1991). For the Northwest Connector, the northern three supports at Bents 15 and 16 and Abutment 17 may suffer liquefaction damage. For the maximum probable water table conditions, the foundations for five supports may experience damage: Bents 6, 11, 15, 16, and Abutment 17.

2.3 Original Design and Construction of the Connector

The Northwest Connector was designed in 1969 in accordance with the AASHO standards of that year. As shown in Fig. 2.2, the Connector is a 2540 ft long, sixteen–span concrete box girder bridge. Beginning at Abutment 1, the alignment has a 1018 ft length on a 1200 ft radius curve, a 1268 ft length on a 1300 ft radius curve, and a 254 ft straight segment ending at Abutment 17. The central portion of the bridge has a vertical curve of 900 ft radius with a maximum profile grade of 4.74%.

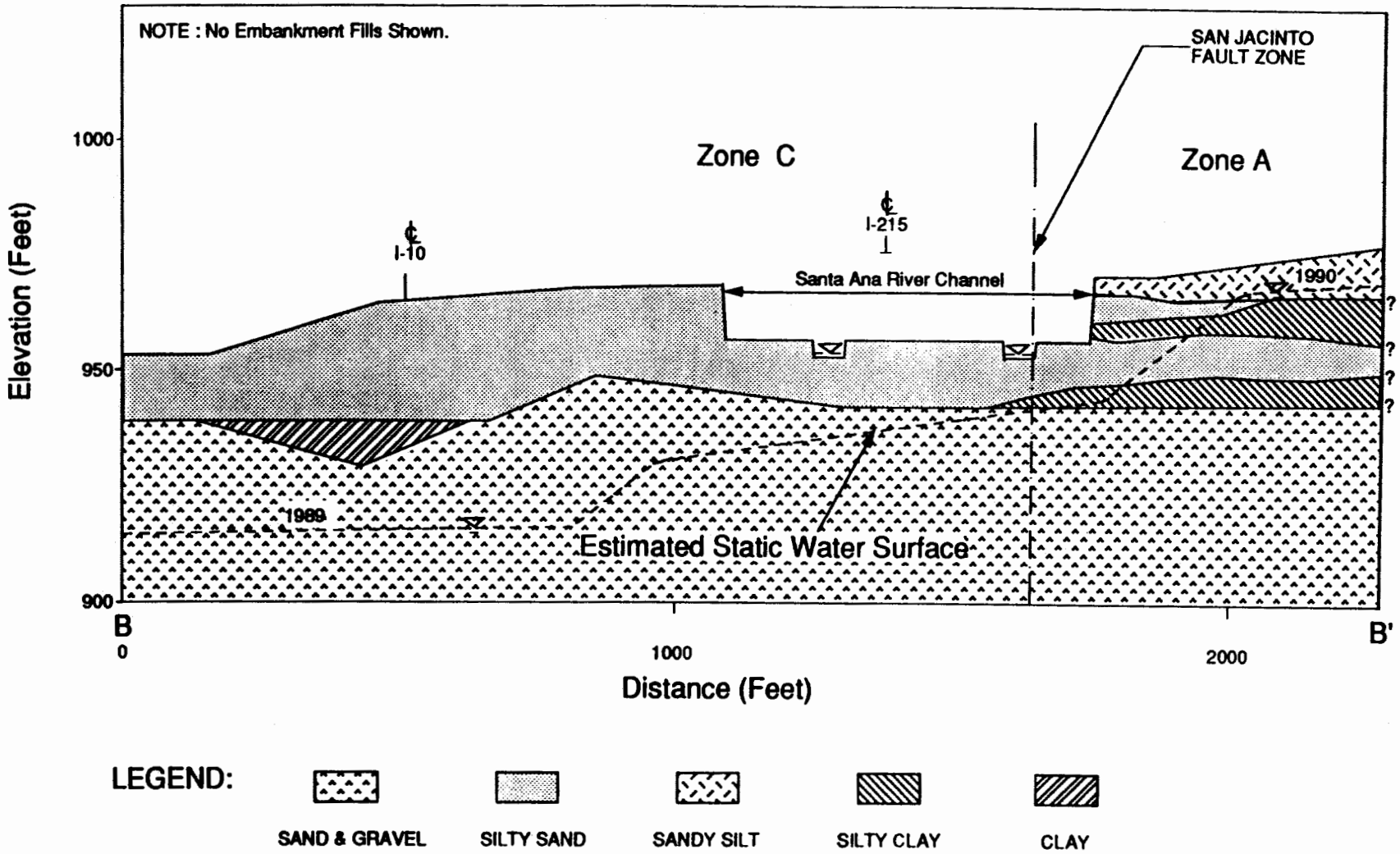

Figure 2.3 Soil Profile along line B–B' in Fig. 2.1 (Jackura, 1991).

The structural system consists of six frames, connected at five intermediate hinges. The hinges are designated by the spans in which they are located: Hinge 3, Hinge 7, Hinge 9, Hinge 11, and Hinge 13. The frames have a cast in–place box girder superstructure supported by two to four single column bents. The box girders in two frames (Hinge 3 to Hinge 7, and Hinge 9 to Hinge 11) are post–tensioned in the longitudinal direction. The spans of the four conventionally reinforced frames range from 75 ft to 155 ft. The spans of the two post–tensioned frames range from 183 ft to 204 ft. The column height (from top of pile cap to the box girder soffit) varies from 24 ft for Bent 16 to 77 ft for Bent 5. The soil overburden at Bents 2 and 16 is 20 ft and 9 ft, respectively; the overburden at Bents 10 and 11 is 10 to 12 ft.; the overburden at the other bents is 4 to 5 ft. Most of the bents are oriented without skew, with the exception of Bents 11 to 15. Bent 11 has the most skew at 24 degrees.

The only available information about the materials used in the construction of the Connector are the specified allowable stresses. The allowable stress for concrete is 1300 psi, except 1200 psi is specified for deck slabs. This translates to 28–day compressive strengths of approximately 3000 psi. The prestressed frames have a specified 28–day compressive strength of 4300 psi for Hinge 3 to Hinge 7 and 3500 psi for Hinge 9 to Hinge 11. All concrete is normal weight. Based on the allowable steel stresses, the reinforcement is Grade 60, except deck slab reinforcement and stirrups are Grade 40 or 50.

Figure 2.4 shows the typical section of the 8 ft deep box girder for the conventionally reinforced concrete frames. The cross–section for the post–tensioned frames has the same overall dimensions, but the interior girders are 12 in. thick instead of 10 in. All the girders are flared near the bent caps, as are the soffits.

The original single column bents, shown in Fig. 2.4(a), have an octagonal cross–section, with overall dimensions of 8 ft by 5.5 ft, and are flared in both directions near the top. The longitudinal reinforcement in the columns consists of #11, #14, or #18 bars in one or two rings. The columns in Bents 4, 5, and 6, have the most longitudinal reinforcement at 7.6 percent. The transverse reinforcement consists of various arrangements of #4 stirrups spaced at 12 in. The longitudinal column reinforcement is extended straight into the bent cap 5.5 ft, except for Bents 4 and 7 which are designed to release moments at the column–bent cap connection. The bent cap is 9.5 ft wide and 8 ft deep, with top longitudinal reinforcement varying from 36 to 54 #11 bars. Transverse reinforcement consists of various arrangements of #6 stirrups at 12 in. The connection between the column and pile cap is provided by dowels, lap spliced forty bar–diameters with the longitudinal reinforcement.

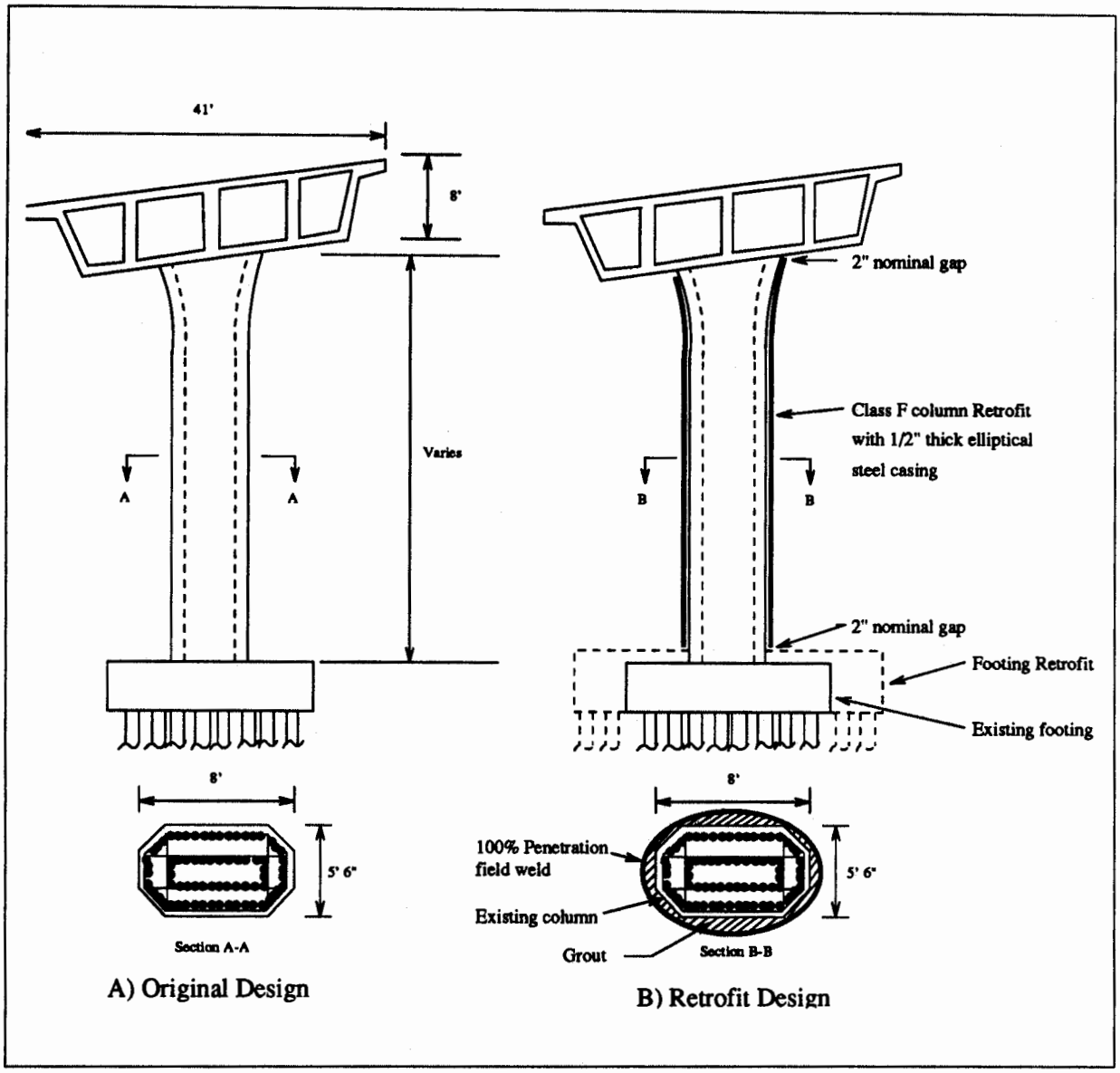

Figure 2.4 Single Column Bent and Box Girder Cross–Section.

The original foundations for the single column bents consist of a pile cap (without top reinforcement) and reinforced concrete piles. The largest foundations (for Bents 4, 5, and 7) have a 24 ft by 23 ft pile cap, 6.75 ft thick, and 48 piles. The smallest pile cap (for Bents 12 and 13) has a 21 ft by 15 ft pile cap, 4.75 ft thick, and 28 piles. The piles are spaced three to four feet on center. All piles are 70 ton, except for 100 ton piles for Bent 2. Although the as–built plans are not clear about the piles used in construction, it appears that they are one foot square

precast prestressed piles. The pile lengths range from 21 ft for Bent 5 to 50 ft for Bent 8.

At the diaphragm abutments, the box girder is integral with a 13 ft high backwall. The tapered wingwalls are 18 ft long. The connection between the backwall and the five foot wide pile cap is provided by #6 dowels at 12 in. Abutment 1 has nine 72 ft long piles, five vertical and four battered at 1:3; Abutment 17 has seven 43 ft piles, four vertical and three battered.

The five intermediate hinges in the superstructure have a seat width of 32 inches or 36 inches, of which 2 inches is specified to be expanded polystyrene and a joint seal (see Fig. 2.5). The condition of the hinges at the time of the earthquake is not documented. All hinges are straight, except for Hinges 11 and 13 which have 23 and 13 degree skew, respectively. The support for the girders at a hinge is provided by elastomeric bearing pads. Although it was not possible to determine material specification for the pads, the plans show they are 4 to 5.5 in. thick. Relative transverse displacement at a hinge is prevented by a shear key. The sides of the shear keys have 1/4–inch joint filler.

Since the South Connector Overcrossing at the Interstate 5/Route 14 interchange collapsed in the San Fernando earthquake because of excessive longitudinal displacement at the hinge seats, Caltrans specified installation of seven cable restrainer units at the hinges of the Northwest Connector (as was done later in the Phase I seismic retrofit program statewide). There are no vertical restrainer cables at the hinges.

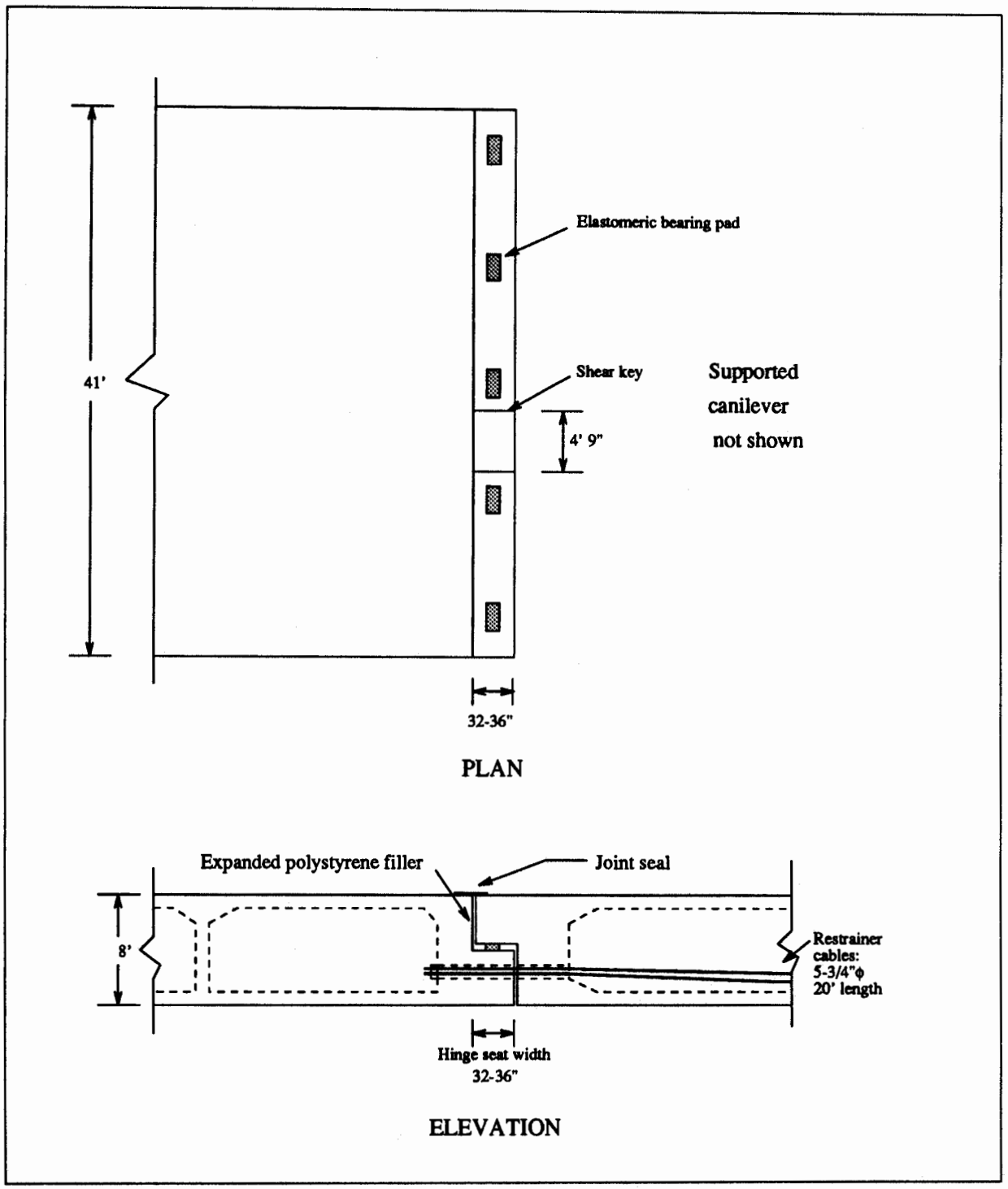

Figure 2.5 Typical Intermediate Hinge.

2.4 Seismic Retrofit

The decision to retrofit the Northwest Connector (and the Southwest Connector) was based on the importance of the bridge, known deficiencies in the original design (Roberts, 1991), and the fact that the bridges crossed a mapped fault. The features of the extensive retrofit are field–welded steel jackets on most of the bent columns, strengthened pile caps and foundations for the bents with full jacket retrofits, new cable restrainer units for the hinges, and support blocks at the abutments. Figure 2.6 is a general plan of the retrofit design.

A steel jacket provides confinement, shear strength, and flexural ductility for a column subjected to the large lateral displacements expected during an earthquake (Priestley, Seible et al., 1992). The jackets are 1/2–inch thick steel casings in an elliptical shape around the column. The void between the elliptical shell and the octagonal column is pressure filled with cement grout. The jackets are installed within two inches of the footing (and soffit for full length jackets) to prevent the steel casing from increasing the flexural strength of the column.

There are two types of column retrofits: Class F jackets are intended to develop the strength of the column with large rotational ductility in the plastic hinge region; Class P jackets allow a column to rotate below the full flexural capacity (because of the lap splices and dowel connection between the column and pile cap), acting more as a hinge. The difference between the two is that the Class P retrofits have a 1/2–inch thick polystyrene filler around the original columns to inhibit the bond with the cement grout and jacket. For the Connector retrofit, the Class F jackets are full column height, whereas the Class P jackets only extend over the lower eighteen feet of the column. The short embedded columns for Bents 2 and 16 have a combination of Class P retrofit for the lower eighteen feet (mostly embedded) and Class F retrofit for the remainder of the column height. Fig. 2.4(b) shows a typical bent with a full length jacket retrofit from the Caltrans drawings.

The foundations for the ten bents with a Class F retrofit were upgraded to transfer the plastic moment through the pile cap and provide overturning resistance with new piles. This required construction of a larger pile cap, with a top mat of reinforcement and shear reinforcement, encompassing the original pile cap. The largest foundations (for Bents 4, 5 and 7) were upgraded to a size of 33 ft by 31 ft, with a top mat 1.25 ft or 2.25 ft thick, and thirty additional 100 ton piles around the perimeter. The new piles are 16 in. diameter steel pipes (1/2–inch thick), driven to a tip elevation between 895 ft to 918 ft. The piles are filled with concrete to elevation 935 ft. The piles are embedded 8 inches into the new pile cap and six U–shaped stirrups per pile provide pullout resistance.

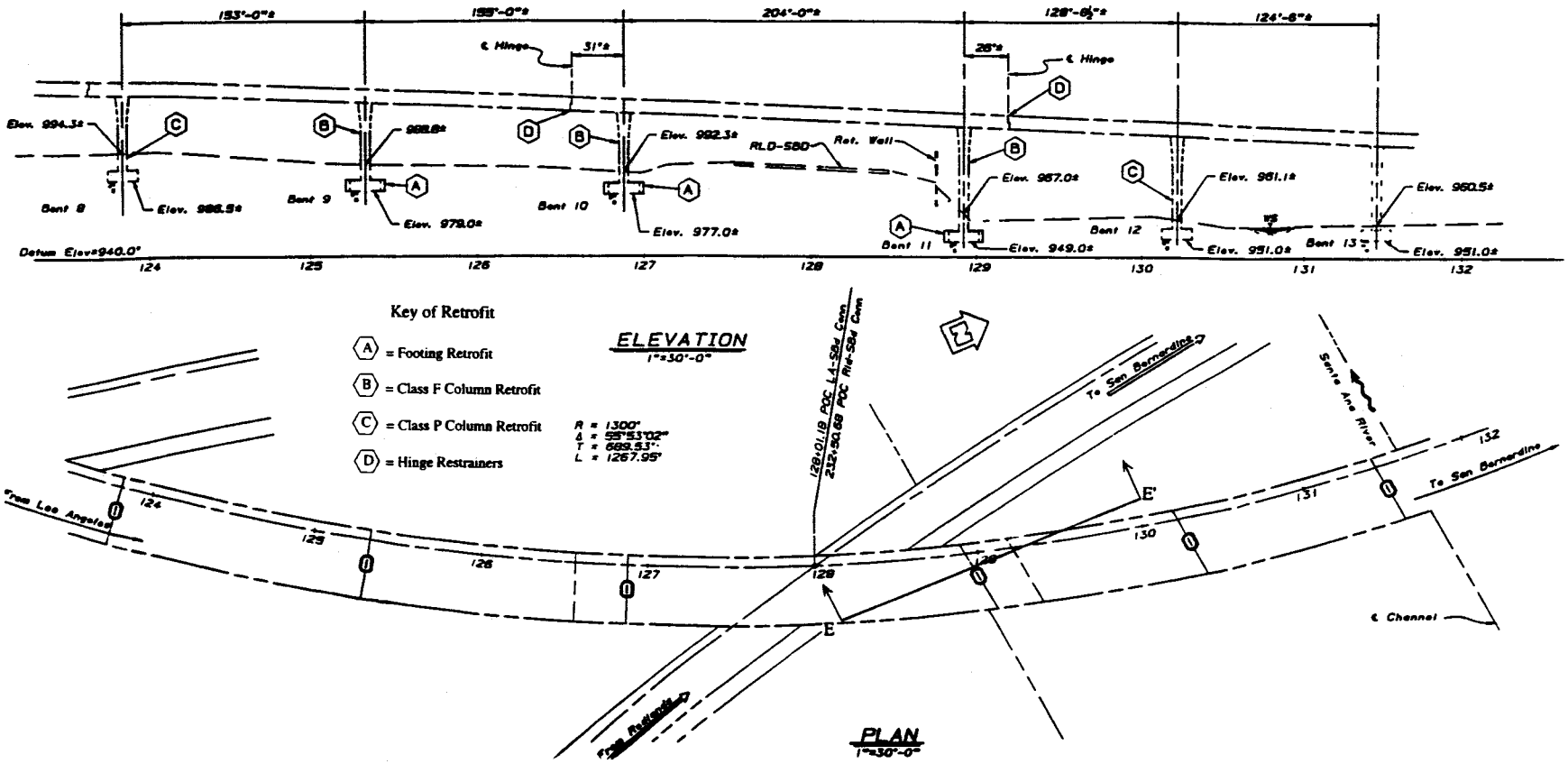

Figure 2.6 General Plan for Seismic Retrofit of Northwest Connector (from Caltrans drawings).

Since there were concerns about the strength of the original diaphragm abutments and the potentially large relative displacements that may develop across the San Jacinto fault, a supplemental support beam was installed in front of each abutment. There is a 1–1/4 inch vertical clearance between bearing blocks on the support beam and the bridge soffit. The support beam will hold the end of the bridge after dropping on to the bearing blocks in the event of a massive abutment failure.

The final retrofit measure was to replace the original restrainers with four cable units (one per cell) at each hinge, using the existing cores through the end diaphragms below the seats. Each cable unit consists of five 3/4–inch diameter twisted strand cables, 20 ft in length.

2.5 Earthquakes Recorded at the Connector

Within a year of the seismic retrofit, the Connector withstood three earthquakes in the Landers sequence. The characteristics of the Joshua Tree earthquake on April 22, 1992, and the Landers and Big Bear earthquakes on June 28, 1992, are summarized in Table 2.2. The Joshua Tree earthquake is considered a precursor to the Landers earthquake, and the Big Bear earthquake is classified as an aftershock (Sieh, Jones et al., 1993). During the current study, the Connector was subjected to the Northridge earthquake on January 17, 1994 (CSMIP, 1994).

The Landers event, with a magnitude of Ms=7.6 (NEIC), was the largest earthquake in California since the 1952 Kern County earthquake. The earthquake resulted from extensive shearing along 53 miles (85 km) on five overlapping faults (Sieh, Jones et al., 1993). The azimuth of the faults is about 10 degrees west of North, although it varies among the five faults. The focal depth was shallow for a California earthquake, an estimated 5.6 miles (9 km). The ground rupture was generally right–lateral strike–slip with an average of 10 ft (3 m) horizontal offset. A maximum horizontal offset of 20 ft (6 m) occurred across a section of one of the faults (Emerson). The maximum vertical displacement of 6 ft (2 m) occurred where the fault bends (USGS, 1992).

Based on broad–band digital seismographic data, Kanamori (1992) concludes that the Landers earthquake consisted of two distinct events from sources about 19 miles (30 km) apart. Each source had a rupture duration of about six to eight seconds, with peaks about ten seconds apart. The seismic moment of the second source is about three time larger than the moment for the first source.

Three hours after the Landers earthquake a magnitude M_S=6.6 earthquake occurred about 19 miles (30 km) west of the Landers epicenter, near Big Bear Lake in the San Bernardino mountains. The focal depth was a shallow 4.3 miles (7

km) and the rupture propagated in a northeast direction, along a previously unmapped left–lateral fault, without evidence of surface rupture.

Table 2.2. Earthquakes and Free–Field Ground Motion Recorded at the Northwest Connector

Event	Magnitude M_s	Epicentral Distance (miles)	Peak Acceleration (g)		Bracketed Duration[b] (sec)
			Horizontal[a]	Vertical	
Joshua Tree[c]	6.3	52	—	—	
Landers	7.6	50	0.089	0.062	26
Big Bear	6.6	28	0.112	0.073	14
Northridge[d]	6.8	72	0.10	0.04	

[a]Instantaneous peak horizontal acceleration.
[b]Time the ground acceleration peaks exceed 0.05 g.
[c]Accelograph not operational.
[d]Based on unprocessed records.

2.6 Observed Earthquake Damage

After the two earthquakes on June 28, 1992, Caltrans maintenance personnel inspected the Connector. The only damage noted in the initial inspection report was spalled concrete in the barrier at Hinge 3. A more extensive Caltrans inspection of the Connector on July 13, 1992, revealed that the left barrier (inside edge of deck) near Hinge 3 spalled an area 8 in. by 6 in. with a depth of 6 in., exposing steel reinforcing bars. Below the deck, the seat of Hinge 3 had three hairline cracks radiating from the reentrant corner of the seat.

Hinges 3, 7, and 9 were inspected from the deck with no other apparent damage. Both sides of Hinges 11 and 13 were inspected by removal of the soffit access plates in one cell of the box girder. There was no evidence of damage to the cable restrainers or brackets.

A report by the Caltrans Post–Earthquake Investigation Team from the Division of Structures described settlement at the hinges, possibly caused by earthquake damage to the elastomeric bearing pads (Yashinksy, Maulchin et al., 1992). Maintenance personnel noted that the expansion joints had had a history of problems and were replaced in 1987. There was no direct inspection of the bearing pads because of the lack of access to the interior of the hinges.

2.7 Strong Motion Instrumentation

The Northwest Connector has been extensively instrumented with a network of strong motion accelerometers by the Office of Strong Motion Studies, California Division of Mines and Geology, in conjunction with Caltrans. The CDMG designation for the Connector is Station No. 23631. After careful study and review the instrumentation was located to record a variety of responses of the bridge. Figure 2.7 shows the location and directions of the thirty–four accelerometers on the Connector.

A sheltered ground motion station is located approximately 825 ft east of the Bent 11 in a parking lot at E and Hospitality Streets in San Bernardino (Station No. 23542). Although a survey of the site was not available for this study, the 825 ft distance was estimated from an Engineering Geology Map of the interchange prepared by Caltrans. The ground motion station is approximately 1400 ft from Bent 8 according to information from CDMG.

The thirty–four force–balance accelerometers on the Connector are cabled to nine digital recorders. The accelerometers have pre–event memory and they are interconnected for time synchronization. The Office of Strong Motion Studies processed the recorded acceleration data for instrument and baseline–corrections, including integration for the velocity and displacement records (Darragh, Cao et al., 1993). The accelerations are sampled at 100 Hz (Δt=0.01 sec.). As a result of bandpass Ormsby filtering, the usable bandwidth for the data is 0.17 Hz to 47.2 Hz (or periods between 5.9 sec. and 0.021 sec.).

The tri–axial ground motion accelerograph is a Kinemetrics SSA–1, and its records were processed in a manner similar to the Connector records. The ground motion recorder is not time synchronized with the Connector recorder, so the relative start time between the free–field records and Connector records must be established by a separate procedure (see Section 4.2).

The terminology for the axes of a curved bridge, longitudinal and transverse, requires clarification. Caltrans defines the longitudinal direction of a curved bridge along the chord between the abutments; the transverse direction is orthogonal to the chord (Caltrans, 1990). In this report the directions based on the chord are called the global longitudinal and global transverse directions. The tangential and radial directions on the curved bridge are called the longitudinal and transverse directions, respectively.

Table 2.3 summarizes the maximum response from the ground motion station. Table 2.4 lists the location of the sensors, direction (longitudinal, transverse, or vertical) and the maximum acceleration and displacement in the Landers and Big Bear earthquakes from the processed records. The records them-

selves will be shown in various forms in this report, but the complete set is not included because of space limitations. The plots of the processed records are available in the CDMG reports (Darragh, Cao et al., 1993).

Table 2.3. Maximum Free–Field Ground

		Landers Earthquake		Big Bear Earthquake	
Channel	Direction	Peak Accel. (g)	Peak Displ. (in.)	Peak Accel. (g)	Peak Displ. (in.)
1	90°	0.077	3.38	0.092	1.38
2	Up	0.062	1.34	0.073	0.44
3	180°	0.087	2.95	0.101	1.23

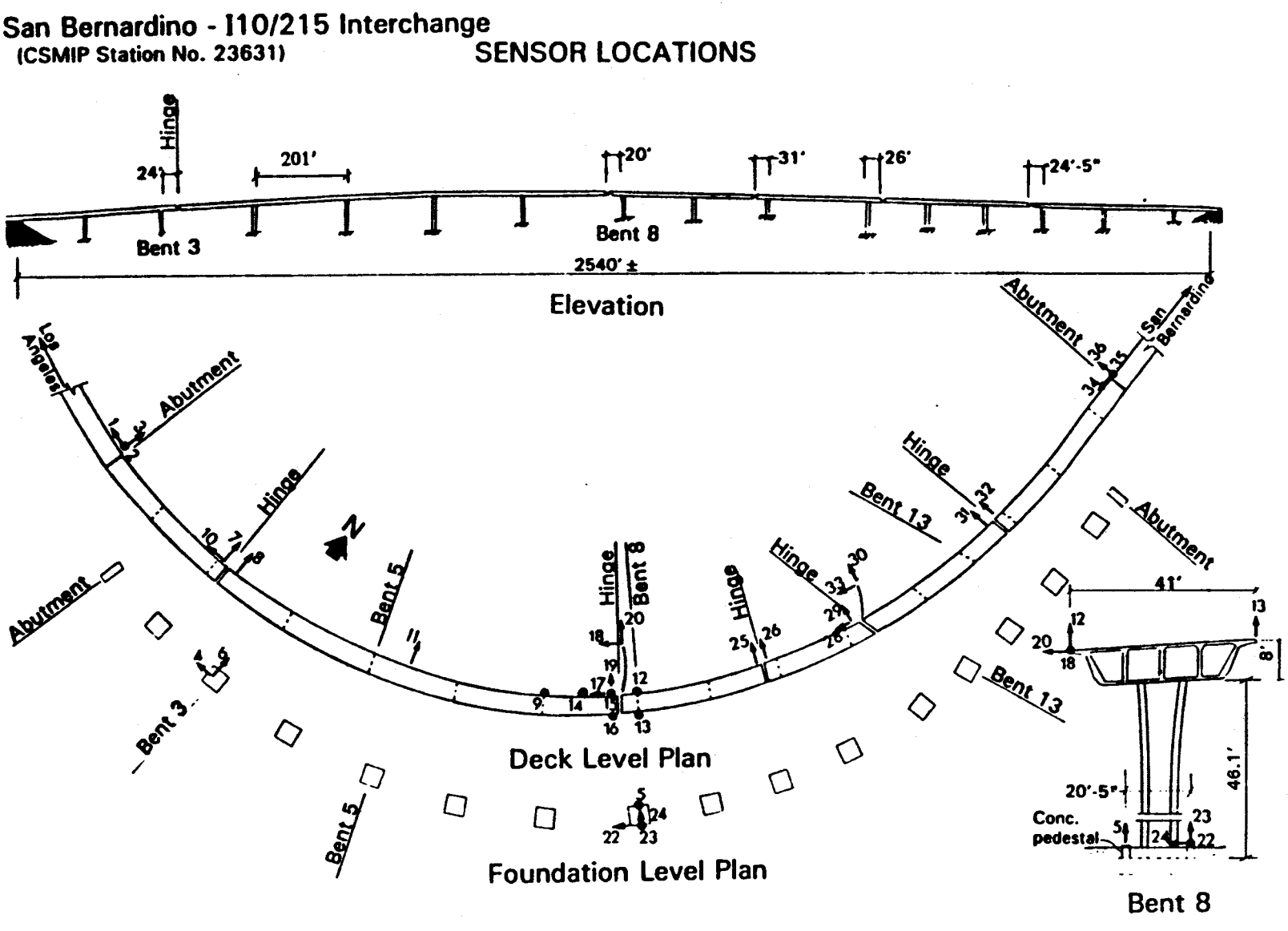

Figure 2.7 Seismic Instrumentation for the Northwest Connector (Darragh, Cao et al., 1993).

Table 2.4. Location of Strong Motion Accelerometers on Northwest Connector and Maximum Response in the Landers and Big Bear Earthquakes

			Landers Earthquake		Big Bear Earthquake	
Channel	Location	Direction	Peak Accel. (g)	Peak Displ. (in.)	Peak Accel. (g)	Peak Displ. (in.)
1	Abut. 1	L	0.535	3.23	0.401	2.04
2	Abut. 1	V	0.187	1.02	0.099	0.33
3	Abut. 1	T	0.243	1.93	0.189	1.26
4	Bent 3, Footing	L	0.103	2.78	0.085	1.07
5	Bent 8, Footing, North Side	V	0.107	1.07	0.075	0.49
6	Bent 3, Footing	T	0.099	2.38	0.110	1.24
7	Hinge 3, West Side	T	0.297	6.30	0.379	5.91
8	Hinge 3, East Side	T	0.553	6.61	0.449	6.22
9	Bent 7, Deck	V	0.197	2.49	0.176	1.89
10	Hinge 3, West Side	L	0.450	3.04	0.344	1.39
11	Midspan, Bents 5 and 6, Deck	T	0.393	9.76	0.287	6.73
12	Bent 8, Deck, North Side	V	0.258	2.36	0.214	2.07
13	Bent 8, Deck, South Side	V	0.354	3.27	0.225	1.49
14	Midspan, Bents 7 and 8, Deck	V	0.372	2.34	0.312	1.95
15	Hinge 7, North Side	V	0.346	2.50	0.311	1.98
16	Hinge 7, South Side	V	0.430	3.31	0.310	1.51
17	Hinge 7, West Side	L	0.638	2.59	0.342	3.11
18	Hinge 7, East Side	L	0.712	1.93	0.565	2.08

L=Longitudinal (tangential); T=Transverse (radial), V=Vertical (up).

Table 2.4 (cont'd). Location of Strong Motion Accelerometers on Northwest Connector and Maximum Response in the Landers and Big Bear Earthquakes

			Landers Earthquake		Big Bear Earthquake	
Channel	Location	Direction	Peak Accel. (g)	Peak Displ. (in.)	Peak Accel. (g)	Peak Displ. (in.)
19	Hinge 7, West Side	T	0.512	10.47	0.496	5.20
20	Hinge 7, East Side	T	0.392	10.28	0.329	4.68
21	Not Used	—	—	—	—	—
22	Bent 8, Footing, South Side	L	0.163	1.34	0.250	1.21
23	Bent 8, Footing, South Side	V	0.072	1.11	0.082	0.49
24	Bent 8, Footing, South Side	T	0.179	4.88	0.147	1.60
25	Hinge 9, West Side	T	0.323	6.38	0.255	3.02
26	Hinge 9, East Side	T	0.298	6.26	0.251	3.00
27	Not Used	—	—	—	—	—
28	Hinge 11, West Side	L	0.281	2.82	0.361	2.35
29	Hinge 11, West Side	T	0.288	7.55	0.302	5.51
30	Hinge 11, East Side	T	0.432	7.68	0.406	5.71
31	Hinge 13, West Side	T	0.357	4.49	0.836	4.02
32	Hinge 13, East Side	T	0.413	4.13	0.450	3.75
33	Hinge 11, East Side	L	0.792	2.81	0.663	2.15
34	Abut. 17	L	0.322	3.28	0.222	1.44
35	Abut. 17	V	0.102	1.03	0.097	0.39
36	Abut. 17	T	0.139	3.16	0.190	1.56

L=Longitudinal (tangential); T=Transverse (radial), V=Vertical (up).

Chapter 3

METHODOLOGY FOR EVALUATION OF EARTHQUAKE RESPONSE

3.1 Introduction

This chapter presents the methodology used in the evaluation of the Northwest Connector in the Landers and Big Bear earthquakes. Several techniques are used to identify the vibration characteristics and evaluate the earthquake response of the structure.

3.2 Summary of Structural Dynamics

The equations of motion for a linear structure subjected to multiple–support motion are summarized in this section. The properties of the structure with N degrees–of–freedom are represented by a mass matrix, $\mathbf{m}$, stiffness matrix, $\mathbf{k}$, a coupling stiffness matrix, $\mathbf{k}_g$, and a damping matrix, $\mathbf{c}$. In this study, classical (or proportional) damping is assumed to model adequately energy dissipation in the structure. The total displacement of the structure is the superposition of "dynamic" response and "pseudo–static" response:

$$\mathbf{u}^t(t) = \mathbf{u}(t) + \mathbf{r}\mathbf{u}_g(t) \tag{3.1}$$

where $\mathbf{u}_g(t)$ is the vector of support displacements and $\mathbf{r} = -\mathbf{k}^{-1}\mathbf{k}_g$ is the matrix of influence vectors for each component of support motion (Clough and Penzien, 1993).

Neglecting the excitation terms proportional to the support velocity, the equations of motion are (Clough and Penzien, 1993):

$$\mathbf{m}\ddot{\mathbf{u}}(t) + \mathbf{c}\dot{\mathbf{u}}(t) + \mathbf{k}\mathbf{u}(t) = -\mathbf{m}\mathbf{r}\ddot{\mathbf{u}}_g(t) \tag{3.2}$$

The undamped eigenvalue problem for the structure, $\mathbf{k}\boldsymbol{\phi}_i = \omega_i^2\mathbf{m}\boldsymbol{\phi}_i$, gives the vibration frequencies, ω_i, and vibration mode shapes, $\boldsymbol{\phi}_i$, for mode i. The

generalized mass for mode i is $m_i^* = \boldsymbol{\phi}_i^T \mathbf{m} \boldsymbol{\phi}_i$, and the vector of generalized influence factors for the support motion is $\mathbf{L}_i = \mathbf{r}^T \mathbf{m} \boldsymbol{\phi}_i$.

The solution for Eq. 3.2 can be represented by mode superposition over $J << N$ vibration modes using generalized coordinates:

$$\mathbf{u}(t) = \sum_{j=1}^{J} \boldsymbol{\phi}_j Z_j(t) \tag{3.3}$$

By orthogonality of the vibration modes, the equations of motion for the generalized coordinates are uncoupled:

$$\ddot{Z}_i(t) + 2\xi_i \omega_i \dot{Z}_i(t) + \omega_i^2 Z(t) = -\frac{1}{m_i^*} \mathbf{L}_i^T \ddot{\mathbf{u}}_g(t) \tag{3.4}$$

in which ξ_i is the damping ratio for vibration mode i.

The solution to Eq. 3.4 can be represented by Laplace transforms. A time-dependent quantity $a(t)$, is related to its Laplace transform $\bar{a}(s)$, by $a(t) = \bar{a}(s)e^{st}$. The Laplace transform of Eq. 3.4 is:

$$\bar{Z}(s) = -\frac{1}{s^2 + 2\xi_i \omega_i s + \omega_i^2} \cdot \frac{1}{m_i^*} \mathbf{L}_i^T \bar{\ddot{\mathbf{u}}}_g(s) \tag{3.5}$$

Since the identification of vibration properties is based on recorded total acceleration, it is necessary to use Eq. 3.1 to represent the Laplace transform of the total acceleration. The influence matrix can be represented in terms of modal contributions:

$$\mathbf{r} = \sum_{j=1}^{J} \frac{1}{m_j^*} \boldsymbol{\phi}_j \mathbf{L}_j^T \tag{3.6}$$

Using Eqs. 3.1, 3.5, and 3.6, the total acceleration vector can be expressed in terms of the support acceleration vector:

$$\bar{\ddot{\mathbf{u}}}^t(s) = \mathbf{H}(s) \bar{\ddot{\mathbf{u}}}_g(s) \tag{3.7a}$$

where,

$$\mathbf{H}(s) = \sum_{j=1}^{J} H_j(s)\mathbf{b}_j^T \tag{3.7b}$$

$$H_j(s) = \frac{2\xi_j\omega_j s + \omega_j^2}{s^2 + 2\xi_j\omega_j s + \omega_j^2} \tag{3.7c}$$

$$\mathbf{b}_j = \frac{1}{m_j^*}\mathbf{L}_j^T\boldsymbol{\phi}_j \tag{3.7d}$$

In Eq. 3.7(a), $[\mathbf{H}(s)]_{nm}$ is the transfer function between support point m and degree-of-freedom n in the structure. The transfer functions are rational polynomials of s, in which the numerator is order $2J-1$ and the denominator is order $2J$. When the Laplace transform is evaluated on the imaginary axis, $s = i\omega$, the functions $\mathbf{H}(i\omega)$ are the frequency response functions. More specifically $\mathbf{H}(i\omega)$ are called transmissibility functions because they give the ratio of ground acceleration (input) to the structure acceleration (output).

3.3 Nonparametric Evaluation

The nonparametric evaluation techniques used in this study are: a) examination of the recorded time histories to ascertain overall characteristics of the earthquake response of the Connector; and b) spectral analysis to obtain the transmissibility functions, in particular identifying the vibration periods. Although numerical results are obtained from spectral analysis, the inherent errors in the procedure mean that the results can only be considered qualitative. A more accurate evaluation of vibration properties uses parametric identification techniques.

3.3.1 Spectral Analysis

The power spectral density and cross-power spectral density functions of the recorded earthquake motions can be used for non-parametric identification of the vibration properties of the structure. For an ergodic and random process with zero mean, the power spectral and cross-power spectral density functions are Fourier transforms of the auto-correlation functions, $R_{xx}(\tau)$ and $R_{yy}(\tau)$, and the cross-correlation function, $R_{xy}(\tau)$, for two processes, x and y (Clough and Penzien, 1993):

$$S_{xx}(\omega) = \frac{1}{2\pi} \int_{-\infty}^{\infty} R_{xx}(\tau) e^{-i\omega\tau} d\tau$$

$$S_{yy}(\omega) = \frac{1}{2\pi} \int_{-\infty}^{\infty} R_{yy}(\tau) e^{-i\omega\tau} d\tau$$

$$S_{xy}(\omega) = \frac{1}{2\pi} \int_{-\infty}^{\infty} R_{xy}(\tau) e^{-i\omega\tau} d\tau$$

Whereas the power spectral density functions, $S_{xx}(\omega)$ and $S_{yy}(\omega)$, are real-valued, the cross-power spectral density function is a complex-valued Hermitian function, $S_{xy}(\omega) = S_{yx}^{*}(\omega)$, in which the asterisk denotes complex conjugation. The power spectral density functions completely characterize the input and output processes.

If process x is the recorded input acceleration (input) for a structure and process y is the recorded acceleration (output) of the structure, the relationship between the two can be expressed in terms of the transmissibility function, $H(i\omega)$ (Ljung, 1987; Pandit, 1991):

$$S_{yx}(\omega) = H(i\omega) S_{xx}(\omega)$$
$$S_{yy}(\omega) = H(i\omega) S_{xy}(\omega)$$

Consequently, the power spectral density functions provide two estimates of the complex-valued transmissibility function:

$$H_1(i\omega) = \frac{S_{yx}(\omega)}{S_{xx}(\omega)} \qquad (3.8)$$
$$H_2(i\omega) = \frac{S_{yy}(\omega)}{S_{xy}(\omega)}$$

In the absence of noise and other errors associated with the discrete Fourier transform (mainly leakage), the two estimates of the transmissibility function should be equal. The absolute value of $H(i\omega)$ gives the transmissibility factor for the structure; the ratio of the imaginary and real components of $H(i\omega)$ is the tangent of the phase angle between the input and output processes.

The coherency function between the input and output processes can be used to judge the quality of the $H(i\omega)$ estimate in the presence of noise. The squared modulus of the coherency is the ratio of the two estimates of the frequency response function (Ljung, 1987; Pandit, 1991):

$$|\gamma(i\omega)|^2 = \frac{H_1(i\omega)}{H_2(i\omega)} = \frac{|S_{xy}(\omega)|^2}{S_{xx}(\omega)S_{yy}(\omega)} \tag{3.9}$$

The squared modulus of the coherency ratio is a function of frequency that varies between zero and unity. It can be shown that the spectrum of the noise is proportional to $1-|\gamma(i\omega)|^2$. A good estimate of the transmissibility function is obtained when the coherency is near unity because the noise is small compared with the response y.

In practice, it is necessary to accept estimates of $H(i\omega)$ with coherency less than unity. The accuracy of the two estimates depends on the noise in the input process and output processes (Mitchell, 1982). It can be shown that $H_1(i\omega)$ is less sensitive to output noise, whereas $H_2(i\omega)$ is less sensitive to input noise. In this study, $H_2(i\omega)$ is used as the estimator for the transmissibility functions. As can be seen from Eq. 3.8, the absolute value of $H_2(i\omega)$ is greater than the absolute value of $H_1(i\omega)$ when the modulus of the coherency is less than unity. Consequently, the $H_2(i\omega)$ estimate gives larger peaks than the $H_1(i\omega)$ estimate.

3.3.2 Periodogram Estimate of Power Spectral Density Function

The periodogram can be used as a measure of the power spectrum of a random signal (Oppenheim and Schafer, 1989). Periodograms are averages of the discrete Fourier transforms of a signal. The transforms can be efficiently computed using the fast Fourier transform (FFT) procedure. The averaging smoothes the Fourier spectrum by reducing the randomness resulting from the estimation procedure.

Before computing periodogram it is necessary to limit the frequency band of the signal to reduce aliasing effects. Since the processed acceleration and displacement records are band limited during the processing, no further filtering is required. As mentioned in Section 2.7, the usable bandwidth of the recorded motion is 0.17 Hz to 47.2 Hz.

Spectral analysis is improved by reducing the high–frequency content of the records. Considering that the important vibration modes of the Connector have frequencies less than 5 Hz (periods longer than 0.20 sec), decimation is performed by lowpass filtering the records and resampling at 10 Hz. The decimated records contain information to one–half the sampling rate (Nyquist frequency) of 5 Hz.

The averaging procedure is based on the method by Welch, as described on page 737 of Oppenheim (1989). To compute the average periodogram, the record is divided into, possibly overlapping, segments. The FFT of the segment, with a

data window is computed. The periodogram is an average of the square of the FFT amplitudes over the segments. It is well–known, however, that there is a tradeoff between smoothness of the estimated frequency response function from the periodograms and error, or bias, relative to the true function. Increasing the number of segments produces a smoother estimate of $H(\omega)$ at the expense of reducing the frequency resolution and eliminating peaks.

The tapering window used for each segment reduces leakage due to the discrete Fourier transform and allows better resolution of peaks in the frequency response function. A window tapers the signal to reduce errors inherent in the discrete Fourier transform, such as leakage. The choice of a window, such as Hanning, Hamming, Bartlett, or Kaiser, requires judgment based on the characteristics of the frequency response function being estimated and the resolution needed to identify peaks in the transmissibility function. A Kaiser window is used for the spectral analysis in this study. The factor for the window is $\beta = 15.7$, which gives sidelobes down 120 dB from the mainlobe, providing excellent tapering (Oppenheim and Schafer, 1989) and a frequency resolution of 0.02 Hz for a sample of 512 points.

3.4 Parametric Identification

There are fundamental problems with identifying vibration properties of a structure by spectral analysis that are related to the application of the FFT to transient response (Pandit, 1991). A more accurate technique for identifying vibration properties is based on representing structural response in the discrete time domain in terms of parameters of a model (Ljung, 1987; Pandit, 1991). The parameters can be estimated by least–squares procedures to minimize the error between the discrete time model and recorded response. The vibration properties of the structure can be determined from the best–fit parameters of the model. Safak (1991) has presented an excellent summary of parametric identification of building vibration properties from earthquake records. Other identification procedures for structural response are described in the literature (Katafygiotis, 1991; Beck and Katafygiotis, 1992).

In this study a single input, single output model is used for determining vibration frequencies and damping ratios of the Connector. A multiple output model would be needed to identify mode shapes, and a multiple input model would be needed to determine the pseudo–static influence matrix, $\mathbf{r}$. When restricted to single input in Eq. 3.7, the matrix $\mathbf{b}_j$ is a scalar for the one input DOF (support point) and one output DOF, and $\mathbf{H}(s)$ is scalar of the transmissibility function between the input and output.

To develop a parametric representation, the continuous response in the Laplace domain can be transformed to discrete time assuming the input and output are constant over each time step, Δt. Using the zero–order hold method, the transfer function in discrete time can be represented as a Z–transform (Astrom and Wittenmark, 1990). The Z–transform of Eq. 3.7 restricted to single input and output is written as (Safak, 1991):

$$H_j(z) = \frac{\beta_{1j} z^{-1} + \beta_{2j} z^{-2}}{\alpha_{2j} z^{-2} + \alpha_{1j} z^{-1} + 1}$$

where the correspondence with the continuous case is apparent. The Z–transform of the scalar $\mathbf{H}(s)$ can be expanded as a rational polynomial:

$$H(z) = \frac{b_1 z^{-1} + b_2 z^{-2} + \ldots + b_{2J} z^{-2J}}{1 + a_1 z^{-1} + a_2 z^{-2} + \ldots + a_{2J} z^{-2J}} \tag{3.10}$$

The order of the model is $2J$.

The Z–transform in Eq. 3.10 has the following relationship between the input $x(t)$ and output $y(t)$:

$$\begin{aligned} &y(t) + a_1 y(t-1) + a_2 y(t-2) + \ldots + a_{2J} y(t-2J) = \\ &b_1 x(t-1-d) + b_2 x(t-2-d) + \ldots b_{2J} x(t-2J-d) \end{aligned} \tag{3.11}$$

where d is a time delay between input and output. This model involves auto–regression of the input and output histories and is called ARX for auto–regressive extended (Ljung, 1987) or ARV for auto–regressive vector (Pandit, 1991).

The $4J$ coefficients in the autoregressive expression of Eq. 3.11 are evaluated by a linear least squares procedure that minimizes the error between the recorded input and output and the model (Safak, 1991). Once the coefficients in Eq. 3.10 are known, the poles of the Z–transform are the roots of the denominator:

$$1 + a_1 z^{-1} + a_2 z^{-2} + \ldots + a_{2J} z^{-2J} = 0 \tag{3.12}$$

The complex–valued roots are denoted $z_1, z_2 \ldots z_{2J}$. For a stable system all the poles lie within the unit circle in the complex plane.

The poles of the Z–transform are related to the poles of the transmissibility function by the sampling interval, Δt (Astrom and Wittenmark, 1990):

$$s_i = \frac{1}{\Delta t} \ln z_i \tag{3.13}$$

The poles of the transmissibility function in Eq. 3.7 are in complex conjugate pairs:

$$s_j, s_j^* = -\xi_j \omega_j \pm i\omega_j \sqrt{1-\xi_j^2} \tag{3.14}$$

Given the poles from Eq. 3.13, the vibration frequency and damping ratio of mode j can be determined from Eq. 3.14:

$$\omega_j = \sqrt{s_j s_j^*}$$

$$\xi_j = -\frac{\mathrm{Re}(s_j)}{\omega_j}$$

Issues related to accuracy of the model and selection of order and delay are discussed in the references (Ljung, 1987; Pandit, 1991; Safak, 1991).

3.5 Structural Modeling and Dynamic Analysis

The final method used in the evaluation of the earthquake response of the Connector is to create models of the structure, perform dynamic analysis with the models, and compare the computed earthquake response with the recorded response. The bridge is modeled by a "stick model" consisting of one–dimensional frame elements to represent the columns and the box girder. Since there was no obvious damage to the bridge in the earthquakes, it is appropriate to use an elastic model for the dynamic analysis. Standard dynamic analysis methods are employed to solve the equations of motion for bridges, as described by Fenves (1992).

To account for the opening and closing of the hinges, nonlinear gap elements and tension–only elements are used in the model. A dynamic analysis program, SADSAP, provides this type of nonlinear analysis capability (Wilson, 1992). The analysis method employs the following concepts (Wilson, Suharward et al., 1994):

1. Load–dependent Ritz vectors are used as a basis for reducing the number of DOF instead of eigenvectors. The Ritz vectors are generated using the inertia loads and concentrated loads that produce hinge opening.

2. An initial stiffness linearization is used for all the linear elements in the reduced basis. Consequently, the uncoupled modal equations are valid for the entire solution history.

3. The nonlinear forces from the compression–only and tension–only elements are placed on the right–hand side of the modal equations. Iteration for each time step is used to evaluate the nonlinear forces and converge to an equilibrium solution.

4. Within the iterations for a time step, the modal equations are solved exactly assuming the loads and nonlinear forces vary as a linear function over the time step.

The solution procedure is very efficient for large models with a small number of nonlinear one–dimensional elements. This is the case for the model of the Connector in which nonlinear elements are only used to represent the hinges and restrainers.

Chapter 6 presents the modeling of the Connector and the comparison of the computed and recorded responses in the two earthquakes.

Chapter 4

FREE–FIELD AND SUPPORT MOTION

4.1 Introduction

This chapter presents the free–field ground motion and its relationship with the support motion at four locations for the Connector. The free–field ground motion station is located approximately 825 ft east of Bent 11 of the Connector.

4.2 Free–Field Ground Motion

To evaluate the recorded free–field ground motions, it is necessary to transform the horizontal acceleration records to principal axes. At sites with a large epicentral distance, the principal axes should correspond with the direction to the epicenter (Kubo and Penzien, 1977). The principal directions are determined from the covariance matrix for the horizontal ground acceleration components:

$$\boldsymbol{\mu} = \frac{1}{N}\sum_{i=1}^{N} \mathbf{a}_i \mathbf{a}_i^T$$

where the vector $\mathbf{a}_i$ contains the acceleration values for the two horizontal components at time step i. The eigenvectors of the 2x2 covariance matrix, $\boldsymbol{\mu}$, are the direction cosines for the principal directions and the eigenvalues are the mean square amplitudes of the ground acceleration in the principal directions.

Table 4.1 gives the azimuths of the principal axes computed over the bracketed duration for each free–field ground acceleration record and the peak and root–mean–square accelerations in the principal directions. The bearing from the site to the Landers epicenter is approximately along the computed principal axis of 251°–71°. The Big Bear epicenter had about the same bearing from the site as the Landers epicenter, although the computed principal axis of 41°–221° is in a more northerly direction by about ten degrees. The free–field ground accelera-

tion records in the principal directions are shown in Figs. 4.1 and 4.2 for the Landers and Big Bear earthquakes, respectively.

Table 4.1. Principal Directions of Free–Field Ground Motion

	Major Principal Direction			Minor Principal Direction		
Event	Azimuth	Peak Accel. (g)	RMS Accel. (g)	Azimuth	Peak Accel. (g)	RMS Accel. (g)
Landers	251°	0.083	0.028	161°	0.088	0.027
Big Bear	41°	0.109	0.015	311°	0.072	0.012

The pseudo–acceleration response spectra, with five percent damping, for the horizontal free–field ground acceleration in the principal axes are shown in Fig. 4.3. The Big Bear earthquake has larger spectral ordinates than the Landers earthquake for vibration periods less than one second. For periods greater than three seconds, the spectral ordinates of the Landers earthquake are about twice that of the Big Bear earthquake. It is expected that the Landers earthquake has more long period energy than the Big Bear earthquake because it is a larger magnitude and longer duration event. For both earthquakes the pseudo–acceleration for the major principal axis is greater than the value for the minor principal axis only in the short period range. For periods greater than about 1.5 sec, the minor principal axis has larger pseudo–acceleration ordinates than the major axis.

The spectra for both earthquakes have a peak near a period of 1.8 to 1.9 sec. This peak may be associated with the characteristic vibration period of the deep alluvial site. To examine this explanation, downhole tests at the site provide an average shear wave velocity of 1580 ft/sec for the alluvial sands (Jackura, 1991). The presumed depth to bedrock is 1000 ft. Based on these data the characteristic site period should be 2.5 sec. The calculated period is longer than the period of the peak in the earthquake response spectra, but the assumed depth to bedrock could be in error by 25 percent.

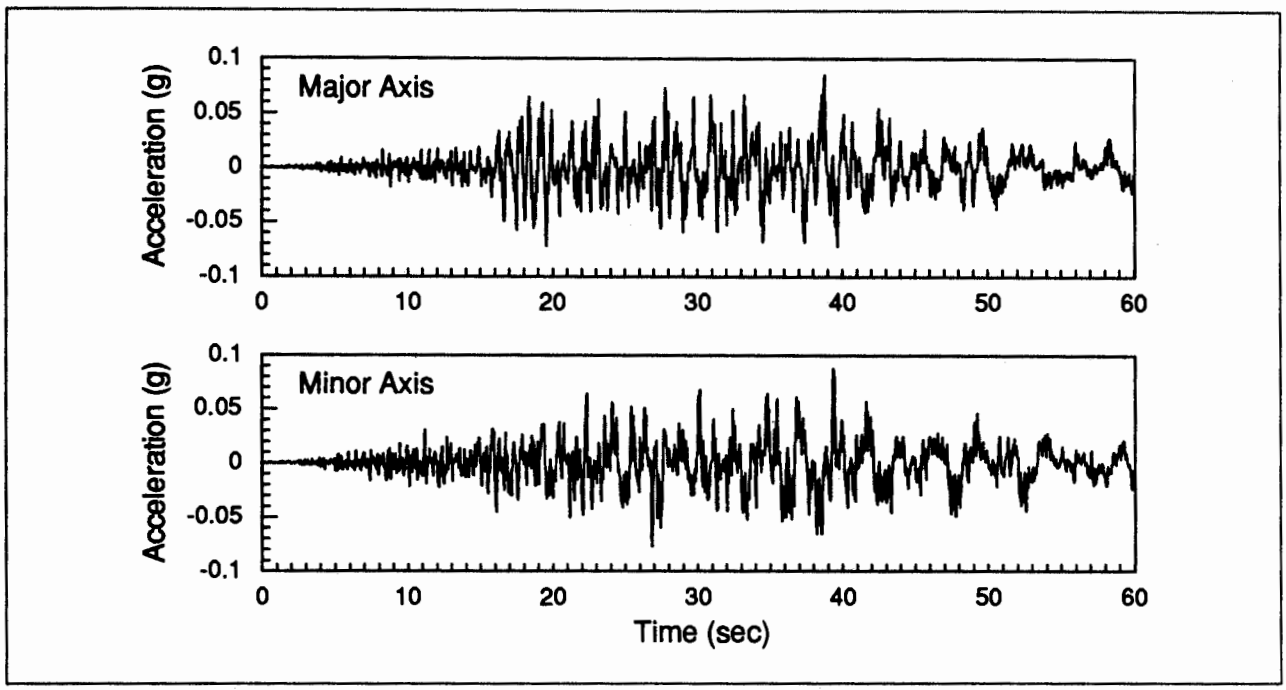

Figure 4.1 Landers Free–Field Ground Acceleration in the Principal Major Axis (251°) and Principal Minor Axis (161°).

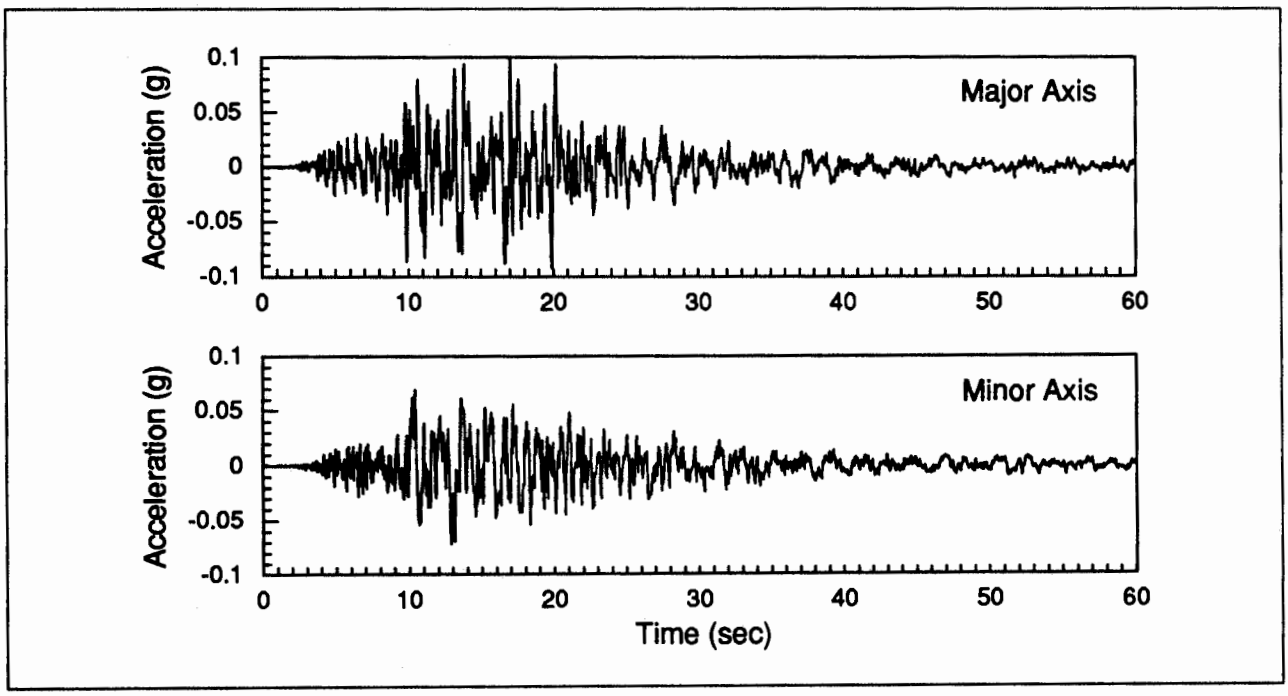

Figure 4.2 Big Bear Free–Field Ground Acceleration in the Principal Major Axis (41°) and Principal Minor Axis (311°).

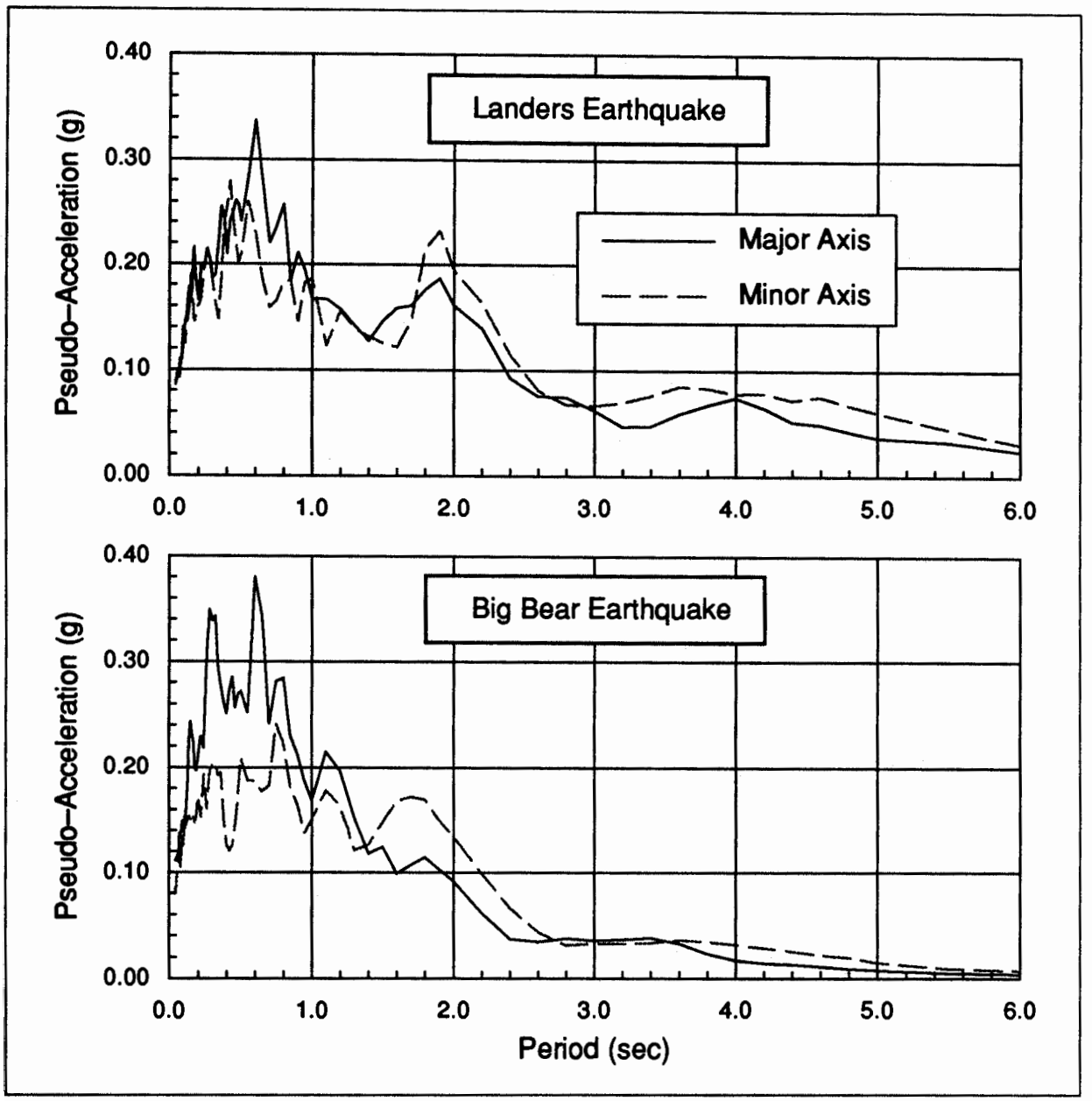

Figure 4.3 Response Spectra (5 percent damping) for Landers and Big Bear Free–Field Ground Motion in the Principal Axes.

The response spectra for ground motion in the principal axes can be compared with the smooth design response spectrum used by Caltrans. Figure 4.4 shows the ARS spectrum appropriate for the site (Caltrans, 1990). The S.7GD51 ARS spectrum corresponds to a peak ground acceleration of 0.7g and an alluvial site with soil depth greater than 150 ft. Also shown in Fig. 4.4 is the ARS spectrum reduced by a Z factor of four, a typical value of the reduction factor to account for inelastic behavior and seismic risk for single column bents (Caltrans,

1990). In the short period range, less than one second, the spectra for the recorded earthquakes in their major principal axis exceed the reduced ARS/Z spectrum. For longer periods the design spectrum envelopes the spectra for two earthquakes, except for the peak for the Landers earthquake near 1.9 sec.

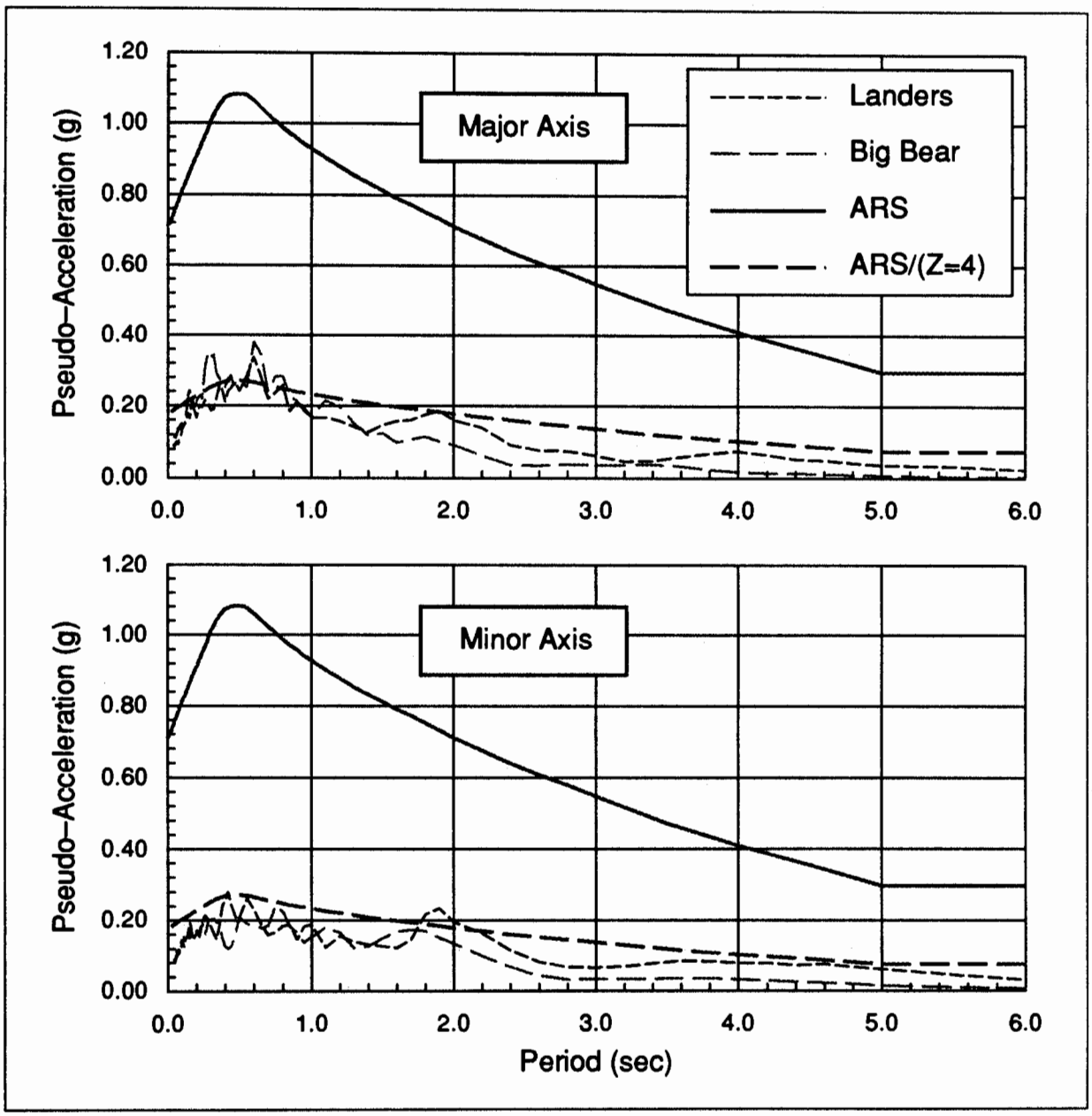

Figure 4.4 Response Spectra (5 percent damping) for Landers and Big Bear Free–Field Ground Motion in the Principal Axes Compared with Caltrans ARS Design Spectrum.

As will be shown in subsequent chapters, the important vibration modes of the Connector have periods between 1.0 and 1.7 sec. The reduced design spectrum envelopes the spectra for the recorded motion in this period range. There is not, however, a large difference between the reduced ARS/Z spectrum and the recorded spectra, so the forces developed in the Connector during the Landers and Big Bear earthquakes approached the nominal design strength of the columns.

4.3 Synchronization of Free–Field and Support Motion Records

The free–field ground motion records were not time synchronized with the records from the Connector. Although the recorders received a radio signal that provides absolute time, the time coding could not be interpreted. However, the thirty–four channels on the Connector have a common time synchronization. CDMG estimated that the Connector records lagged the free–field records by two to three seconds for the Landers earthquake, and the lag was 0.6 to 0.8 sec for the Big Bear earthquake.

The purpose of this section is to estimate the time lag between the recorded free–field and structure records. Considering the lack of a precise survey and the wave propagation properties of the site, the synchronization procedure must be approximate. To determine the time lag, the following assumptions are made:

- Wave propagation effects are neglected and it is assumed that the vertical motion at the free–field location and the footing of Bent 8, separated by 1400 ft, are in–phase.

- The processed vertical ground displacement records are used to determine the time lag because they are least affected by soil–structure interaction.

The time lag between Channel 23 for the Connector relative to the free–field Channel 2 is determined by computing the correlation coefficient between the processed displacement records. The correlation is computed for a time window from 20 sec to 40 sec in the free–field record, during which the largest vertical ground displacement occurs for both earthquakes.

Figure 4.5 shows the correlation coefficient between the two vertical displacement records for time lags near the values estimated by CDMG. The correlation is maximized for a time lag of 1.96 sec for the Landers earthquake and 0.64 sec for the Big Bear earthquake. Figure 4.6 shows the vertical displacement history for the free–field and the vertical displacement at the footing for Bent 8 with the specified time lag.

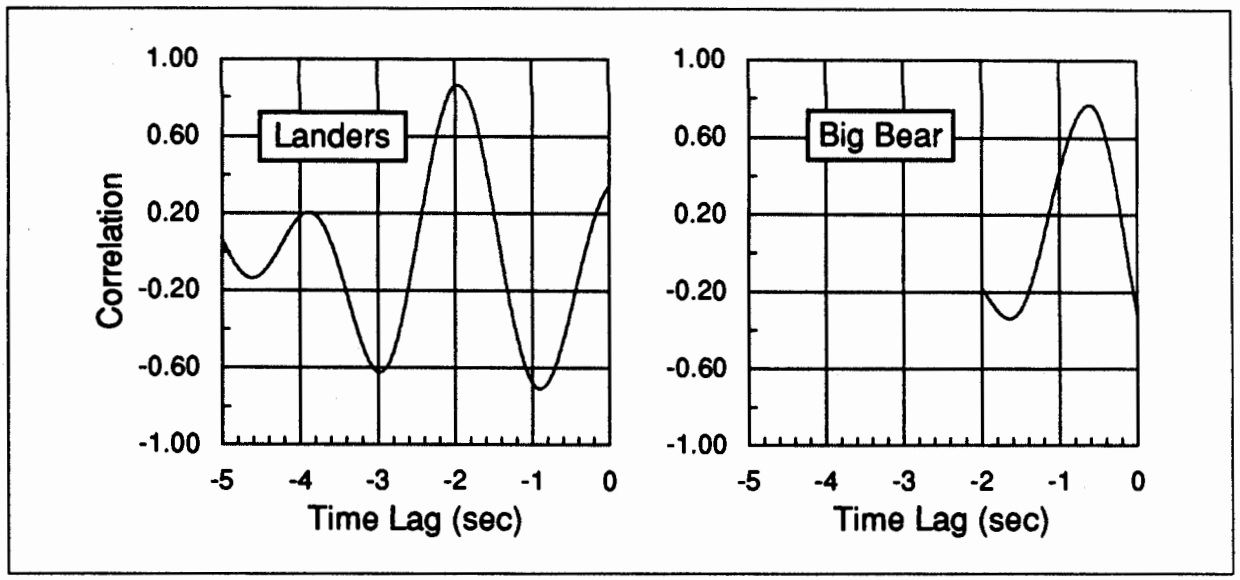

Figure 4.5 Correlation Coefficient Between Free–Field Vertical Displacement and Bent 8 (Footing) Vertical Displacement.

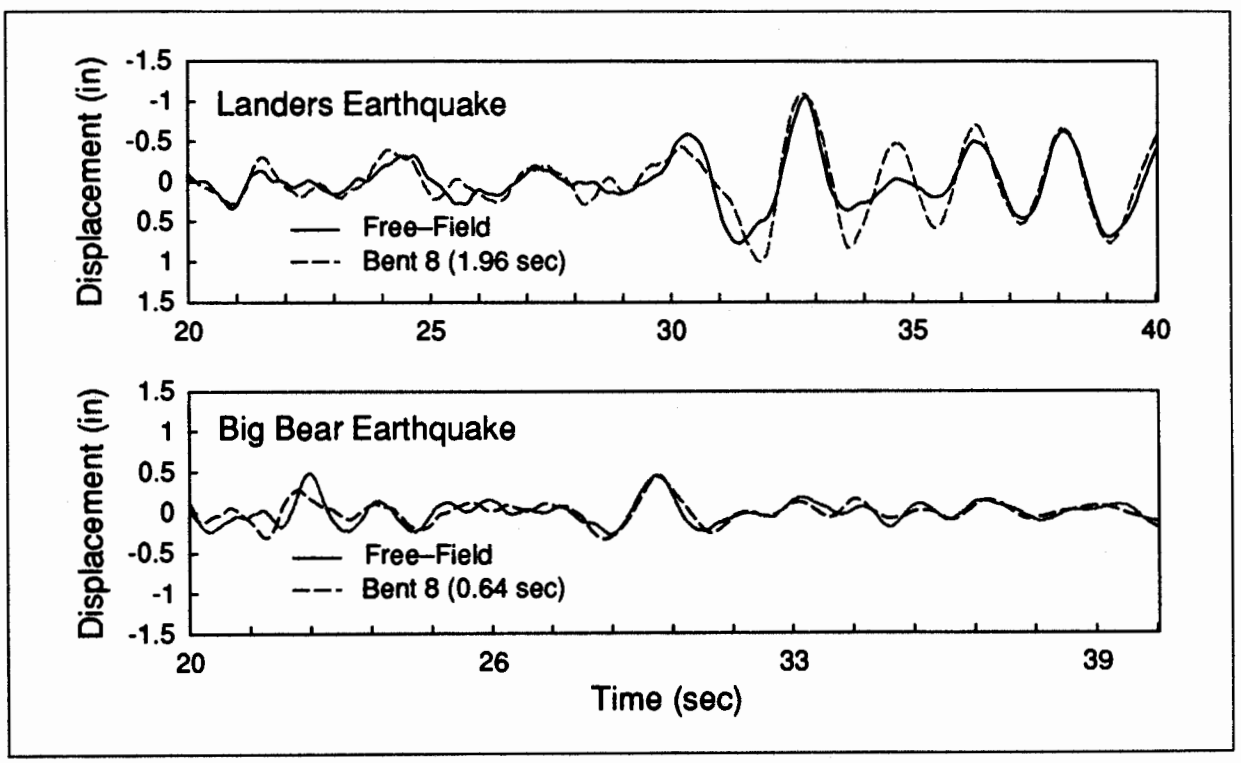

Figure 4.6 Free–Field Vertical Displacement and Bent 8 Footing Vertical Displacement with Time Lag.

Based on this correlation study, it is assumed that the Connector records lag the free–field records by 1.96 sec for the Landers earthquake and 0.64 sec for the Big Bear earthquake.

4.4 Support Motion for the Connector

The input motions for the Connector were recorded at four supports: Abutments 1 and 17, and Bents 3 and 8. Figures 4.7 and 4.8 show the displacement histories at the four supports in the global longitudinal direction (parallel to chord) and global transverse direction (perpendicular to chord) for the two earthquakes. The heavy line in Figs. 4.7 and 4.8 is the free–field displacement histories in the same directions, accounting for the aforementioned time lags.

As can be seen from Figs. 4.7 to 4.8, the displacement histories are similar at the four supports and the free–field location. There are several causes of the differences between the five records:

- Different site response because of varying soil profile along the alignment.
- Random incoherence of the ground motion.
- Wave propagation across the site.
- Modification of the free–field motion by soil–structure interaction.

Although the overall input motion at the four locations is similar to the free–field motion, the differences in the input motion must be understood in order to assess the importance of multiple–support excitation of the Connector.

As a first step, Table 4.2 gives the maximum difference in support displacement between pairs of the four supports for each earthquake. The maximum relative displacement between the abutments is 3.04 inches and 2.58 inches for the Landers and Big Bear earthquakes, respectively. The relative displacements from Table 4.2 are plotted as a function of the distance between the supports in Fig. 4.9. Generally, the relative displacements are larger for Landers than for Big Bear, except for the short distance between Bents 3 and 8. These relative support displacements are small for a 2540 ft long bridge; they should be easily accommodated as pseudo–static displacements, primarily at the hinges. The relative displacements are significantly less than a strain of 0.003 produced by a 50 degree change of temperature in the superstructure.

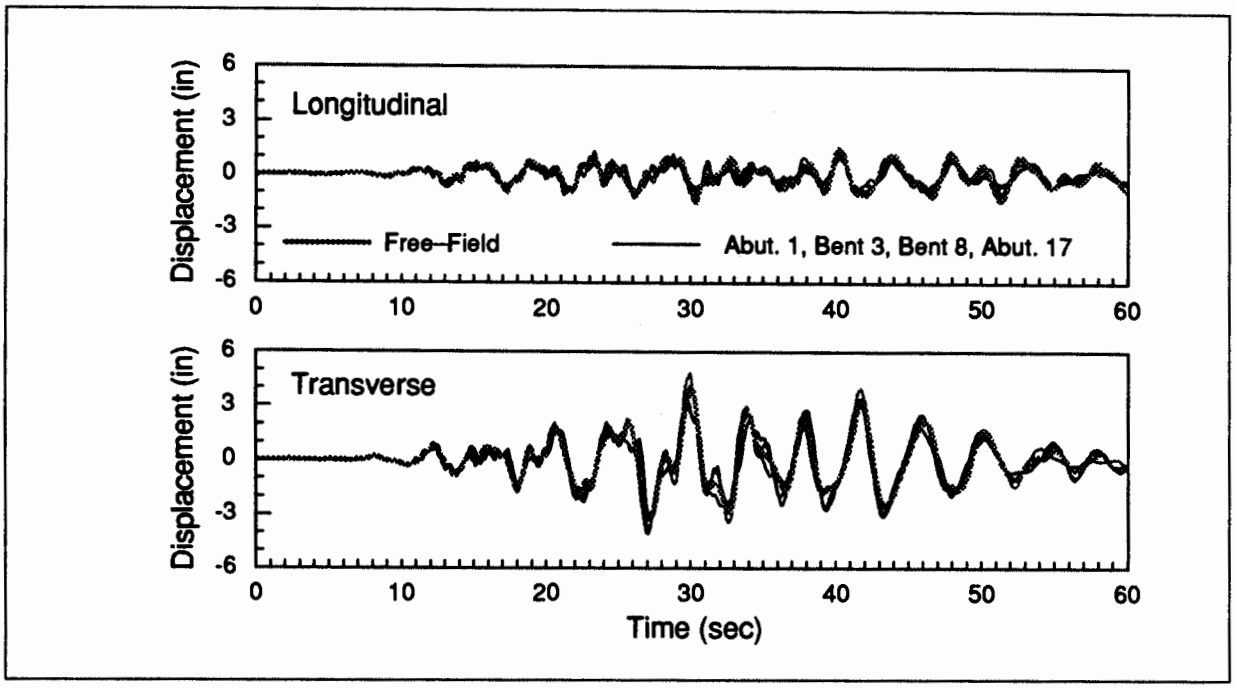

Figure 4.7 Horizontal Displacement at Four Supports and Free–Field in Global Longitudinal and Transverse Directions for the Landers Earthquake.

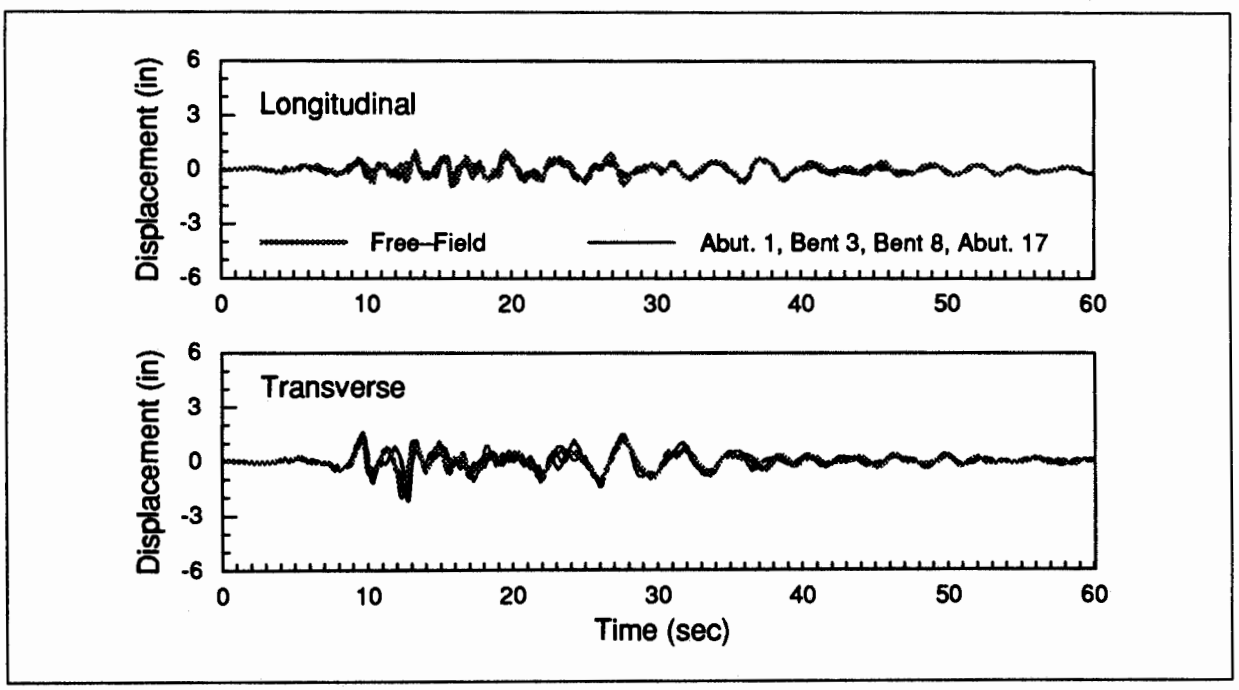

Figure 4.8 Horizontal Displacement at Four Supports and Free–Field in Global Longitudinal and Transverse Directions for the Big Bear Earthquake.

Table 4.2. Maximum Relative Horizontal Displacement Between Four Supports

Relative displacements (in inches) for Landers earthquake above the diagonal.

	Abut 1	Bent 3	Bent 8	Abut 17
Abut 1		0.57	2.18	3.04
Bent 3	0.88		2.15	2.53
Bent 8	1.69	1.11		1.67
Abut 17	2.58	2.18	1.26	

Relative displacements (in inches) for Big Bear earthquake below the diagonal.

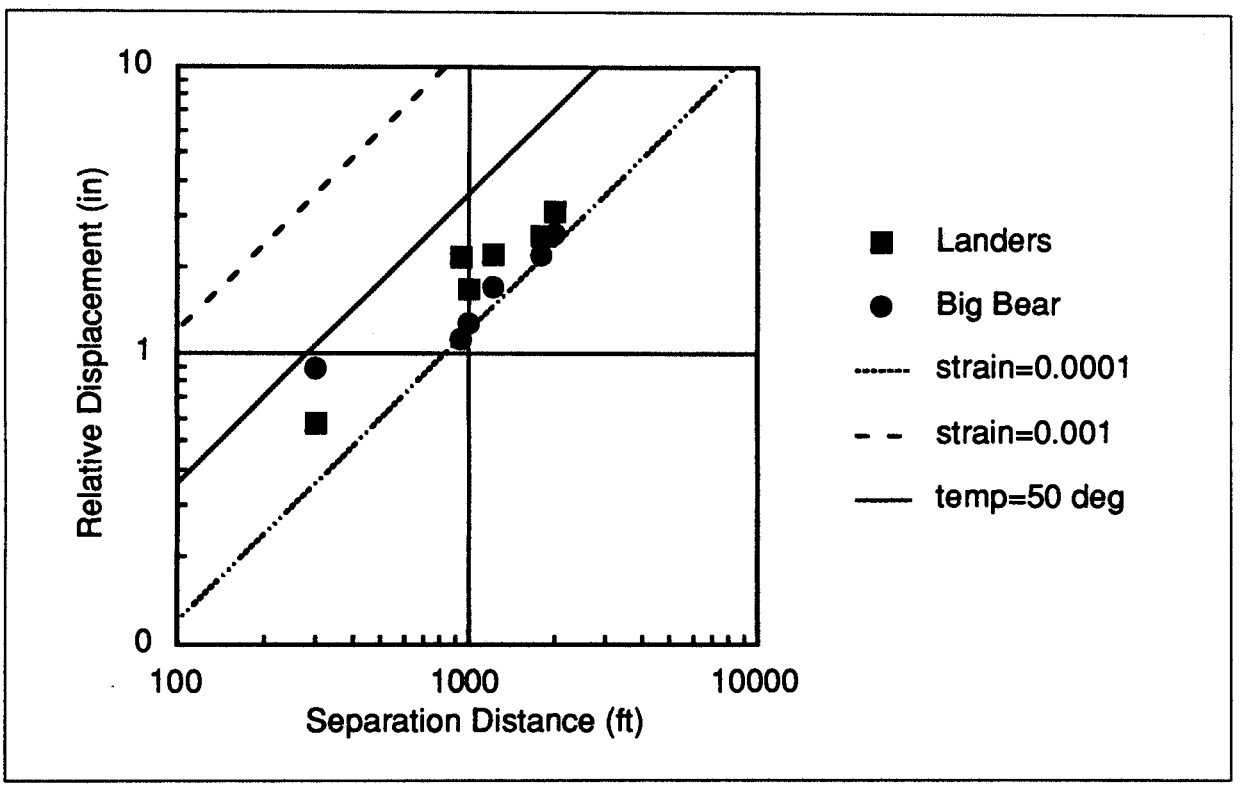

Figure 4.9 Maximum Relative Displacement Between Supports as a Function of Distance Between Supports.

4.5 Coherency of the Free–Field and Support Acceleration

The horizontal ground motion at the free–field location and the four supports of the structure are somewhat different, as shown in Figs. 4.7 and 4.8. The coherency of two ground motions is one way of characterizing the variation of ground motion. Although some of the difference in motion is due to soil–structure interaction effects, it is useful to compute the coherency between the Bent 8 support motion and the support motion at the other three supports.

The modulus of the coherency function is computed by the procedures described in Section 3.3 using periodogram estimates of the power spectral density functions for the free–field and support motions. Consistent with the use of the coherency in ground motion studies, the function is presented as $|\gamma(i\omega)|$ instead of $|\gamma(i\omega)|^2$, as defined in Eq. 3.9. A Bartlett window is used for the tapering instead of the Kaiser window, as recommended by previous studies of ground motion incoherence (Abrahamson, 1985; Hao, 1989).

Figures 4.10 and 4.11 plot the coherency functions between the gloabl transverse input motion at Bent 8 with the global transverse input motion at Abutment 1, Bent 3, and Abutment 17. The distance between Abut 1–Bent 8 is 1239 ft; Bent 3–Bent 8 is 969 ft; Abut 17–Bent 8 is 1017 ft.

For both earthquakes the input motion at Abutment 1 and Bent 3 is fairly coherent with the Bent 8 motion up to a frequency of 2 Hz, with the exception of several frequencies that are the vibration frequencies of the Connector. At these frequencies, soil–structure interaction are significant and produce low coherence. In contrast, the input motion at Abutment 17 is less coherent with the Bent 8 motion compared with the other support motions. One possible explanation for the difference is that the site conditions at Abutment 17, on the northwest side of the San Jacinto fault (and higher water table) are different than at the other supports with recorded input motion on the southeastern side of the fault.

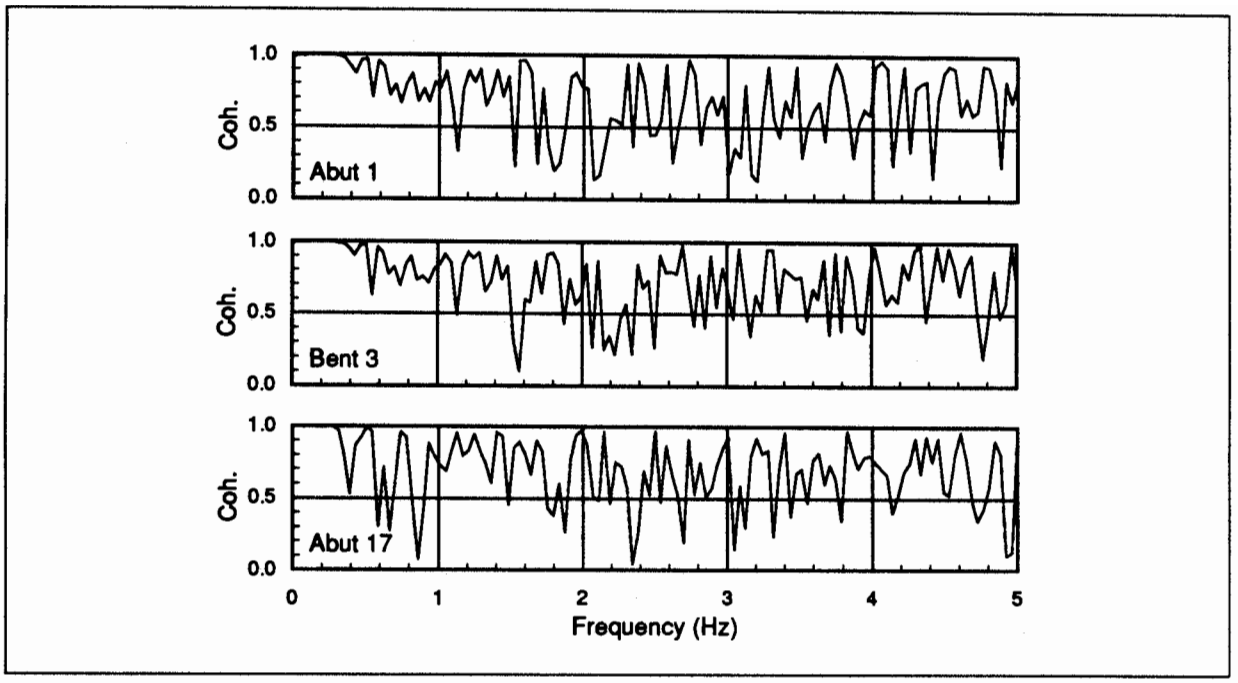

Figure 4.10 Coherency Function Between Bent 8 Global Transverse Support Motion and Global Transverse Motion at Three Supports for Landers Earthquake.

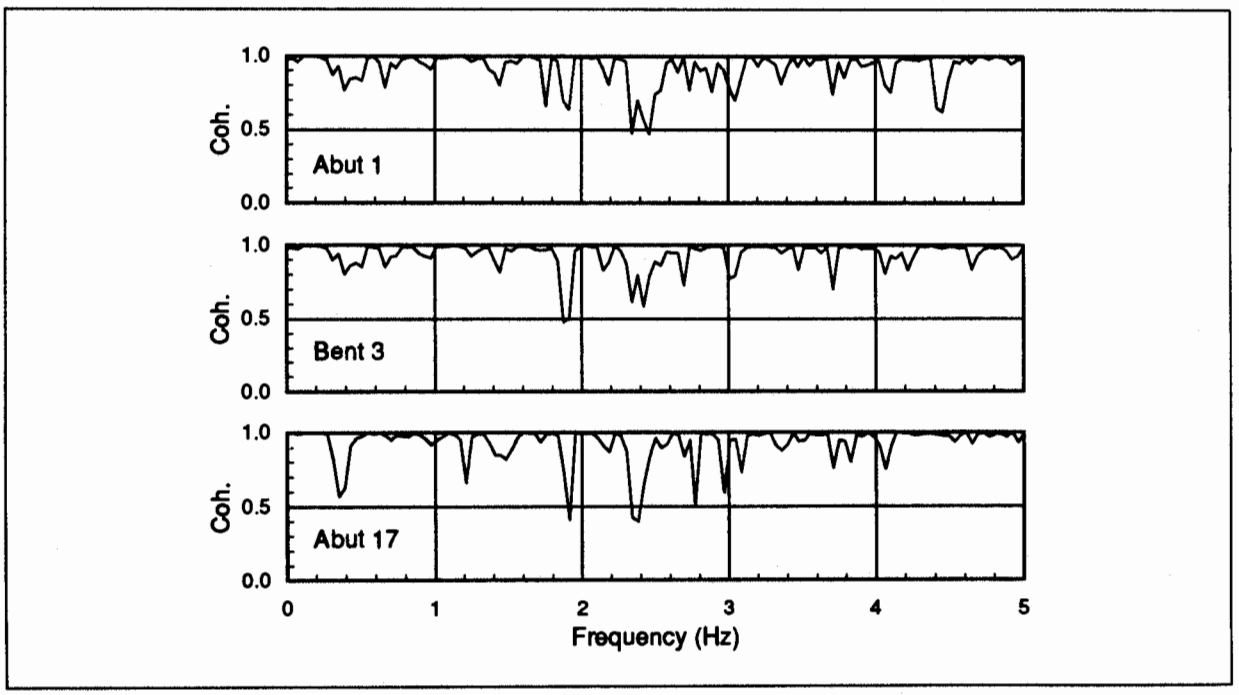

Figure 4.11 Coherency Function Between Bent 8 Global Transverse Support Motion and Global Transverse Motion at Three Supports for Big Bear Earthquake.

In general, the input motion for the Big Bear earthquake is more coherent compared with the Landers earthquake. This observation may be due to the fact that the Big Bear earthquake was smaller than the Landers earthquake and at a shorter epicentral distance. The Big Bear earthquake had a smaller extended source effect than Landers (which involved five fault segments), and the propagation effects were less at the shorter epicentral distance.

These coherency functions, although they include soil–structure interaction effects, are comparable with coherency functions computed from recorded motion at the SMART 1 array in Taiwan (Abrahamson, 1988). For several of the events recorded at the array, the coherency for separation distances of about 300 m (similar to the distances in Figs. 4.10 and 4.11) is greater than 0.95 for 1 Hz, and greater than 0.8 for 2 Hz.

Considering Fig. 4.9 for the pseudo–static effects of the input motion, and Figs. 4.10 and 4.11 for the coherency effects for frequencies less than 2 Hz, it may be concluded that the spatial variation of the input motion is not significant within the range of important vibration frequencies for the Connector.

Chapter 5

EVALUATION OF EARTHQUAKE RESPONSE

5.1 Introduction

The evaluation of the earthquake response of the Connector involves identification of the vibration characteristics by: (i) examination of the recorded acceleration and processed displacement records to ascertain overall characteristics of the earthquake response; (ii) nonparametric evaluation using spectral analysis to obtain the transmissibility functions for identifying the vibration periods and modes of the structure; and (iii) parametric evaluation to determine vibration periods and damping ratios.

5.2 Recorded Displacement Response

The processed records allow evaluation of the structural displacements relative to the supports and opening–closing displacements of the hinges. There are some limitations to computing relative displacements from acceleration records. The subtraction introduces error, in addition to the noise in the displacement records. However, the large signal–to–noise ratio for the digital records means that the difference in displacements is fairly accurate. Secondly, the baseline correction in the processing obscures any residual displacement.

5.2.1 Response of Bent 8 and Bent 3

Bent 8, near the center of the Connector, is instrumented to provide detailed response in the transverse and longitudinal directions. Figure 2.7 shows the instrumentation for Bent 8. The transverse deformation of the column at Bent 8 can be computed because the vertical channels on the pile cap give the base rotation. The displacement at the top of the column due to pile cap rotation and deformation of the column is computed from:

$$u_{col} = u_{20} - \left(\frac{8.0\text{ ft}}{41.0\text{ ft}}\right)\cdot(u_{13} - u_{12}) - u_{24}$$

$$u_{base} = \left(\frac{46.10\text{ ft}}{20.42\text{ ft}}\right)\cdot(u_{23} - u_5)$$

$$u_{def} = u_{col} - u_{base}$$

where u_{col} is the displacement at the top of the column relative to the pile cap, considering the rotation of the box girder; u_{base} is the displacement at the top due to rotation of the pile cap; u_{def} is the deformation of the column; and u_i is the processed displacement record for channel i. The 46.10 ft column length for Bent 8 is from the as–built drawings.

Figure 5.1 shows the displacements at the top of the Bent 8 column for the Landers and Big Bear earthquakes. The dotted line is the displacement at the top due to the pile cap rotation, u_{base}, and the solid line is the displacement at the top due to column deformation and pile cap rotation, u_{col}. The rotation of the pile cap is in–phase with the transverse displacement at the top of the column. The difference in the two histories is the deformation of the column, which is a maximum of 4.76 in. for Landers (drift=0.86%), and 2.98 in. for Big Bear (drift=0.54%). As described in the response evaluation of the Connector in Chapter 6, the deformation of the Bent 8 column in the Landers earthquake is large enough to begin yielding the longitudinal reinforcement.

The pile cap rotation produces displacements at the top of the column as a result of soil–structure interaction: 0.63 in. for Landers and 0.47 in. for Big Bear. Rotational flexibility due to soil–structure interaction affects the stiffness and hence vibration period of a single degree–of–freedom system in the following manner:

$$\frac{\tilde{T}}{T} = \sqrt{1 + \frac{kL^2}{k_\theta}} \tag{5.1}$$

where $\tilde{T}$ and T are the flexible base and fixed base vibration periods, respectively; k and k_θ are the fixed base stiffness of the structure and rotational stiffness of the foundation, respectively; and L is the height of the structure. Evaluating Eq. 5.1 using the maximum values for the transverse displacements of Bent 8, the effect of foundation flexibility on the period is:

$$\frac{\tilde{T}}{T} = \sqrt{1 + \frac{u_{base,\max}}{u_{def,\max}}}$$

For Landers, the stiffness ratio is 0.13 and the period ratio is 1.06. For Big Bear, the stiffness ratio is 0.16 and the period ratio is 1.08. It is difficult to estimate the stiffness of the structure to within about 15 percent, but these soil–structure interaction effects are at about the limit for which they should be considered.

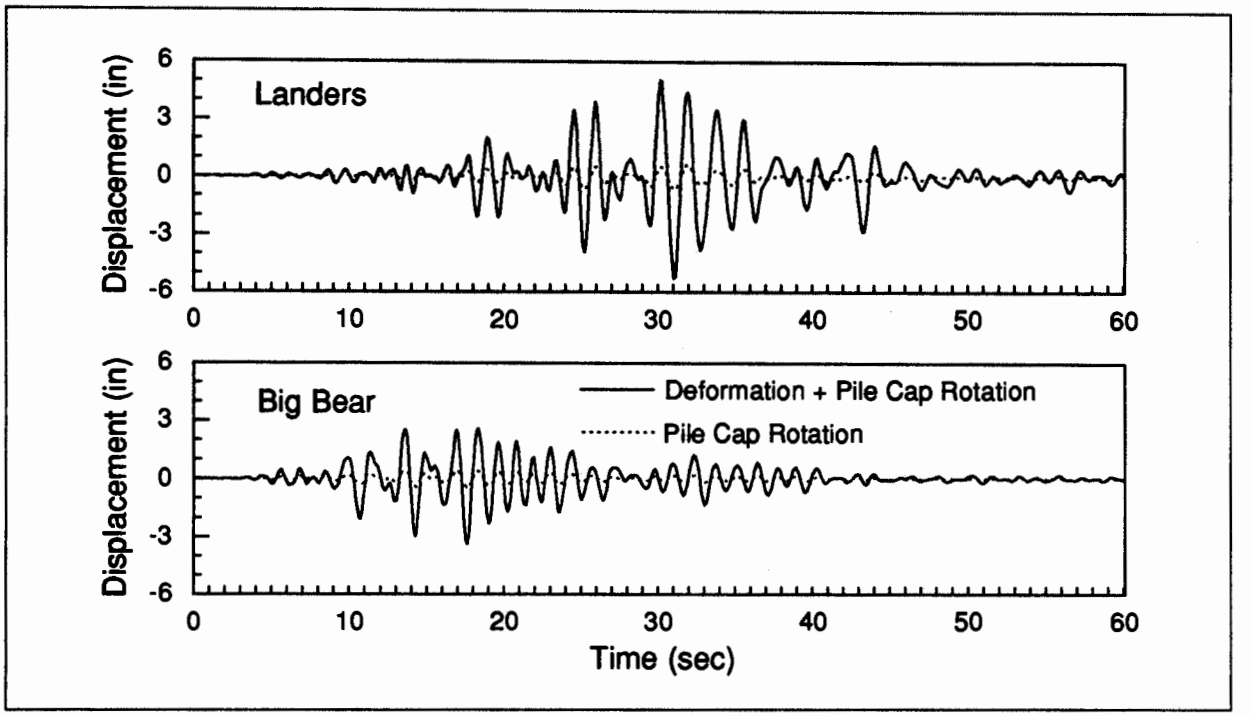

Figure 5.1 Transverse Displacement at Top of Bent 8 Column.

The trajectory of horizontal motion of the deck at Bent 8 and Bent 3 relative to the respective pile caps gives an overall picture of the response of the Connector at the two locations. The plots in Figs. 5.2 confirm that the response is predominantly in the transverse direction for the Landers earthquake. This results from the stronger input motion in the transverse direction, as described in Section 4.4, and the transverse components in the lower vibration modes. The trajectories in Fig. 5.3 for the Big Bear earthquake also show predominant transverse motion, but the displacement at the taller Bent 3 (column length is 51.40 ft) is greater than the displacement at Bent 8.

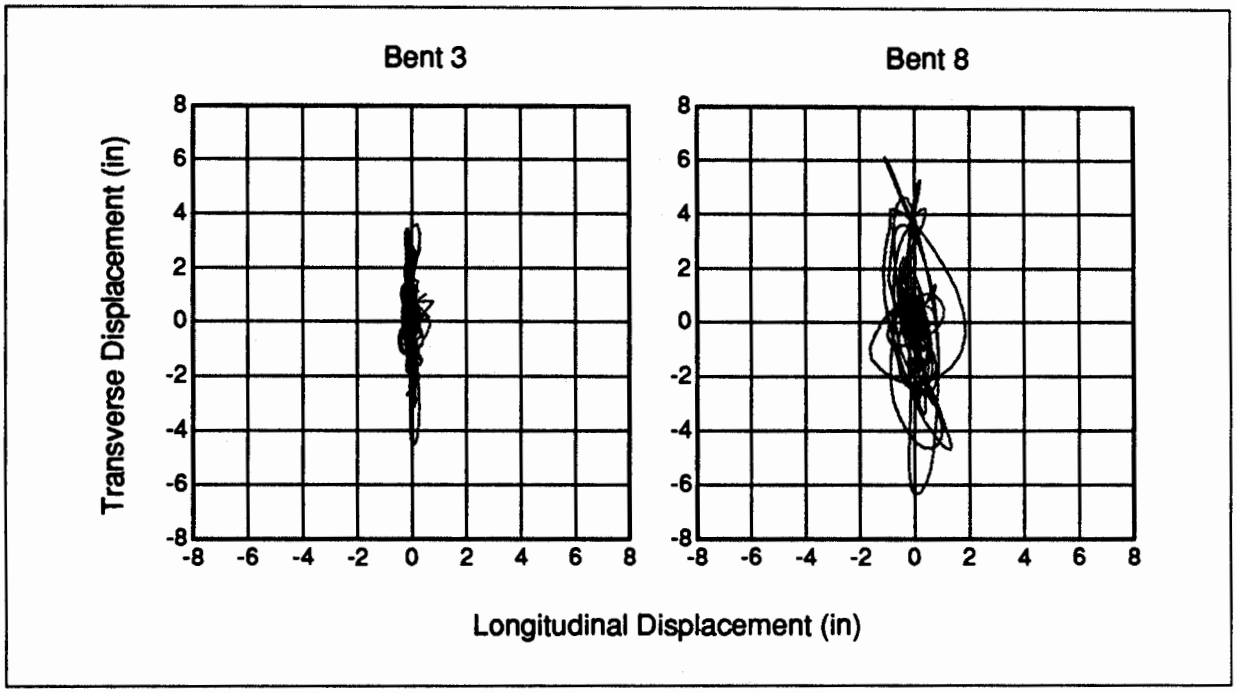

Figure 5.2 Trajectory of Horizontal Motion at the Deck Relative to Pile Cap in Landers Earthquake.

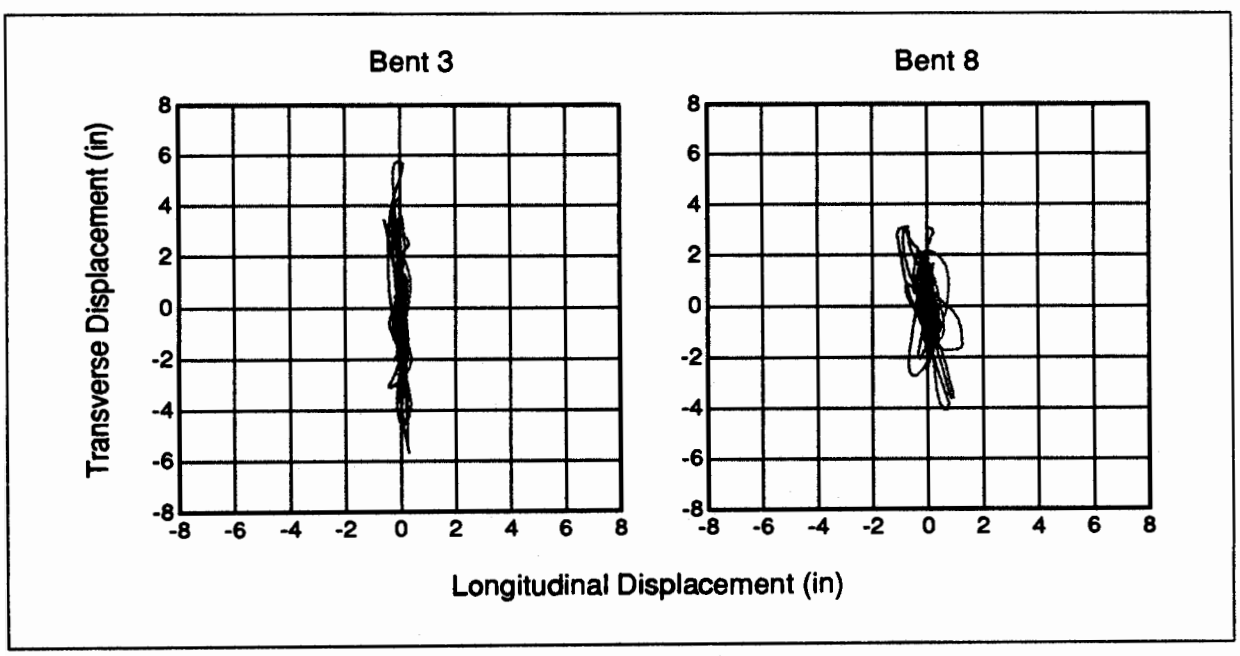

Figure 5.3 Trajectory of Horizontal Motion at the Deck Relative to Pile Cap in Big Bear Earthquake.

5.2.2 *Horizontal Hinge Response*

Intermediate hinges are provided in bridges for releasing strain due to temperature changes and post–tensioning during construction. The hinges allow relative longitudinal displacement, but transverse displacement is restricted by shear keys. The opening and closing of the hinges during an earthquake is a major concern because of the possibility of unseating. The instrumentation allows determination of relative hinge displacements on the inside edge of the superstructure. It is not possible to determine the displacements at the outside edge or rotations of the hinges about a vertical axis.

Figures 5.4 and 5.5 show the acceleration records in the longitudinal direction across Hinge 7 (near Bent 8) for the two earthquakes. The acceleration spikes result from impact of the adjacent frames, as the hinge pounds closed. More pounding is evident for Landers than for Big Bear. Some of the spikes at a channel are caused by pounding at Hinge 3 and axial wave propagation through the box girder. The acceleration records at Abutments 1 and 17 also have some acceleration spikes, which are caused by wave propagation from pounding at adjacent hinges (Hinge 3 and Hinge 13, respectively). A recent study of hinge pounding in the Landers earthquake using wave propagation analysis is described by Malhotra et al. (1994).

The longitudinal opening–closing displacements at Hinge 7 and Hinge 11 (inside edge of the deck) are shown in Figs. 5.6 and 5.7 for the two earthquakes. The maximum hinge displacements are given in Table 5.1. Hinge 7 has the largest opening: 1.41 in. for Landers and 1.70 in. for Big Bear. The closing of the hinge (negative displacement) is harder to discern. From Fig. 5.6, Hinge 7 closes at most about 1/2–inch during the first 25 sec of the Landers earthquake. Later the maximum closing displacement is about one inch, indicating that polystyrene filler material (nominally 2 in. thick) in the hinge crushed during the strong motion response. The opening at Hinge 11 is less than the opening of Hinge 7, and the maximum closing displacement is 0.86 in. Several of the closing excursions show the high frequency oscillation associated with pounding.

Comparing Fig. 5.7 with Fig. 5.6, Hinge 7 opens more in the Big Bear earthquake than in Landers. The maximum closing displacement is nearly 1.5 in., possibly indicating accumulated crushing of filler in the hinge in the second earthquake. The response of Hinge 11 is similar for the two earthquakes.

As described in Section 2.2 the barrier on the inside edge of the deck near Hinge 3 spalled and exposed reinforcing bars. The seat of Hinge 3 had three hairline cracks radiating from the reentrant corner. Channel 10 near Hinge 3 had four major peaks of acceleration near 0.45 g in the Landers earthquake, which is characteristic of the type of pounding that can damage the hinges.

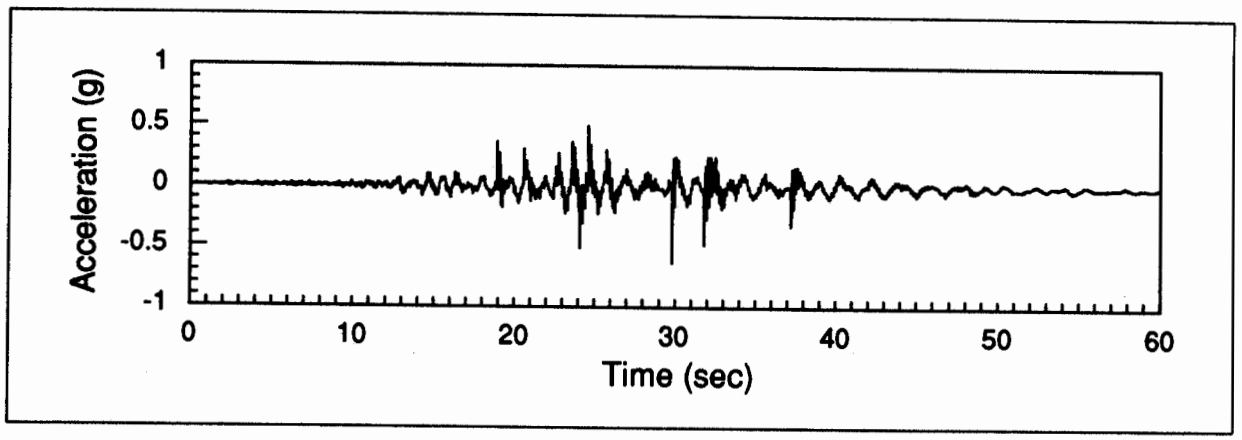

Figure 5.4 Longitudinal Acceleration of Deck at Hinge 7 in Landers Earthquake (Channel 17).

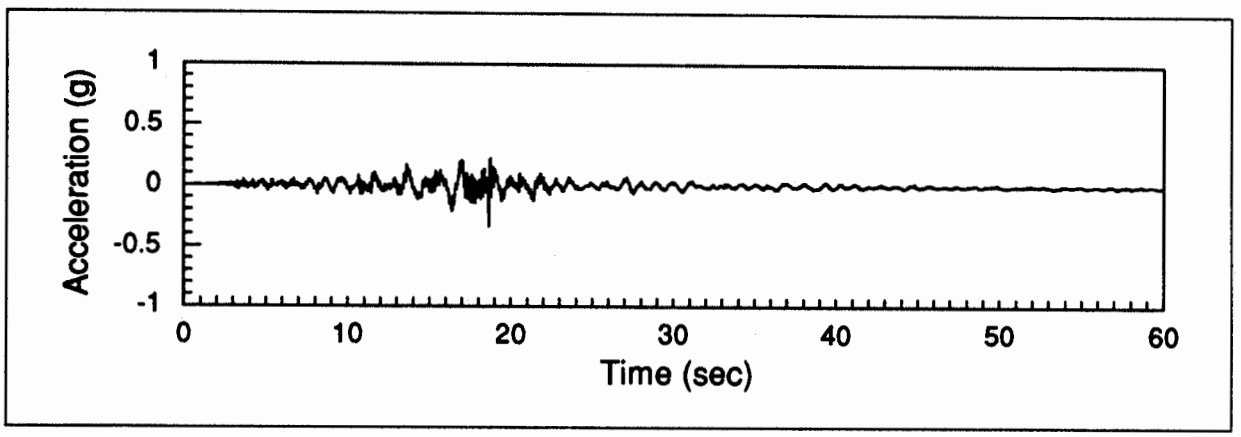

Figure 5.5 Longitudinal Acceleration of Deck at Hinge 7 in Big Bear Earthquake (Channel 17).

Each hinge has a shear key to restrict relative transverse motion of adjacent frames. The shear keys have a nominal 1/4–inch gap, with polystyrene filler, which presumably allows that much relative transverse displacement at the hinges. The instrumentation provides the relative transverse motion at all five hinges in the Connector. The relative transverse displacements for Hinge 3 and Hinge 7 are shown in Figs. 5.8 and 5.9 for the two earthquakes.

The transverse displacement for Hinge 3 is typical of the displacements for Hinges 9, 11, and 13. The relative motion shows high frequency vibration during the first eight seconds, with a maximum displacement of about 1/4–inch. Subsequently, the frequency reduces to about 1 Hz with larger displacements. The maximum transverse displacement at Hinge 3 is 0.35 in. for Landers and 0.41 in. for Big Bear.

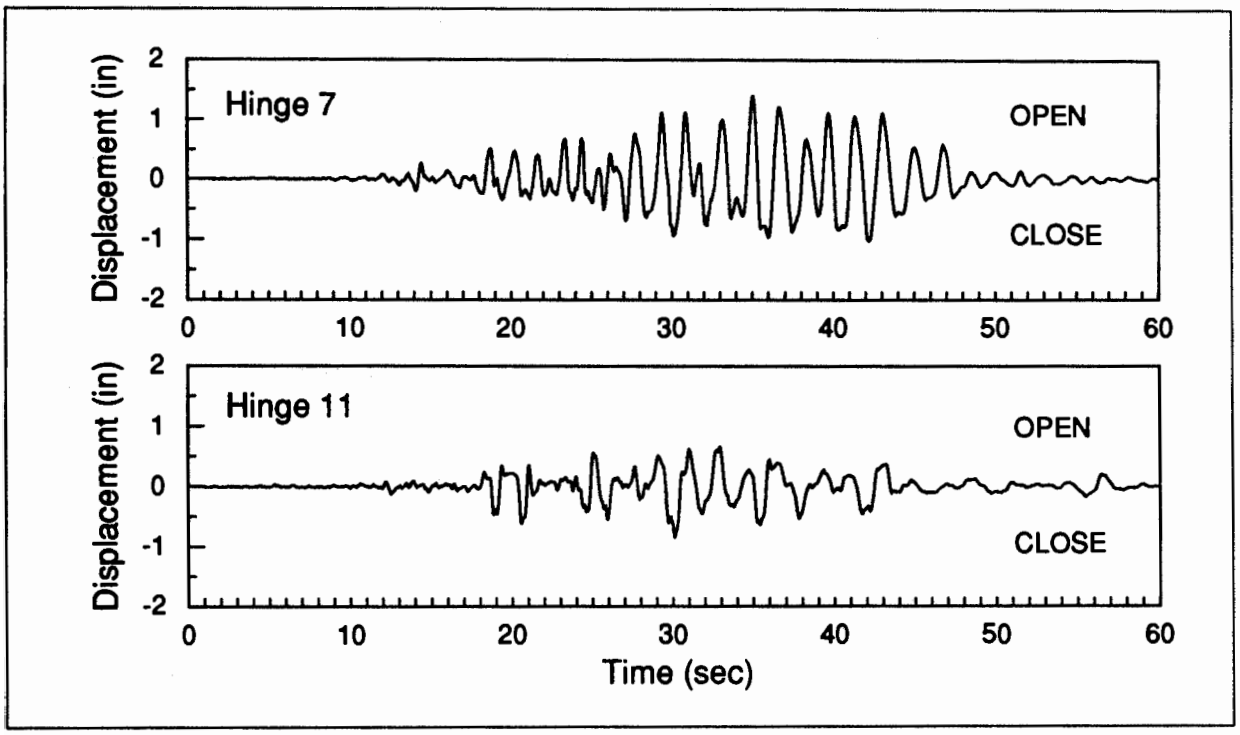

Figure 5.6 Relative Longitudinal Displacement of Hinges in Landers Earthquake.

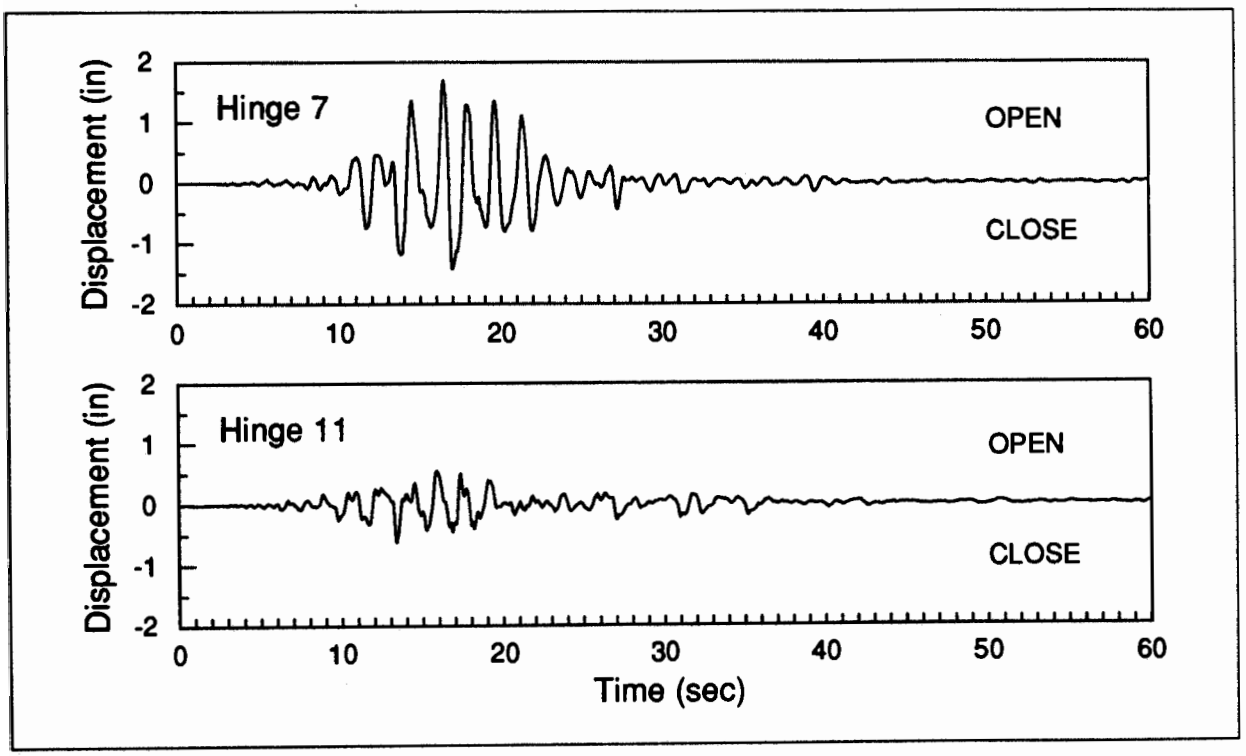

Figure 5.7 Relative Longitudinal Displacement of Hinges in Big Bear Earthquake.

Table 5.1. Maximum Longitudinal Opening and Closing Displacements of Hinges (Inside Edge of Box Girder)

		Maximum Displacement (in.)	
Earthquake	Hinge Number	Opening	Closing
Landers	H7	1.41	1.03
Landers	H11	0.67	0.86
Big Bear	H7	1.70	1.44
Big Bear	H11	0.56	0.63

As shown by Figs. 5.8 and 5.9, the relative transverse displacement of Hinge 7 is substantially different than Hinge 3. There is little displacement for the first 18 sec in Landers and the first 10 sec in Big Bear. However, larger displacements then occur at a frequency of approximately 0.5 Hz. The maximum relative displacement is 0.47 in. for Landers and 0.61 in. for Big Bear.

Although the condition of the shear keys before the earthquakes, twenty years after construction, and the condition after the earthquakes is not known, some conjecture can be made based on the recorded response. During the early parts of the Landers earthquake, when the motion is small, the keys limit the transverse displacement to the nominal gap in some hinges (such as Hinge 3); and friction and perhaps excess filler or debris nearly eliminate all transverse displacement in the other hinges (such as Hinge 7). As the motion increases, local crushing of concrete at the key allows larger transverse displacements. When the Big Bear earthquake occurs, the shear keys have been "loosened-up" by the earlier Landers earthquake, exhibiting more relative transverse displacement. The shear keys are effective in limiting the relative displacement to a maximum of 0.61 in. compared with a transverse displacement of nearby Bent 8 of over 5 in. The maximum relative transverse displacements, however, are greater than the nominal 1/4-inch gap, indicating the shear keys likely suffered minor local damage.

5.2.3 *Vertical Hinge Response*

One concern about the seismic performance of hinges is the possibility that torsion of the box girder may cause vertical lift-off and pounding on the elastomeric bearing pads (Williams and Godden, 1976). Figures 5.10 and 5.11 show the vertical displacement at the inside and outside edges of Hinge 7. The relative vertical displacement at the outside edge is less than 0.20 in. opening and 0.27 in. closing for both earthquakes, and it is most likely caused by deformation of the pads.

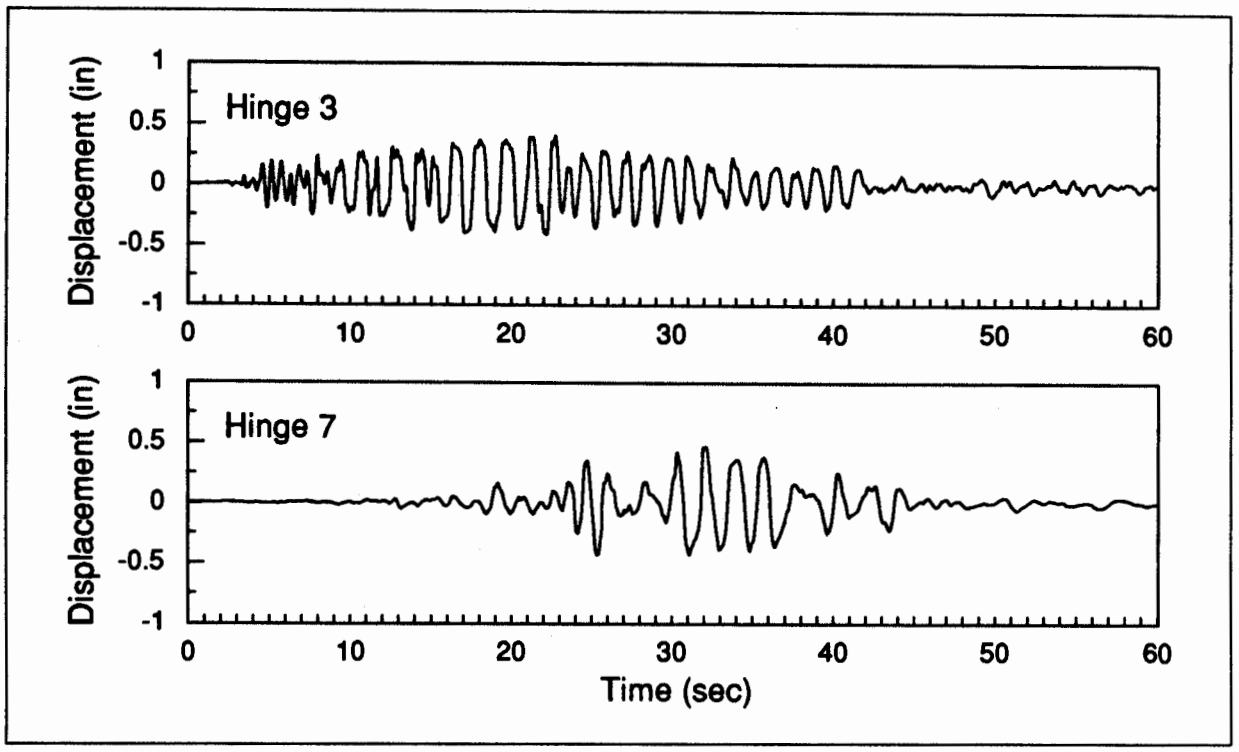

Figure 5.8 Relative Transverse Displacement of Two Hinges in Landers Earthquake.

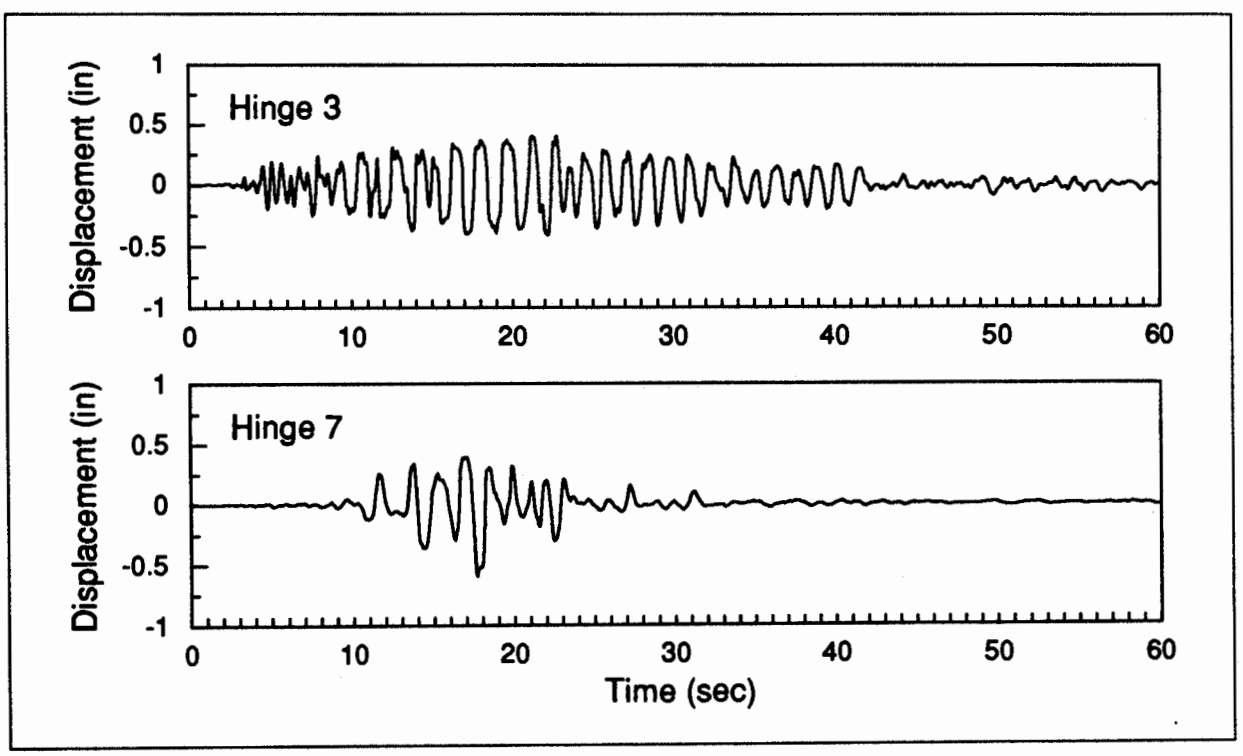

Figure 5.9 Relative Transverse Displacement of Two Hinges in Big Bear Earthquake.

In contrast, the relative vertical displacements at the inside edge are larger. The maximum relative opening is 0.34 in. and 0.39 in. for Landers and Big Bear, respectively. The maximum relative closing is 0.55 in. and 0.36 in. for Landers and Big Bear, respectively. It seems likely that slight lift–off and pounding occurred on the inside edge of the Hinge 7, with rotation about the outside edge. Caltrans personnel noted possible settlement at the hinges after the earthquakes. The damage to the elastomeric bearing pads may have been caused by the response on the inside edge of the bridge indicated in Figs. 5.10 and 5.11.

In the Northridge earthquake the unprocessed acceleration records for the Connector show that the vertical motion at Hinge 7 may have been different (CSMIP, 1994). The records for channels 15 and 16 on the outside edge of the box girder have acceleration spikes, indicating vertical lift–off and impact on the outside edge. There is out–of–phase motion between the two vertical channels on the inside edge also, as in the Landers and Big Bear earthquakes.

5.3 Spectral Analysis

The spectral analysis techniques described in Section 3.3 are used to estimate the vibration characteristics of the Connector. Although numerical results are obtained, inherent difficulties with this type of nonparametric evaluation mean that the results can only be considered qualitative.

5.3.1 Transmissibility Functions

The transmissibility functions are computed from an input acceleration in one direction relative to the output acceleration at various locations in the superstructure. As shown in Section 4.4, the predominant input motion is in the transverse direction. Two transverse input motions are used to compute transmissibility functions: the support acceleration for Bent 8 (Channel 24), and the free–field ground acceleration (Channel 3). The free–field ground motion is modified to account for the time lag with respect to the structure records. Based on the information in Sections 5.3 and 5.4, the input motions are assumed to be uniform for the frequency range of interest (0 to 2 Hz).

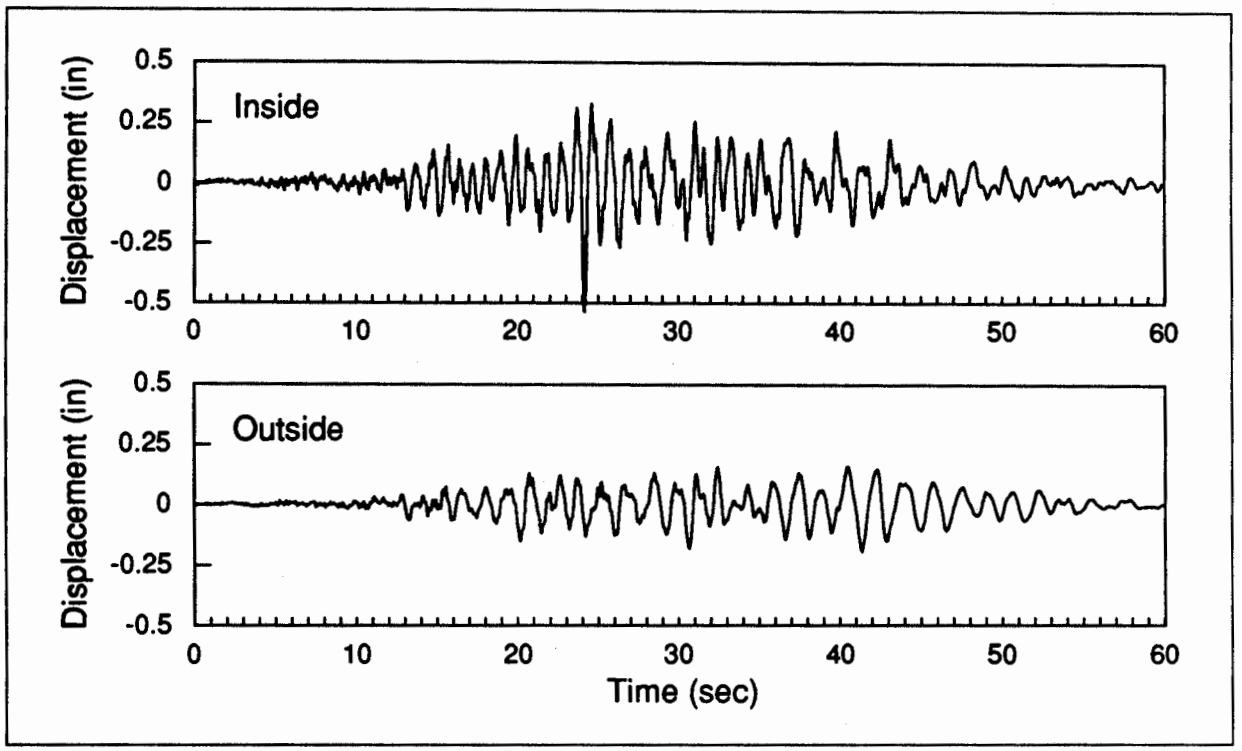

Figure 5.10 Relative Vertical Displacement for Hinge 7 in Landers Earthquake.

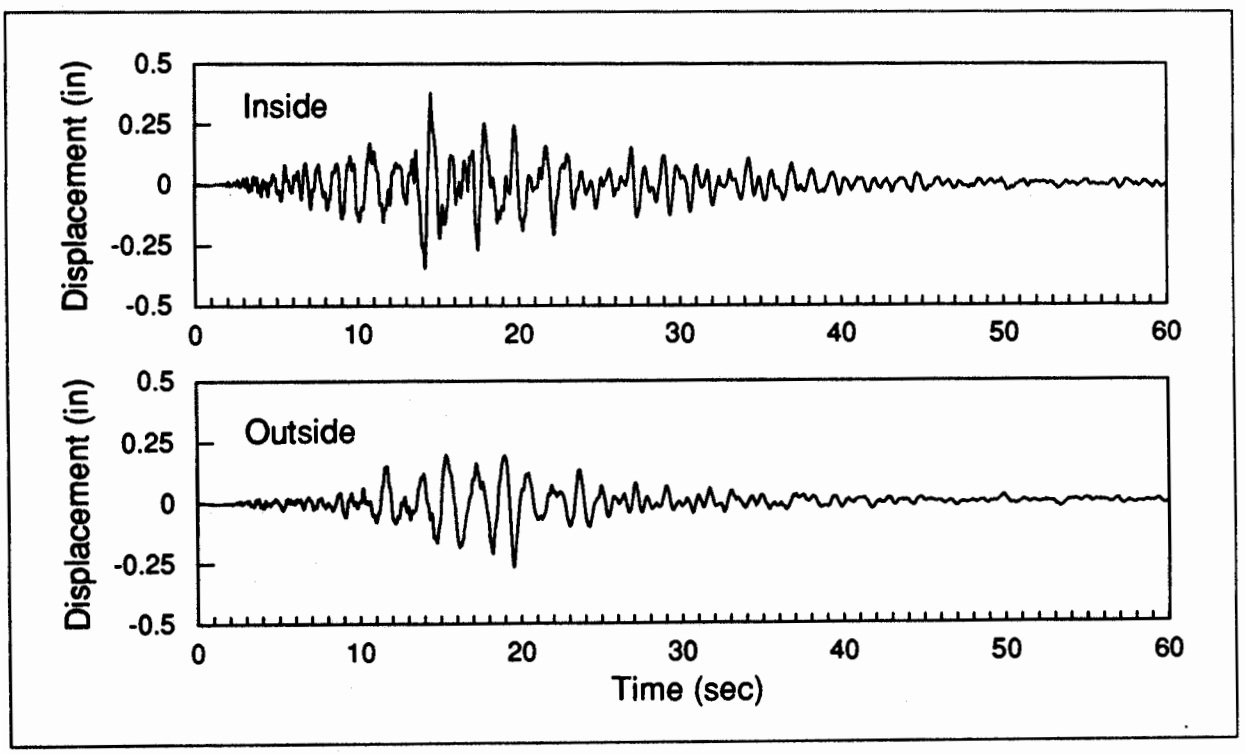

Figure 5.11 Relative Vertical Displacement for Hinge 7 in Big Bear Earthquake.

The output motions are the recorded accelerations at various channels on the superstructure in the transverse and longitudinal directions. For each input–output pair, three quantities are plotted as a function of frequency:

- Absolute value of the transmissibility function.
- The phase angle, in degrees, of the transmissibility function.
- The coherence function for the transmissibility estimate.

Table 5.2 lists the cases for which the transmissibility functions are computed.

Table 5.2. Transmissibility Functions from Spectral Analysis

Input Motion	Output Motion of Superstructure	Earthquake	Figure Showing Functions
Bent 8, Transverse (Channel 24)	Transverse	Landers	Fig. 5.12
Bent 8, Transverse (Channel 24)	Longitudinal	Landers	Fig. 5.13
Bent 8, Transverse (Channel 24)	Transverse	Big Bear	Fig. 5.14
Bent 8, Transverse (Channel 24)	Longitudinal	Big Bear	Fig. 5.15
Free–Field (Channel 3)	Transverse	Landers	Fig. 5.16

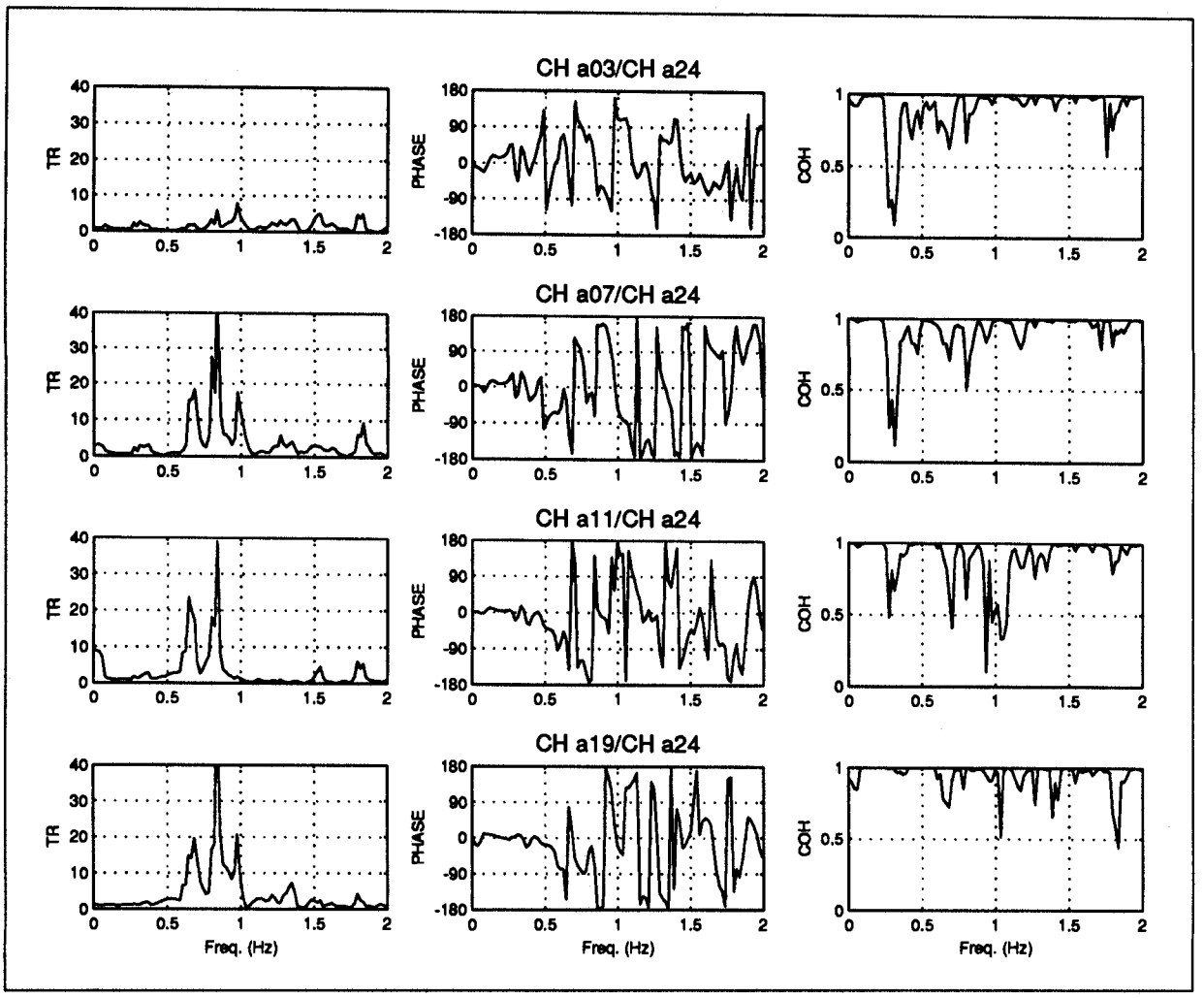

Figure 5.12 Transmissibility Functions Between Bent 8 Support Acceleration in Transverse Direction (Channel 24) and Transverse Accelerations in Superstructure for Landers Earthquake.

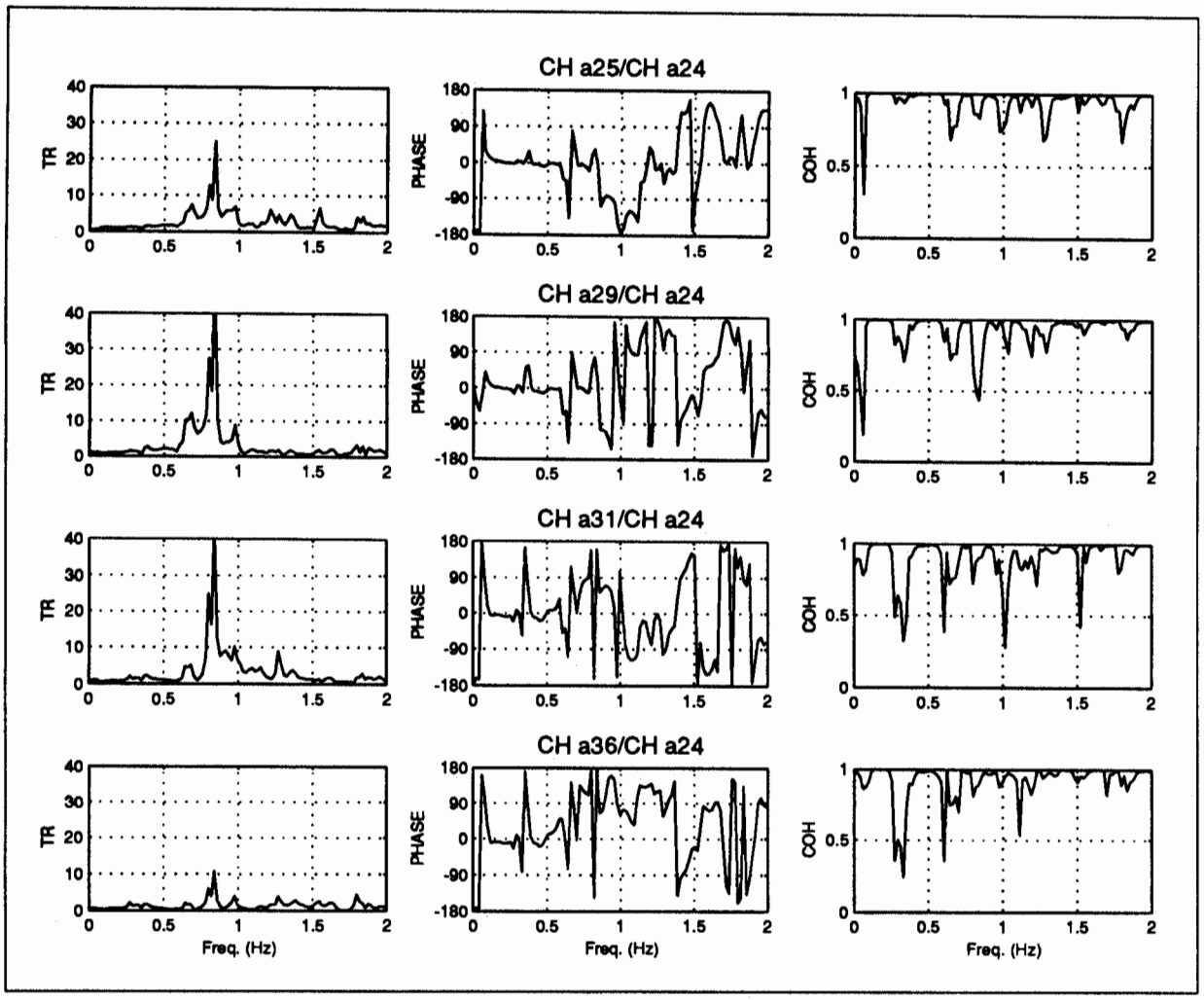

Figure 5.12 Transmissibility Functions Between Bent 8 Support Acceleration in Transverse Direction (Channel 24) and Transverse Accelerations in Superstructure for Landers Earthquake (continued from previous page).

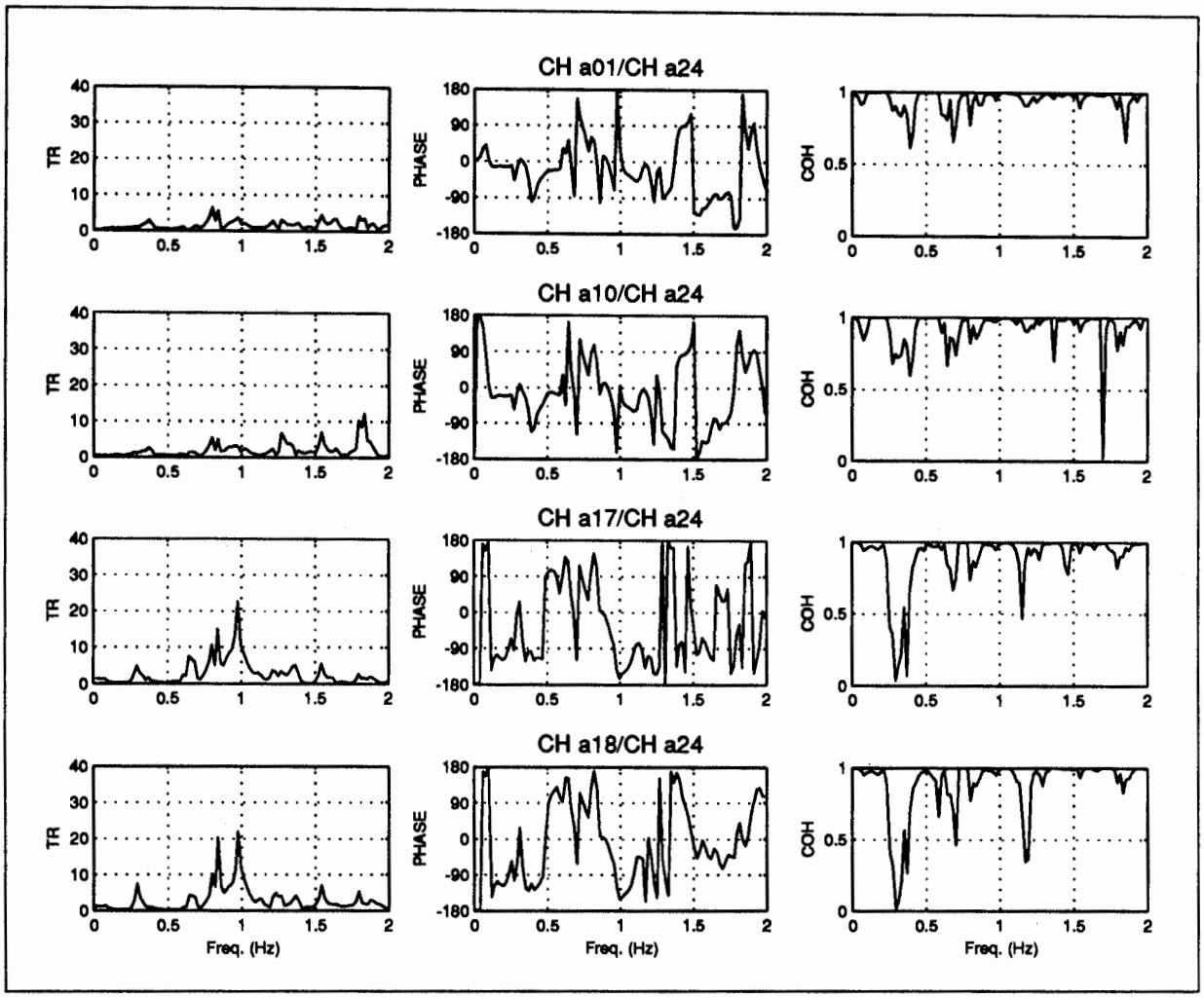

Figure 5.13 Transmissibility Functions Between Bent 8 Support Acceleration in Transverse Direction (Channel 24) and Longitudinal Accelerations in Superstructure for Landers Earthquake.

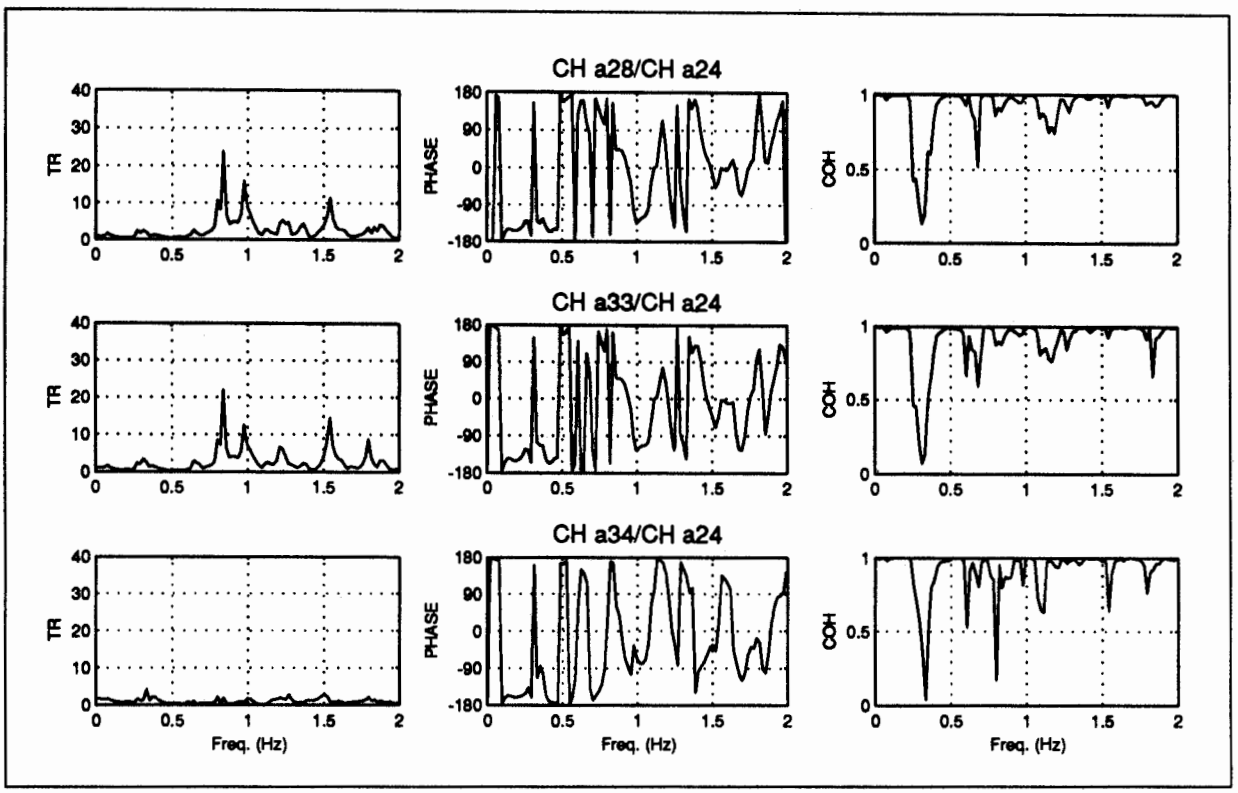

Figure 5.13 Transmissibility Functions Between Bent 8 Support Acceleration in Transverse Direction (Channel 24) and Longitudinal Accelerations in Superstructure for Landers Earthquake (continued from previous page).

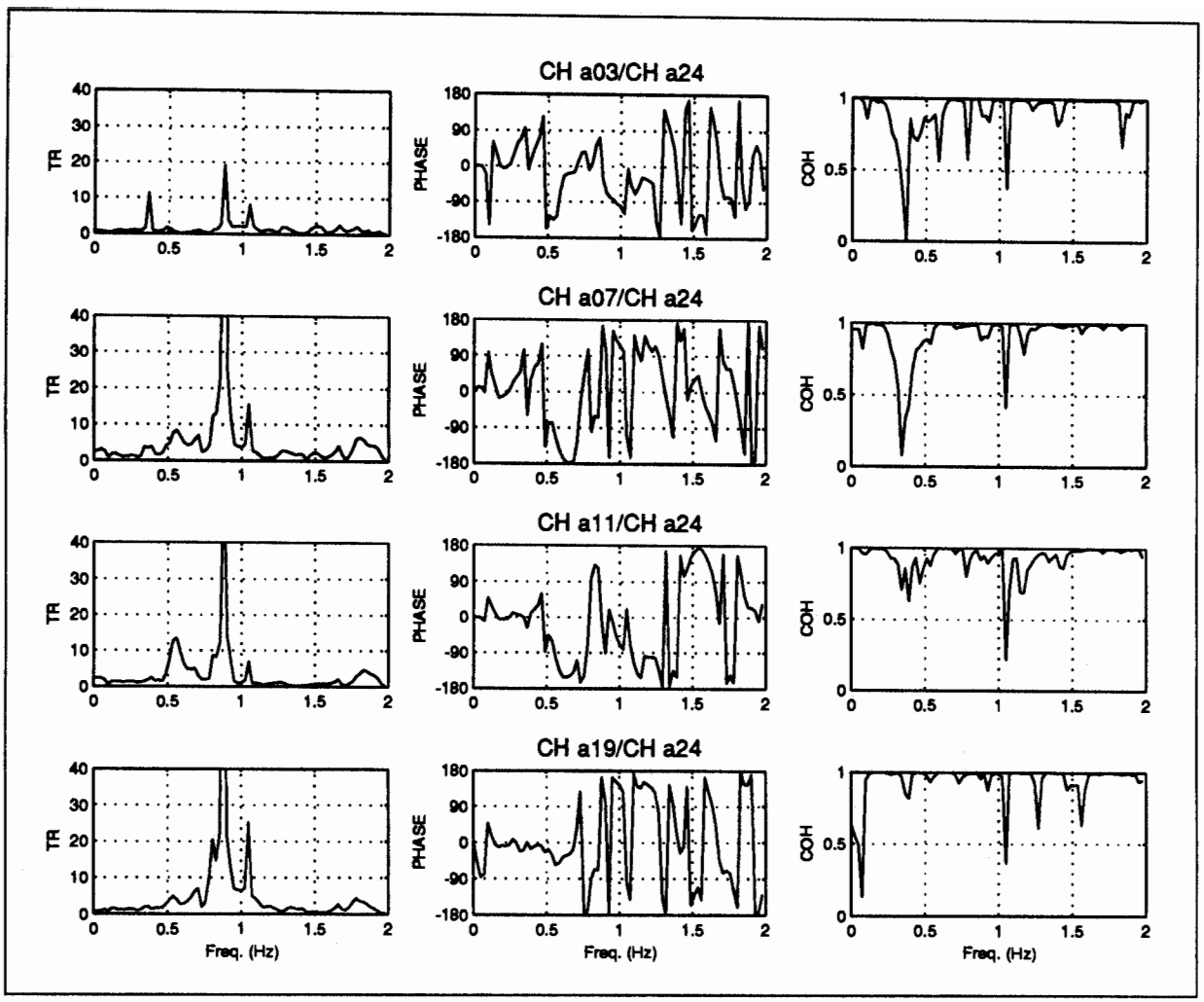

Figure 5.14 Transmissibility Functions Between Bent 8 Support Acceleration in Transverse Direction (Channel 24) and Transverse Accelerations in Superstructure for Big Bear Earthquake.

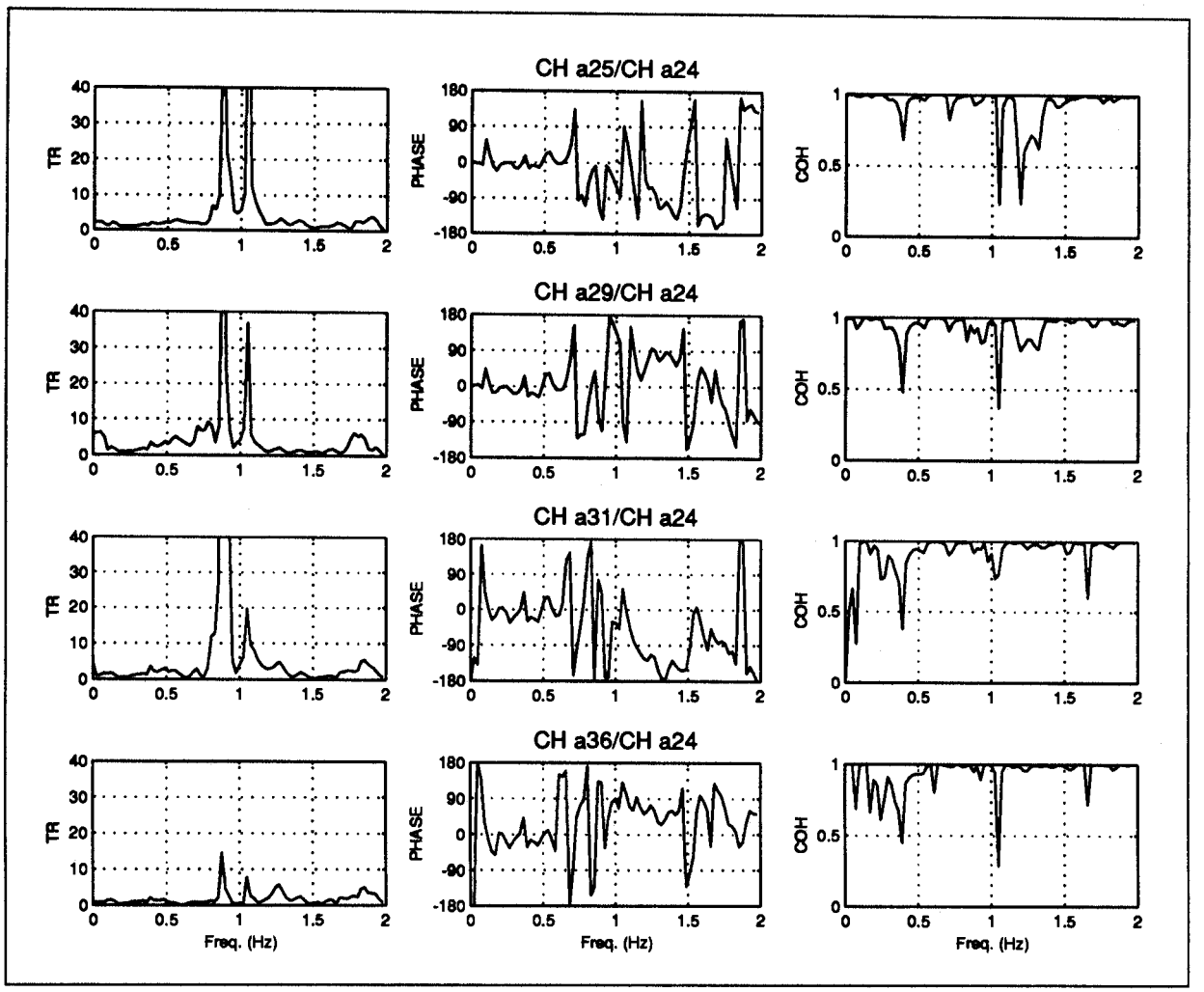

Figure 5.14 Transmissibility Functions Between Bent 8 Support Acceleration in Transverse Direction (Channel 24) and Transverse Accelerations in Superstructure for Big Bear Earthquake (continued from previous page).

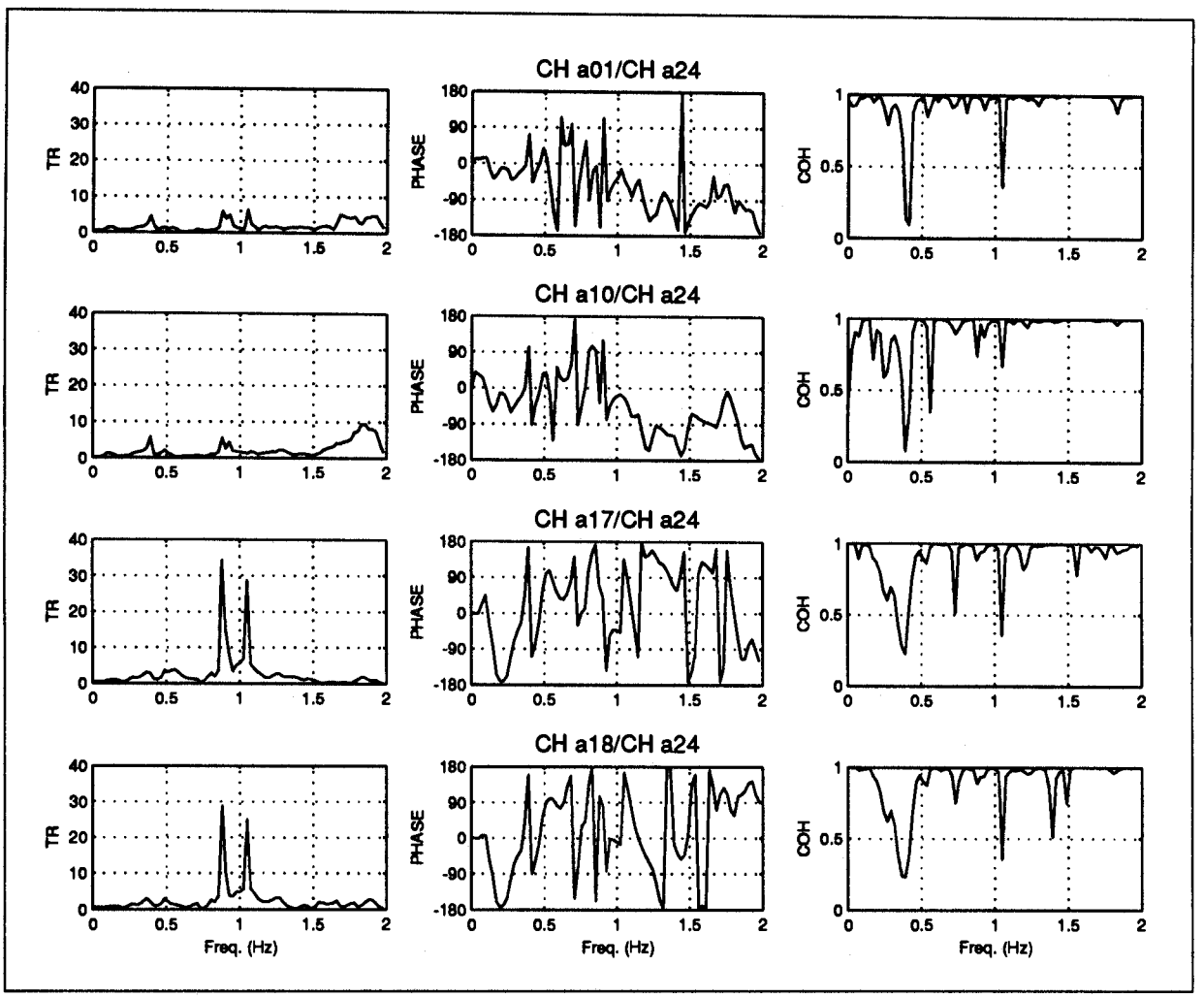

Figure 5.15 Transmissibility Functions Between Bent 8 Support Acceleration in Transverse Direction (Channel 24) and Longitudinal Accelerations in Superstructure for Big Bear Earthquake.

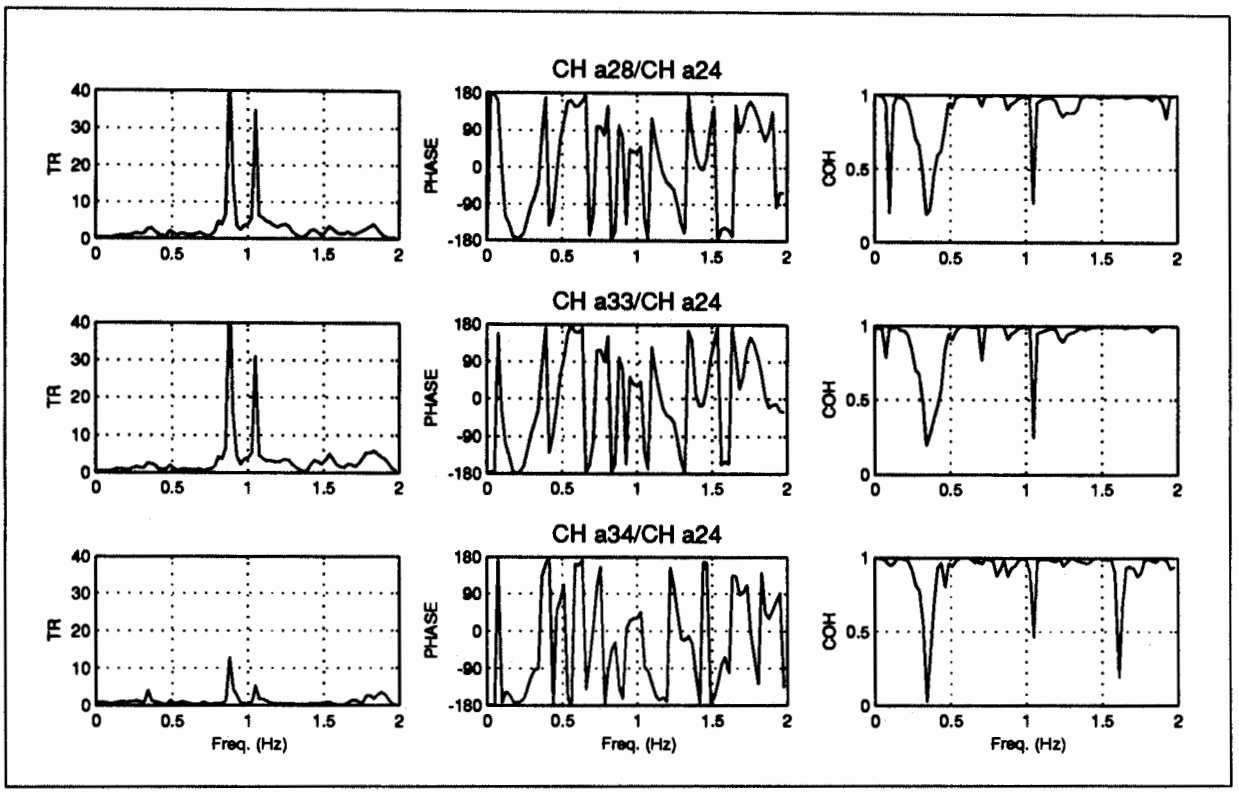

Figure 5.15 Transmissibility Functions Between Bent 8 Support Acceleration in Transverse Direction (Channel 24) and Longitudinal Accelerations in Superstructure for Big Bear Earthquake (continued from previous page).

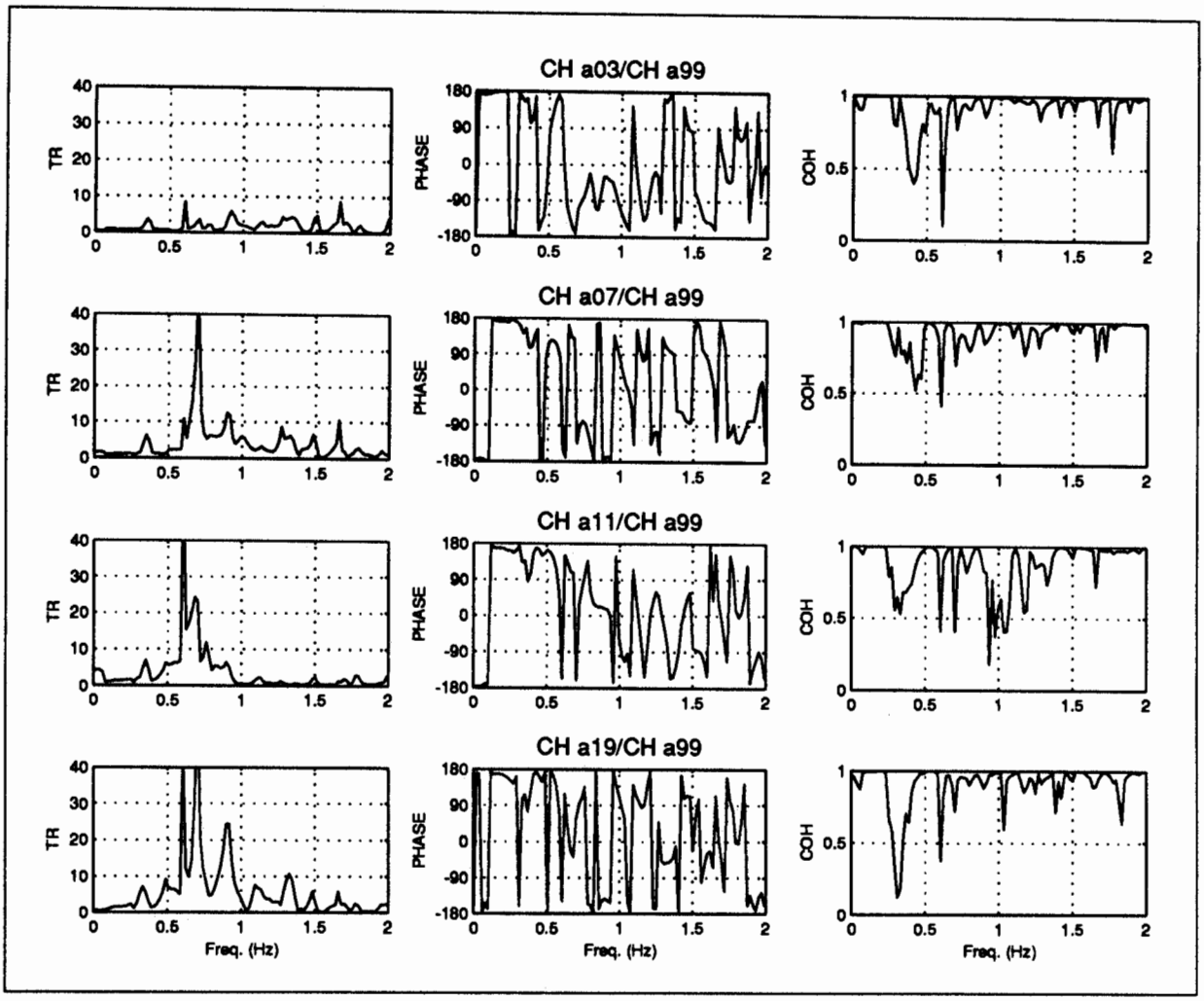

Figure 5.16 Transmissibility Functions Between Free-Field Acceleration (Channel 3) and Transverse Accelerations in Superstructure for Landers Earthquake.

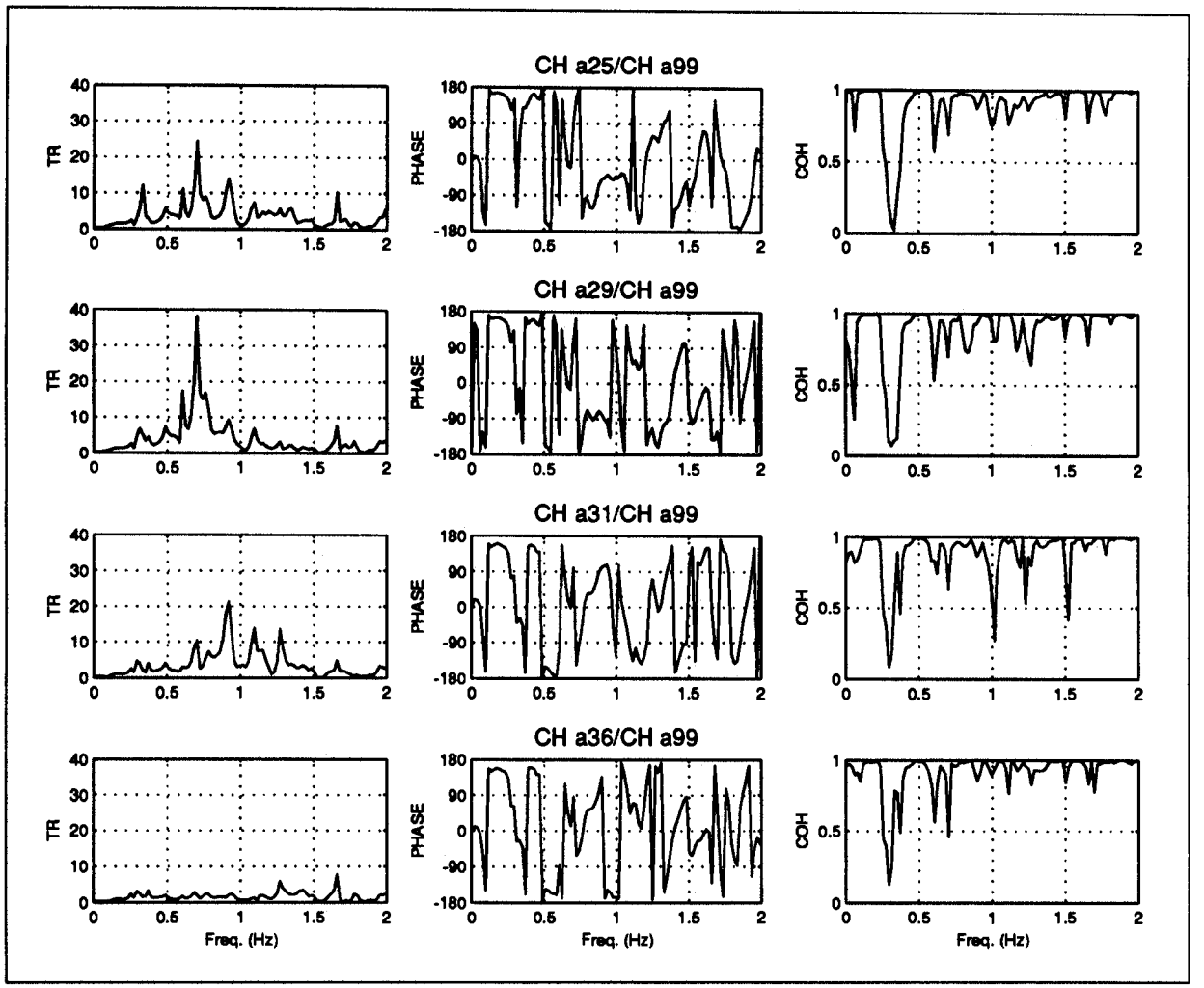

Figure 5.16 Transmissibility Functions Between Free-Field Acceleration (Channel 3) and Transverse Accelerations in Superstructure for Landers Earthquake (continued from previous page).

5.3.2 *Vibration Properties*

The transmissibility functions obtained from spectral analysis identify the frequencies of excitation with high amplification. These are the resonant frequencies of the structure, each of which corresponds to a vibration mode. Since the differences between phase angles for the channels at a resonant frequency are not exactly 0^o or 180^o (indicating non–proportional damping in the structure), the characterization of the vibration modes is qualitative.

From Figs. 5.12 and 5.13 for the Landers earthquake, the fundamental vibration mode has a frequency of 0.664 Hz, or a period 1.51 sec. Comparing the relative magnitudes and phase angle of the peaks at the fundamental frequency, the vibration mode is predominantly transverse and symmetric. The amplitude of the mode is largest for Channels 7, 11 and 19, between Bents 3 and 8. The channels at the abutments have very little response at the fundamental frequency.

The second mode in Landers has a frequency of 0.840 Hz (period of 1.19 sec) and has a substantially larger amplification than the fundamental mode. The predominant response is also transverse and it appears to be the first antisymmetric mode. There is fairly large longitudinal motion at Channels 29 and 33, about one–half the transverse motion at Bent 11.

The third vibration mode has a frequency of 0.977 Hz (period of 1.02 sec). From the phase angles, it is antisymmetric also, although there is substantial longitudinal motion. The third mode also has relatively large peaks at the transverse abutment channels.

Yet higher modes are associated with peaks at 1.270 Hz (0.787 sec), 1.543 Hz (0.648 sec), and 1.836 Hz (0.545 sec).

Figs 5.14 and 5.15 show the transmissibility functions for the Connector in the Big Bear earthquake. Although several channels have a peak at the low frequency of 0.366 Hz, the coherence is small, so this peak can be rejected. The fundamental mode of the structure in the Big Bear earthquake has a frequency of 0.562 Hz (period of 1.78 sec), with most of the motion transverse at Channel 11 near the tall Bent 3. The peaks have a wider bandwidth compared with the corresponding peaks for the Landers earthquake, indicating a larger amount of damping.

The second mode in the Big Bear earthquake has a small peak at 0.806 Hz (1.24 sec), which is closely spaced to the third mode at 0.879 Hz (1.14 sec). The third mode has larger amplification than the second mode. The fourth mode has a frequency of 1.05 Hz (0.952 sec). The third and fourth modes in Big Bear

correspond with the second and third modes in Landers, shifted to a slightly higher frequency because of the extra mode. For the Big Bear earthquake, the peaks at higher frequency are broader and less distinct than for the Landers earthquake.

Finally, Fig. 5.16 shows the transmissibility functions for the Connector in the Landers earthquake using the free–field ground motion (Channel 3) as the input. The characteristics of the peaks in Fig. 5.16 (using free–field motion) are similar to that of Fig. 5.12 (using Bent 8 support motion). There are small shifts in frequencies, but these are mostly associated with the support flexibility due to soil–structure interaction.

5.4 Parametric Evaluation

The parametric evaluation techniques summarized in Section 3.4 are used to identify the vibration frequencies. A single input–single output model is used with the Bent 8 transverse support acceleration (Channel 24) and various transverse acceleration records from the superstructure. Model verification to determine the best fit gave polynomials of order 50 (sufficient for representing 25 modes) with no time delay between the input and output. Table 5.3 summarizes the results of the identification along with the vibration periods from spectral analysis.

The periods from the spectral analysis and parametric identification are similar, with the exception of the second mode for the Landers earthquake. The spectral analysis gives a mode with a period of 1.19 sec, whereas the parametric identification gives a mode with a period of 1.30 sec. It appears the latter procedure identifies a broader range of periods with a peak at 1.30 sec than the former, because of the large damping of 11 percent. It is possible that there are two closely spaced modes in this period range, which are identified differently by the two methods.

5.5 Summary of Vibration Properties

The most significant finding of the identification of the vibration properties is the difference in the fundamental mode period of the Connector in the Landers and Big Bear earthquakes. The fundamental period lengthens from 1.56 sec in Landers to 1.75 sec in Big Bear. The change in period implies a 25 percent reduction in the stiffness of the bridge. Although there is little change in the second mode, the periods of the third and fourth mode are longer in the Big Bear earthquake. The other noticeable difference between the two earthquakes is that the damping ratio increases in the first and third mode, although it decreases in the second mode.

The lengthening of the vibration periods and generally increased damping indicate that the bridge "softened" in the Landers earthquake. Since the forces in the columns were less than the yield strength, it is unlikely that the softening was due to structural damage although cracking of the concrete columns and slippage of the steel jackets is possible. A more likely explanation is that the soil and pile foundations loosened in the Landers earthquake due to compaction and/or gapping of soil surrounding the piles, or changes in the groundwater between the two earthquakes. This soil behavior provided a larger compliance in the Big Bear earthquake. Another possibility is that the crushing of filler material in the hinges during the Landers earthquake allowed larger displacements between adjacent frames in the Big Bear earthquake (as evidenced by larger longitudinal hinge opening), producing a more flexible bridge. Once the processed records from the 1994 Northridge earthquake are available (CSMIP, 1994), it would be interesting to examine the vibration properties for comparison with the properties from the two 1992 earthquakes.

Table 5.3. Identified Vibration Periods and Damping Ratios

	Landers Earthquake			Big Bear Earthquake		
	Spectral Analysis	Parametric Identification		Spectral Analysis	Parametric Identification	
Mode	Period (sec)	Period (sec)	Damping Ratio (%)	Period (sec)	Period (sec)	Damping Ratio (%)
1	1.51	1.56	3.1	1.78	1.75	8.2
2	1.19	1.30	11.0	1.24	1.29	2.1
3	1.02	0.98	5.0	1.14	1.09	15.0
4	0.79	0.83	7.0	0.95	0.96	7.0

Chapter 6

STRUCTURAL MODELING AND ANALYSIS

6.1 Introduction

Structural modeling and earthquake analysis are a central step in the design of new bridges and evaluation of existing bridges. There is always the question about how well the models can predict the earthquake response of a bridge. An important objective of the current study is to model the Northwest Connector and compute its response to the Landers and Big Bear earthquakes. The approach is to apply modeling and dynamic analysis procedures typically used for bridge design. The computed responses are compared with the recorded responses from the earthquakes to assess the effectiveness of the analysis methods.

Since the structural components of the Connector did not experience inelastic deformations in the earthquakes, it is appropriate to use linear elastic models for the components. The opening and closing of the intermediate hinges, however, is nonlinear and that behavior is represented in the model. Although the behavior of the foundation and soils is nonlinear, as evidenced by the change in soil–structure interaction effects, the foundations are modeled as linearized springs.

The dynamic analyses are performed using the computer program SADSAP (Wilson, 1992). The program includes standard linear frame elements and nonlinear compression–only elements and tension–only elements. A model of the intermediate hinges is constructed using the nonlinear elements.

6.2 Model of the Connector

The three–dimensional model of the Connector consists of 353 frame elements and 20 nonlinear elements. The complete model, shown in Fig. 6.1, has approximately 1750 degrees–of–freedom.

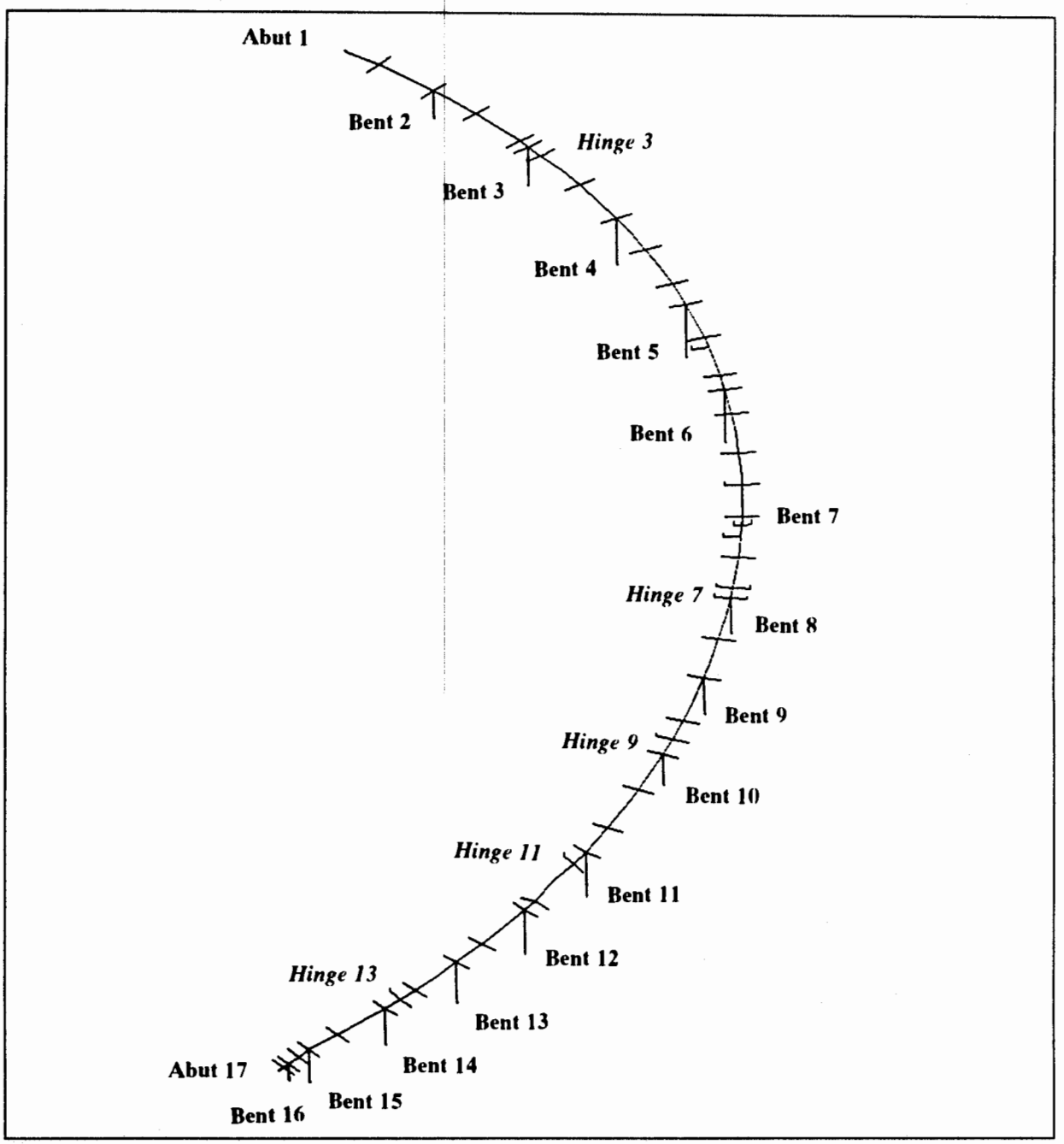

Figure 6.1 Model of Northwest Connector.

The frame elements are located at the elastic centroid of the members using the gross section properties, modified for assumptions about effective width, cracking, and level of deformation. The assembly of the elements reflects the joint size, eccentricities, and offsets from the member centerlines. The transverse superstructure elements, shown in Fig. 6.1, are massless and rigid elements that serve two purposes: modeling the diaphragms at the intermediate hinges, as described below; and for visualizing the twisting of the box girder in the plots of displaced configuration.

Since traffic was light at the time of the earthquakes, the mass of the superstructure is based only on the calculated dead load; mass due to live load is not included.

6.2.1 Superstructure

The 2540 ft long concrete box girder superstructure consists of six frames. The superelevation is neglected in determining the section properties of the box girder. The assumed concrete properties for the superstructure are listed in Table 6.1. The 28–day compressive strength is based on the allowable stresses specified in the drawings, and the strength is increased by 20 percent to account for overstrength. The modulus of elasticity is based on standard expressions (ACI, 1989) using the assumed f_c', and no reduction is made for creep. The unit weight of concrete is assumed to be 150 lb/ft^3.

The box girders for the conventionally reinforced and prestressed frames are similar except the latter has thicker girders. For the conventionally reinforced spans, the gross moments of inertia are multiplied by 0.75 to account for cracking. There is no reduction from the gross section for the prestressed spans. Shear deformation in the vertical and transverse direction is included in the model.

For each span, two section properties for the box girder are used. Within one–quarter span of the bent, section properties for bending about the transverse axis and torsion are reduced to account for the smaller effective width near the bent cap for transfer of moments to the column. The effective width near the bent cap is the center $3D$ of the box girder, where D=8 ft is the transverse width of the column. The middle one–half of the spans has no reduction for effective width. Table 6.2 summarizes the section properties for the model of the box girder.

Each span of the box girder is modeled by four or five elements. The translational mass is lumped at the nodes. The mass coefficients for the horizontal DOF are lumped at the nodes on the centerline. To account for the rotational mass moment of inertia about the longitudinal axis of the box girder (twisting), 40 percent of the vertical mass is lumped at the ends of the transverse elements, and the remainder is lumped at the centerline DOF.

Table 6.1. Concrete Properties for Box Girder Superstructure

Frame	Section	Type	Design f_c' (psi)	Assumed f_c' (psi)	Assumed E (ksi)
1	Abut 1–H3	Reinforced	3000	3600	3420
2	H3–H7	Prestressed	4300	5160	4090
3	H7–H9	Reinforced	3000	3600	3420
4	H9–H11	Prestressed	3500	4200	3690
5	H11–Abut 17	Reinforced	3000	3600	3420

Table 6.2. Section Properties for Model of Box Girder Superstructure

Type	Effective Width	Rectangular Moments of Inertia[a] I_{22} (ft^4)	I_{33} (ft^4)	Torsional Moment of Inertia J (ft^4)
Prestressed	Full	683	7930	2314
Prestressed	Partial	447	7930	1252
Reinforced	Full	491	5450	1719
Reinforced	Partial	323	5450	929

[a] I_{22}, I_{33}= moments of inertia about transverse axis and vertical axis of box girder, respectively.

6.2.2 *Intermediate Hinges*

The nonlinear behavior of the hinges is modeled using the scheme illustrated in Fig. 6.2. The hinge model represents opening–closing with an initial gap, tension–only restrainers with initial slack, and the elastomeric bearing pads. The relative transverse displacement (radial to the alignment) is constrained to zero, regardless of the hinge skew, because the shear keys only allow relative longitudinal displacement (tangential to alignment). In addition, relative vertical displacement and twisting at the hinge is constrained to zero. Consequently, the small transverse displacements and vertical displacements of the hinges in the earthquakes, as shown in Section 5.2, are not represented in the model.

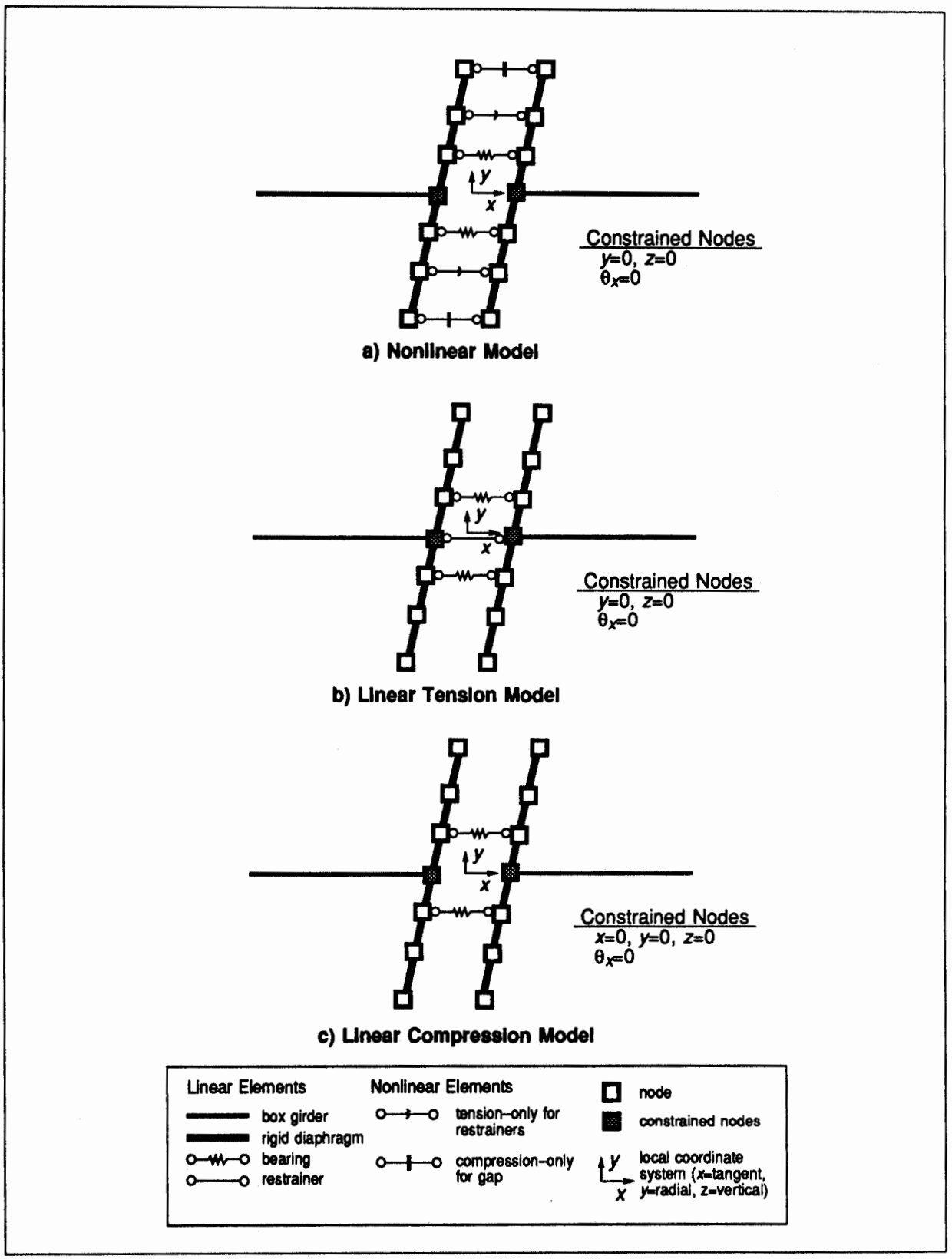

Figure 6.2 Plan View of Models for an Intermediate Hinge.

In the model of Fig. 6.2(a), the diaphragms are represented as rigid elements oriented with the skew of the hinge. The width of the rigid diaphragm elements is the width of the box girder, 41 ft, and they are separated longitudinally 0.1 ft, although the latter number is not important in the model. Compression–only elements are located at the edges of the diaphragms near the two outer girders. Tension–only elements for the restrainers are located at the centroids of the restraining force for the three possible modes of hinge opening. Linear spring elements are located at the centroids of longitudinal bearing force. The compression–only and tension–only elements and linear springs are aligned in the longitudinal direction regardless of the hinge skew.

The stiffness of the tension–only elements for the restrainer cables is based on the specified cross–sectional area of the cables and a modulus of elasticity of 10,000 ksi. Since specifications for the elastomeric bearing pads were not available, the stiffness of the pads is based on the nominal dimensions in the drawings and a shear modulus of 150 psi for the elastomeric material.

The compression–only gap elements have a spring that penalizes closing of the gap. The springs are assigned a stiffness approximately two orders of magnitude greater than the stiffness of the restrainer cables. Although this is a relatively low stiffness, compared with the axial stiffness of the box girder, it provides a compromise between penalizing penetration upon closing of the gap and convergence of the solution. The penetration is as much as 20 percent of the specified closing displacement, as will be shown later.

There is no information about the condition of the hinges before the two earthquakes. Based on the observations of hinge displacement in Section 5.2, the hinges are assumed to initially open 1.5 in. prior to the Landers and Big Bear earthquakes. The restrainer cables are assumed to have an initial slack of 0.5 in. prior to each earthquake. The sensitivity of the bridge response to these assumptions was not investigated.

6.2.3 Columns

Each column is modeled with three frame elements. Rigid offsets at the top represent the eccentricity of the column–cap beam connection. The connection with the bent cap is rigid, except for Bents 4 and 7 which have moment releases about the weak column axis. The distributed mass of the columns is included in the model.

The length of each column is from the soffit to the pile cap, according to the drawings, except for bents with deep overburden (2, 10, 11, and 16). At those bents, the base nodes are located halfway between the pile cap and overburden surface to represent approximately the point of fixity. No attempt was made to locate points of fixity for the columns beyond these assumptions.

The flexural stiffness of the retrofitted columns is affected by the level of deformation and the presence of the steel jackets. One of the parameters in the model is the factor by which the flexural rigidity (EI) based on gross moments of inertia is modified to represent the stiffness of the columns. The modification factor is selected as the primary parameter to match the computed vibration modes with the modes identified from the earthquake response records.

The steel jackets, however, increase the stiffness of the section, although that is not their intent. Based on the test data for steel jacketed columns (Priestley, Seible et al., 1992), the moments of inertia for columns with F–jacket and P–jacket retrofits are increased 15 percent and 10 percent, respectively.

The torsional moment of inertia for the columns is the gross section multiplied by a factor of 0.25 and 0.12 for F–jacket and P jacket columns, respectively, to account for cracking. The gross section properties are used for axial and shear deformation. Table 6.3 gives the gross section properties for the columns without reduction factors.

Table 6.3. Gross Section Properties for Model of Columns

	Rectangular Moments of Inertia[a]		Torsional Moment of Inertia
Condition	I_{22} (ft^4)	I_{33} (ft^4)	J (ft^4)
Original (Gross)	87.6	179	267
Full Jacket Retrofit	101	206	267
Partial Jacket Retrofit	96.3	197	267

[a] I_{22}, I_{33} = moments of inertia about weak axis (bending in longitudinal direction) and strong axis (bending in transverse direction).

6.2.4 *Foundations*

The stiffness of the pile foundations is approximated by translational and rotational springs at the pile cap. The translational spring stiffness is based on a lateral stiffness of 65 kip/in per pile for the firm sandy soils at the site. The stiffness is attributed to all the original and retrofit piles for a foundation.

The rotational stiffness coefficient for the pile foundations are obtained from the foundation rocking observed at Bent 8, as described in Section 5.2.1. Assuming a transverse stiffness coefficient for the column of $3EI/L^3$, the rotational stiffness coefficient is 4×10^7 kip–ft for Landers and 2×10^7 kip–ft for Big Bear. These springs

were applied to all the foundations for rocking about the transverse and longitudinal directions.

The translational and rotational stiffness coefficients were verified by comparing the values computed using methods by Novak (Prakash and Sharma, 1990). The calculations for pin–headed piles use a small strain shear velocity of 1580 ft/sec for the alluvial sands (Jackura, 1991). The stiffness coefficients used in the model are about 50 percent of the calculated value. The stiffness coefficients were accepted because the soil strains would be larger in an earthquake and pile group effects would reduce the effective stiffness. It is recognized, however, that the foundation modeling is approximate.

The translational and rotational mass of the pile caps are lumped at the node for each foundation. Material damping and radiation damping due to soil–structure interaction are neglected.

6.2.5 Abutments

The stiffness coefficients for the diaphragm abutments are based on standard modeling techniques (Caltrans, 1990). A linear model is used for the abutments, since the records did not indicate nonlinear behavior. The longitudinal stiffness is 200 kip/in per foot width of backwall plus the stiffness of the piles, assumed to be 40 kip/in per pile. The soil stiffness is reduced by one–half to recognize it is only effective in compression. The transverse stiffness of the abutments is due to the piles and partial resistance of the wingwalls. The three rotational degrees–of–freedom at the abutments are assumed to be fixed.

For Abutment 1, the longitudinal and transverse stiffness coefficients are 53,500 kip/ft and 42,720 kip/ft, respectively. For Abutment 17, the longitudinal and transverse stiffness coefficients are 52,560 kip/ft and 41,760 kip/ft, respectively. The vertical displacement and rotation about the three axes is constrained to zero at the abutments.

6.2.6 Damping

Energy dissipation occurs in the superstructure, foundations, and soil. Since energy dissipation in the model of the foundations is neglected, damping for the structure should account for all dissipation mechanisms. For design it is typical to assume 5 percent modal damping.

Based on the identified damping ratios in Table 5.3, 3 percent damping for all modes is used for modeling the response of the Connector in the Landers earthquake and 5 percent for all modes in the Big Bear earthquake. More elaborate

damping models could have been used, but the lack of information made it difficult to justify additional assumptions about energy dissipation.

6.2.7 Design Models

A nonlinear model of a bridge, including opening and closing of the intermediate hinges, is not normally used in bridge design. To account for this nonlinear mechanism, it is common to bound the response by two linear models: the tension model and the compression model.

The tension model is intended to capture the response of the bridge when all the hinges are open. At the hinges, there is no longitudinal restraint except that provided by the cable restrainers. The restrainers are represented by a linear truss element located along the centerline of the box girder. This is done to avoid the restrainer elements from developing a moment due to relative rotation of the hinge about the vertical axis. The linear elements for the elastomeric bearing pads are included. The tension model of a hinge is shown in Fig. 6.2(b).

The compression model represents the response of the bridge when all the hinges are closed. In addition to the constraints shown for the tension model, the relative longitudinal displacements are constrained to be zero. The linear elements for the elastomeric bearing pads are included. The compression model of a hinge is shown in Fig. 6.2(c).

6.2.8 Input Motion

Since soil–structure interaction effects are modeled by the foundation springs, the recorded free–field motion is used as the input motion. The three components of free–field ground motion are used: 90°, 180°, and vertical.

6.3 Vibration Properties

The vibration modes identified in Table 5.3 average the nonlinear hinge opening mechanism over the duration of the strong motion. For calibrating the models, the identified properties are compared with the vibration properties of the open hinge model. Although the model vibration modes could have been calibrated with the compression (closed joint model), calibration with the open joint model is more appropriate because of the hinge opening observed in the earthquakes. Table 6.4 compares the vibration periods for the lower modes.

The best–fit open joint model for Landers is obtained by multiplying the gross EI (including effect of steel jackets) from Tables 6.1 and 6.3 by a factor of 1.05. The best fit model for Big Bear is obtained by multiplying the gross EI by a factor of 0.85. For the Big Bear model, the rotational foundation springs are reduced by one–half, in

accordance with the observation in Section 5.2.1, to account for the increased flexibility of the foundations.

The lower vibration modes for the open joint model calibrated for the Landers earthquake are plotted in Fig. 6.3. The mode shapes for the calibrated Big Bear model are similar to the modes for the Landers model.

Table 6.4. Comparison of Identified[a] and Computed Vibration Periods (in seconds) for Open Joint Model

Model Mode		Landers Earthquake		Big Bear	
No.	Type	Identified	Model	Identified	Model
1	1st symmetric	1.56	1.56	1.75	1.74
			1.22[b]		1.33[b]
2	1st antisymmetric	1.30	1.18[c]		1.31
3	2nd symmetric		1.12	1.29	1.23
4	2nd antisymmetric	0.98	0.90	1.09	0.98
			0.81[b]		0.87[b]
			0.80[b]		0.85[b]
5	composite	0.83	0.69	0.96	0.75

[a]Parametrically identified periods from Table 5.3.

[b]Mode of individual frames in longitudinal direction; used for representing hinge displacements in model.

[c]The model period of 1.18 sec compares well with the period of 1.19 sec identified from spectral analysis.

The identified and model modes are matched by examining the type of model mode with the characterization of the mode from spectral analysis, as described in Section 5.3.2. The open joint model modes consisting of longitudinal motion of individual frames are not included in the comparison; only the transverse model modes are included. This is because the longitudinal modes of the individul frames are used in the analysis to represent the hinge displacements. Generally the modes and periods match well, although there is some judgment in interpreting the second and third modes. As shown in Table 5.3 for the Landers earthquake, the parameteric identification gives a second mode period of 1.30 sec, whereas the spectral analysis gives a period of 1.19 sec. The open joint model matches well with the period from spectral identification. For the Big Bear earthquake, the higher modes in the model are somewhat smaller than the corresponding identified periods, indicating that the model may be too stiff. For comparison with the open joint model, the vibration modes of the closed joint (compression) model are shown in Figure 6.4.

6.4 Response Comparison

The earthquake response comparison uses the model with the column properties determined from calibration of vibration properties and the nonlinear hinge model. The nonlinear solution procedure uses Ritz vectors that are generated from the open joint model, neglecting the nonlinear elements (Wilson, 1992). Hence, the Ritz vectors are essentially generated from the tension model since the linear cable restrainer elements have a small effect on the vibration properties. In addition to the inertia forces, the Ritz vector generation includes forces applied at the gap elements so that the vectors are rich in hinge displacements. The response computation uses 25 Ritz vectors, which represents 95 percent of the total mass of the bridge in the horizontal directions and 77 percent of the total mass in the vertical direction.

The load cases considered in the response evaluation are dead load and earthquake ground motion. The time history computation for the response to the free–field earthquake ground motion is performed with a time step of 0.02 seconds.

The recorded total displacements for 29 channels are compared with total displacements computed from the model. Five channels (8, 20, 26, 30, and 32) are not shown since the response comparison is very similar to adjacent channels. Figure 6.5 presents the comparison for the Landers earthquake, and Fig. 6.6 gives the comparison for the Big Bear earthquake. The location of the instruments is again given in Fig. 2.7.

Support Motion

The translational support motion at Abutment 1 (channels 1 and 3), Bent 3 (channels 4 and 6), Bent 8 (channels 22 and 24), and Abutment 17 (channels 34 and 36) is represented very well by the model. This indicates that the selection of springs to represent the abutments and translational stiffness of the pile foundations is acceptable. The vertical flexibility of the abutments is neglected in the model. Yet, the vertical motion at the abutments (channels 2 and 35) is represented well.

The assumption of uniform free–field input is accurate, as can be seen by the model's ability to represent support motion, including soil–structure interaction effects, recorded in the two earthquakes.

Transverse Response

Much of the transverse response of the Connector is captured in the model, although there are some differences between the recorded and computed total displacements. For channel 7, near Bent 3 and Hinge 3, the model has many of the

peaks in the recorded response and the phase is very good, particularly for Landers. However some of the recorded peaks are under estimated by the model.

Channel 11, in Span 5, again represents several of the peaks and phase well. The phasing in channel 11 for Big Bear earthquake is slightly off, especially in the strong motion segment of 15 to 25 seconds. This may indicate that the Big Bear model does not represent the transverse modes of the span well, or nonlinear response changes the characteristics of the bridge or foundation during the earthquake.

The phase of the model response compared with the recorded response is excellent for channel 19, near Hinge 7 and Bent 8. Some of the peaks are under estimated by the model, particularly in the strong motion response (30 to 35 seconds) in the Landers earthquake. The comparison is similar for channel 29, near Hinge 11. The comparison of recorded and computed transverse displacement is excellent for channel 25 (near Hinge 9) and channel 31 (Hinge 13). Overall, the Big Bear models appears to be a little too stiff, since it is under estimating the recorded displacements.

Longitudinal Response

The comparison of model and recorded displacements of the Connector is excellent for channel 10 (Hinge 3), channel 18 (Hinge 7), and channel 28 (Hinge 11). The comparison is not quite as good for channel 17 on the other side of Hinge 7 from channel 18 in the Landers earthquake, although the overall phase and amplitude of the longitudinal displacement is excellent after the strong motion vibration past 35 seconds.

Vertical Response

The vertical response of the bridge in the two earthquakes is captured reasonably well by the model. For example, the close comparison for channel 9 shows that the rotation of the cap beam for Bent 7 is represented in the model. The rotation of the box girder at Bent 8 (channels 12 and 13) is slightly under estimated by the model.

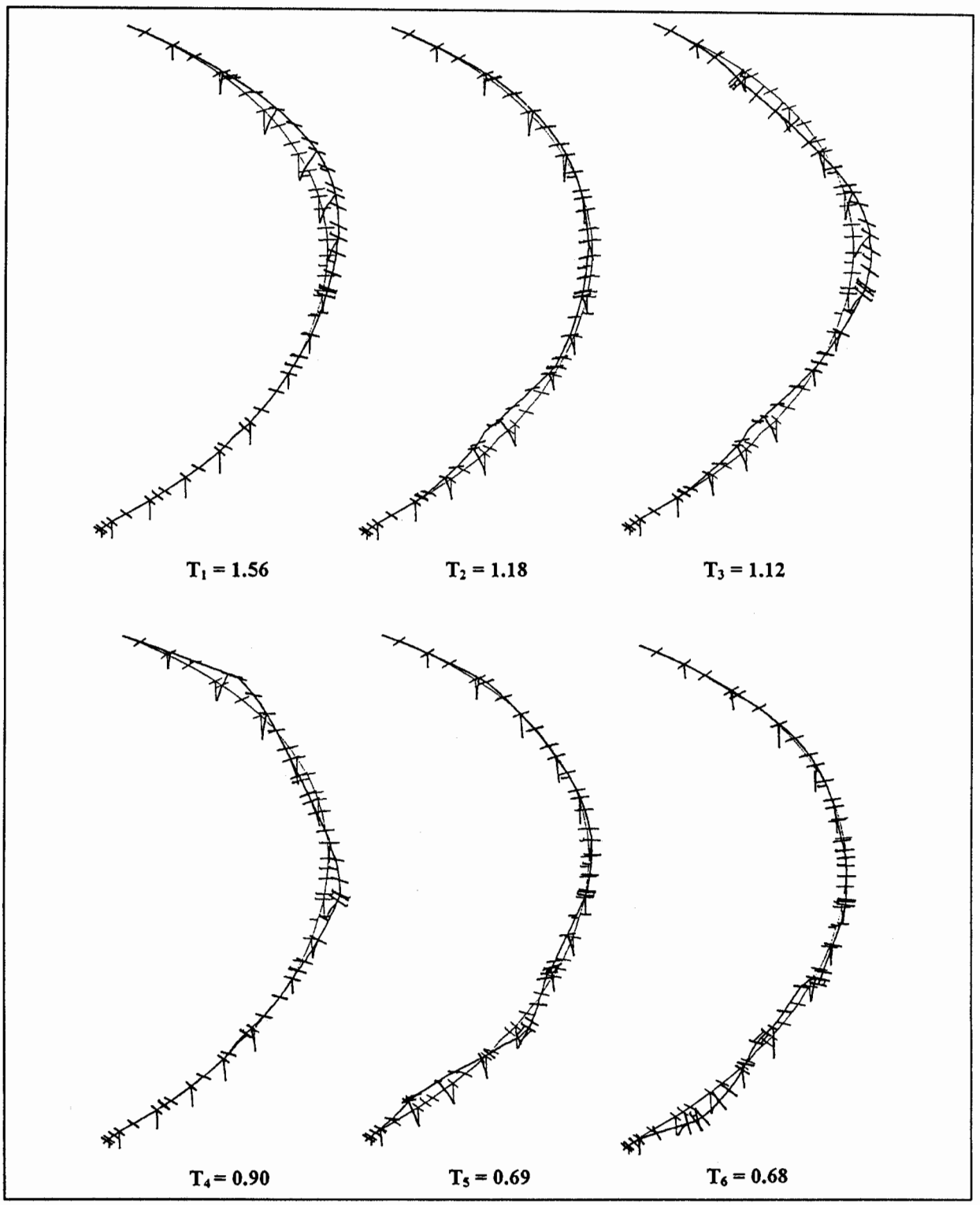

Figure 6.3 Lower Vibration Modes of Open Joint Model for Landers Earthquake.

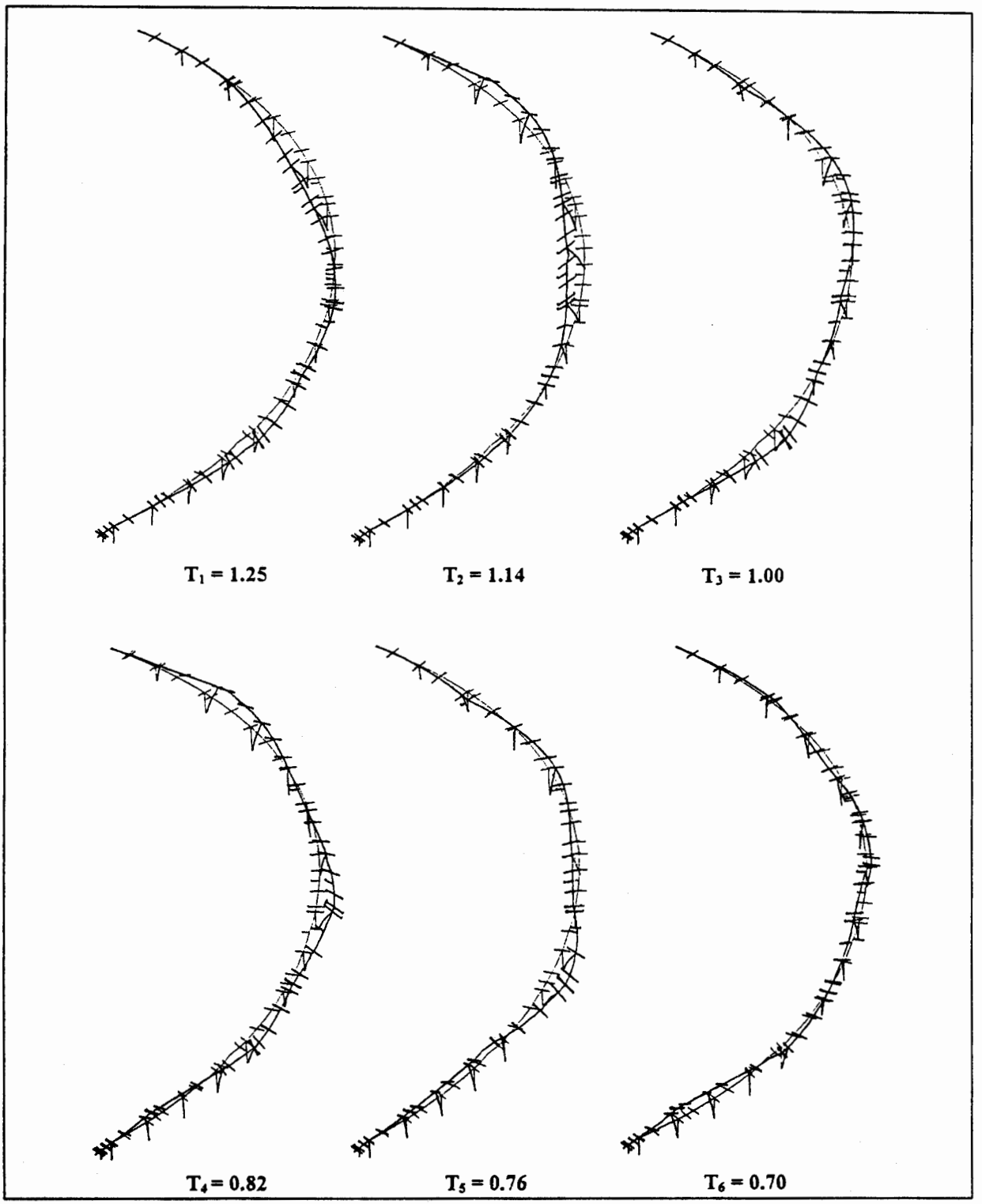

Figure 6.4 Lower Vibration Modes for Compression Model for Landers Earthquake.

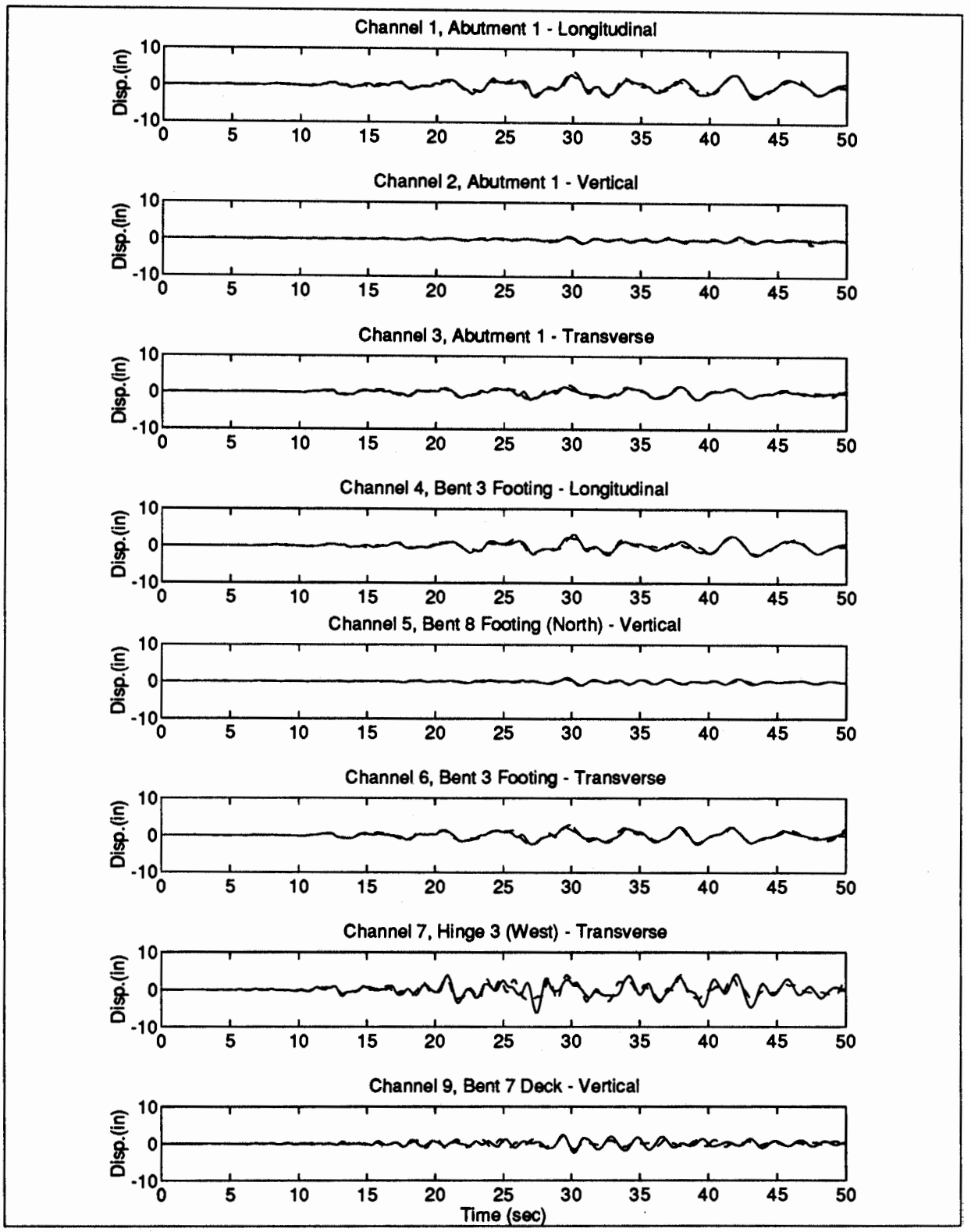

Figure 6.5 Comparison of Recorded Total Displacement (solid line) with Computed Total Displacement (dashed line) for Landers Earthquake.

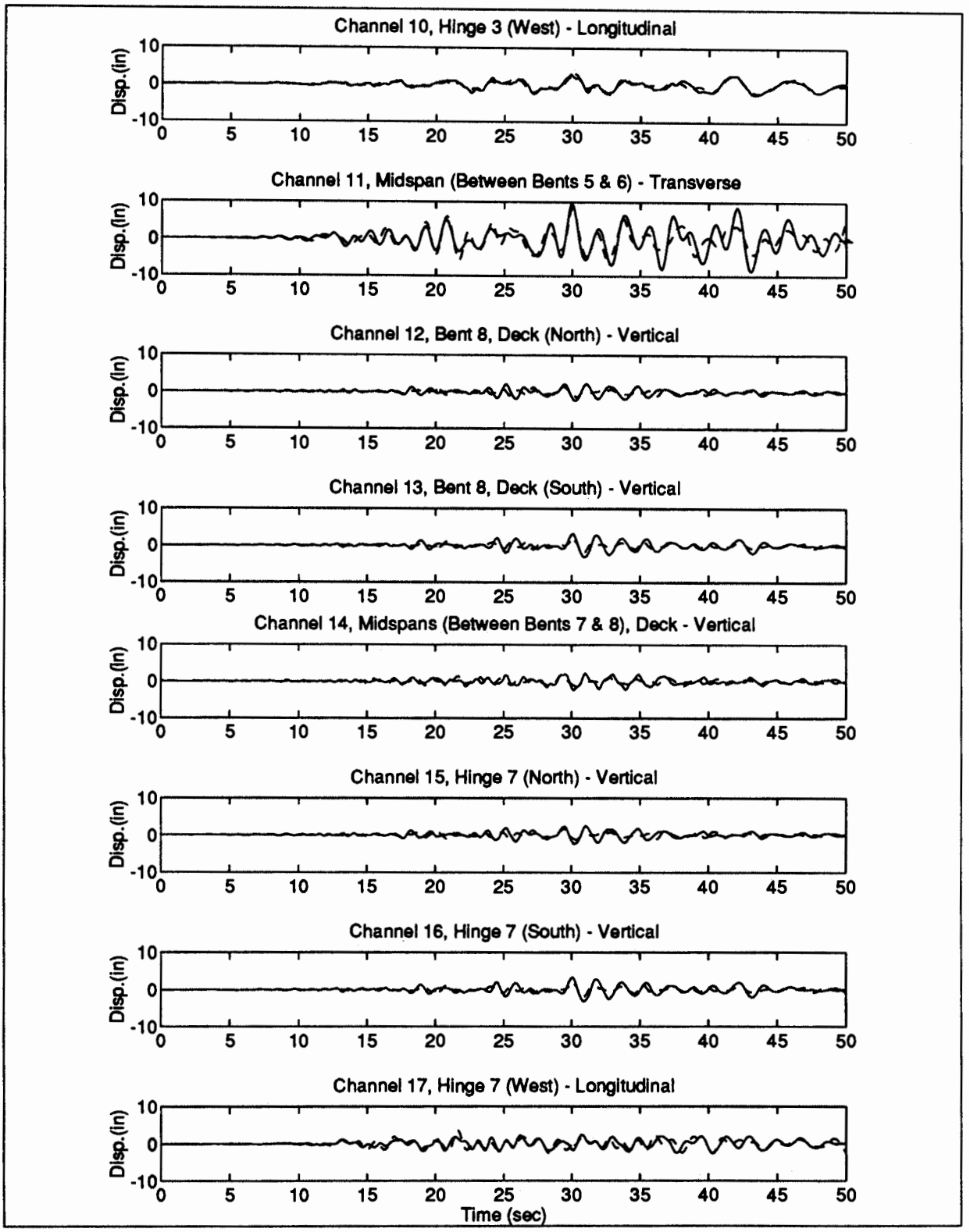

Figure 6.5 Comparison of Recorded Total Displacement (solid line) with Computed Total Displacement (dashed line) for Landers Earthquake (continued from previous page)

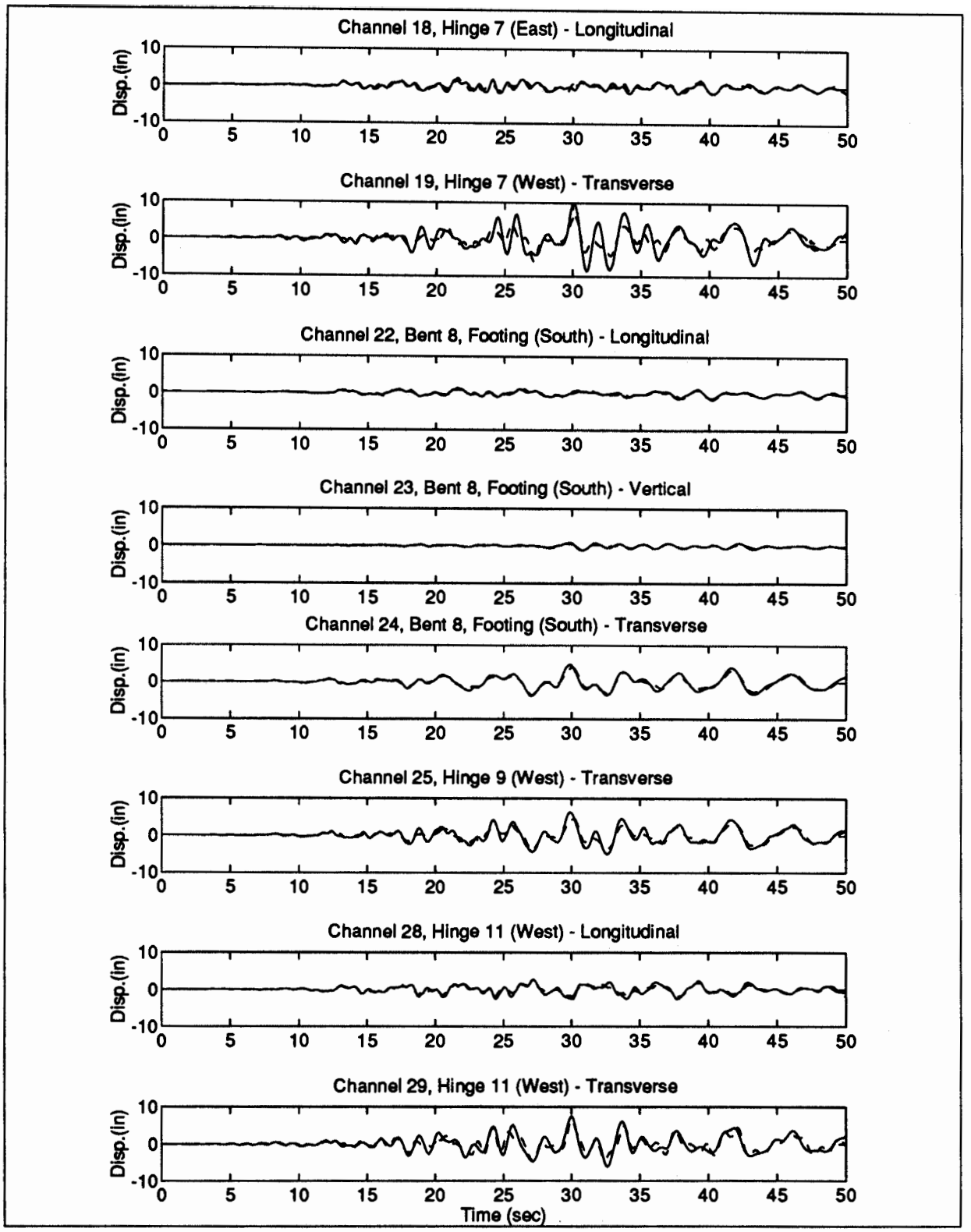

Figure 6.5 Comparison of Recorded Total Displacement (solid line) with Computed Total Displacement (dashed line) for Landers Earthquake (continued from previous page)

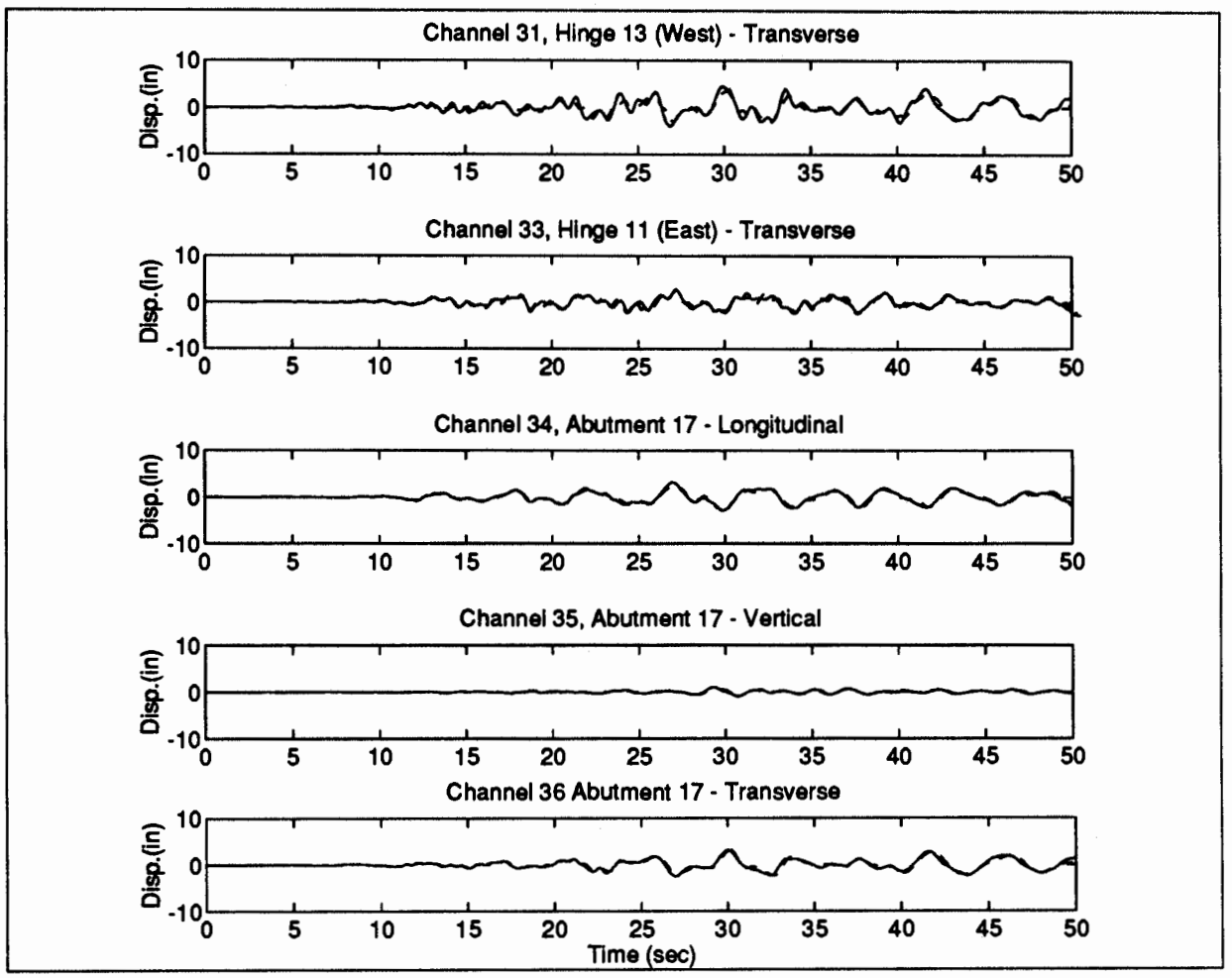

Figure 6.5 Comparison of Recorded Total Displacement (solid line) with Computed Total Displacement (dashed line) for Landers Earthquake (continued from previous page)

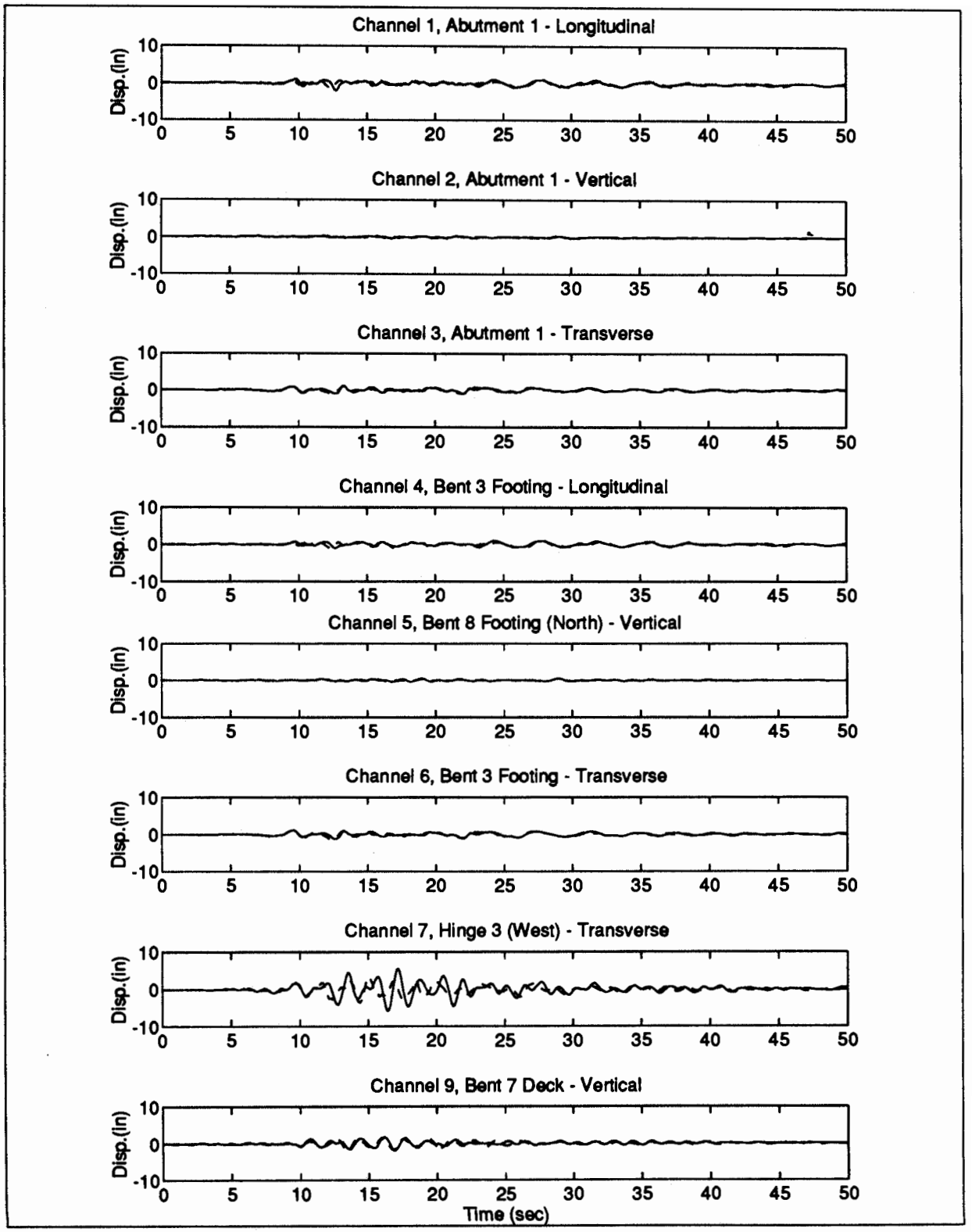

Figure 6.6 Comparison of Recorded Total Displacement (solid line) with Computed Total Displacement (dashed line) for Big Bear Earthquake.

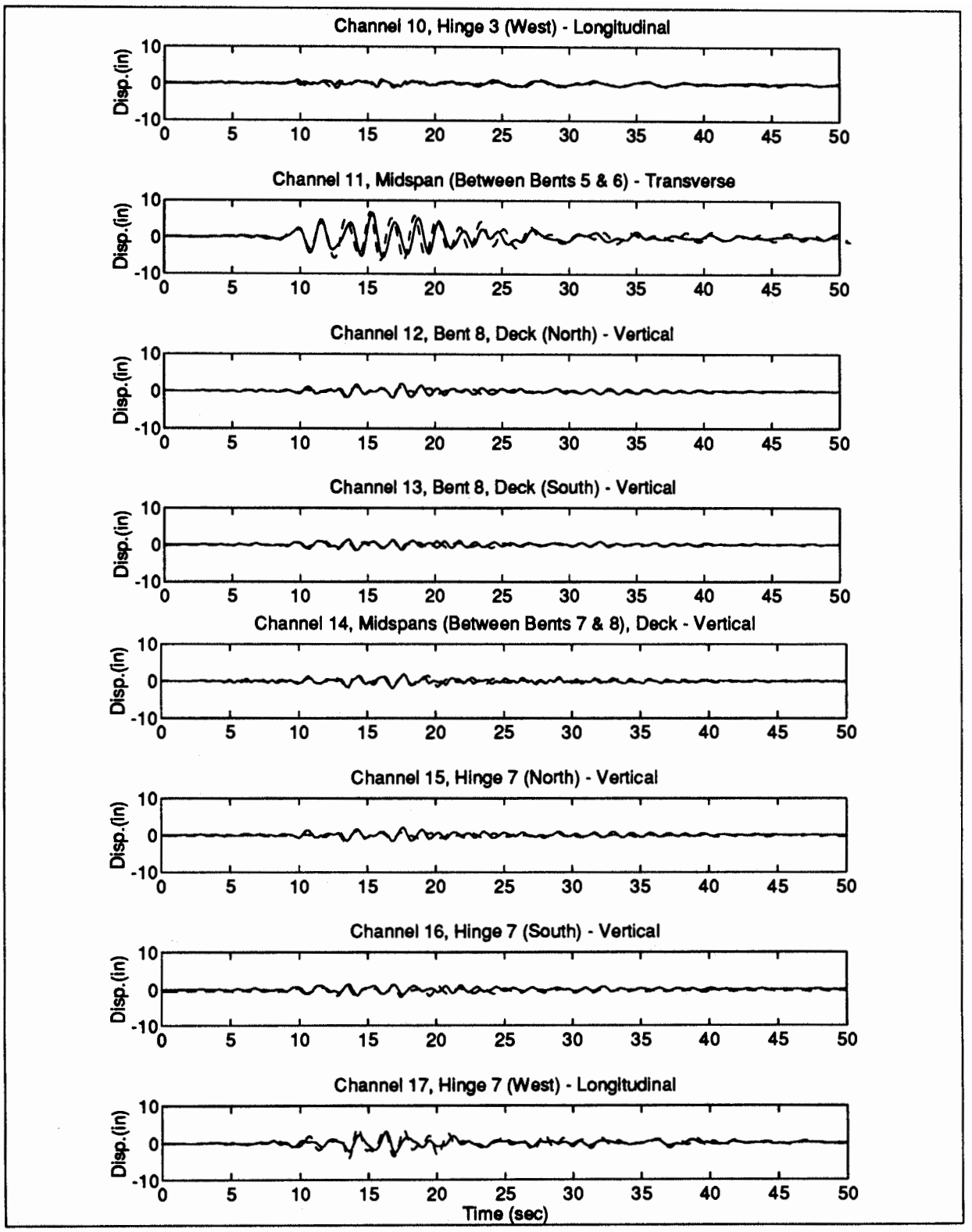

Figure 6.6 Comparison of Recorded Total Displacement (solid line) with Computed Total Displacement (dashed line) for Big Bear Earthquake (continued from previous page).

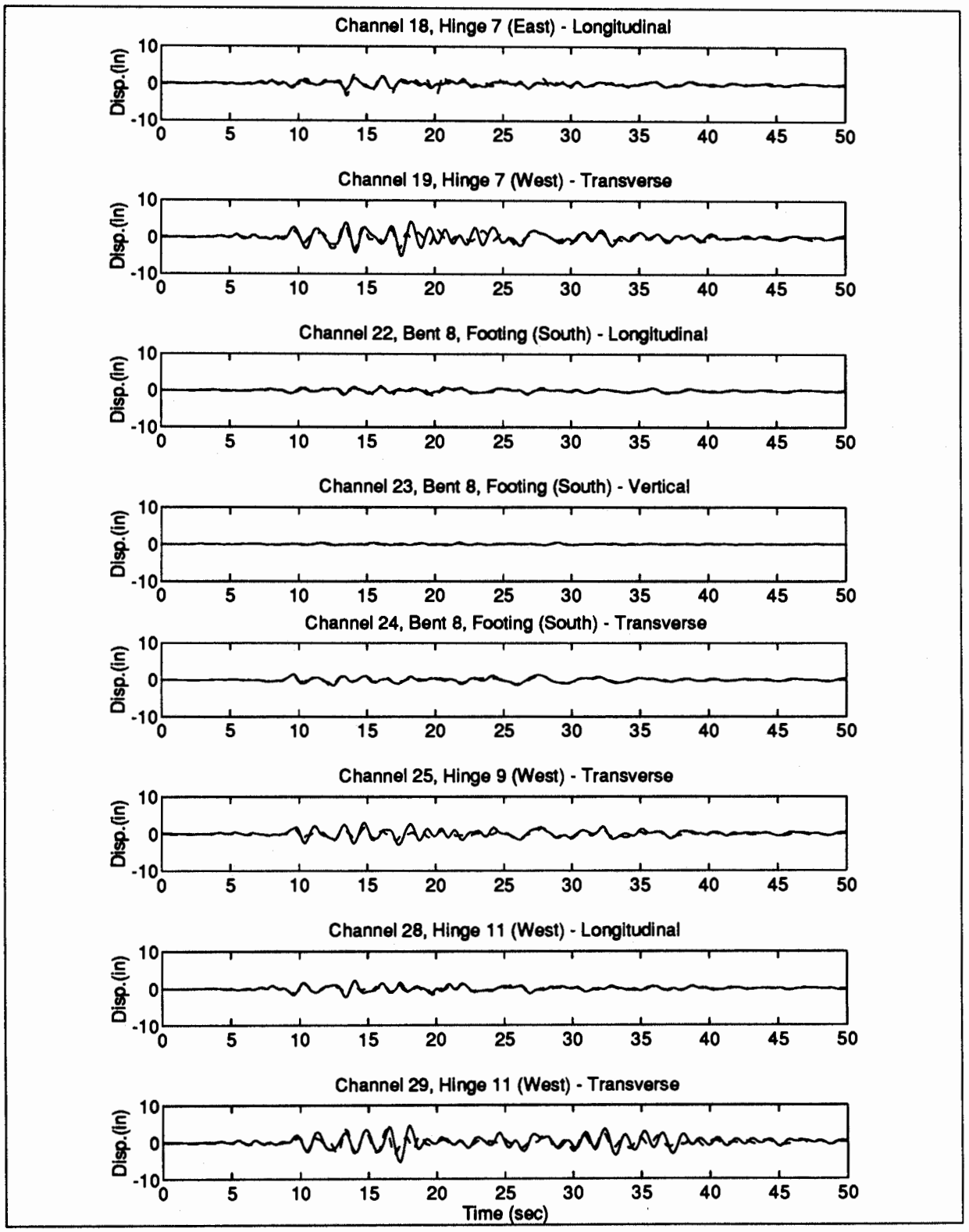

Figure 6.6 Comparison of Recorded Total Displacement (solid line) with Computed Total Displacement (dashed line) for Big Bear Earthquake (continued from previous page).

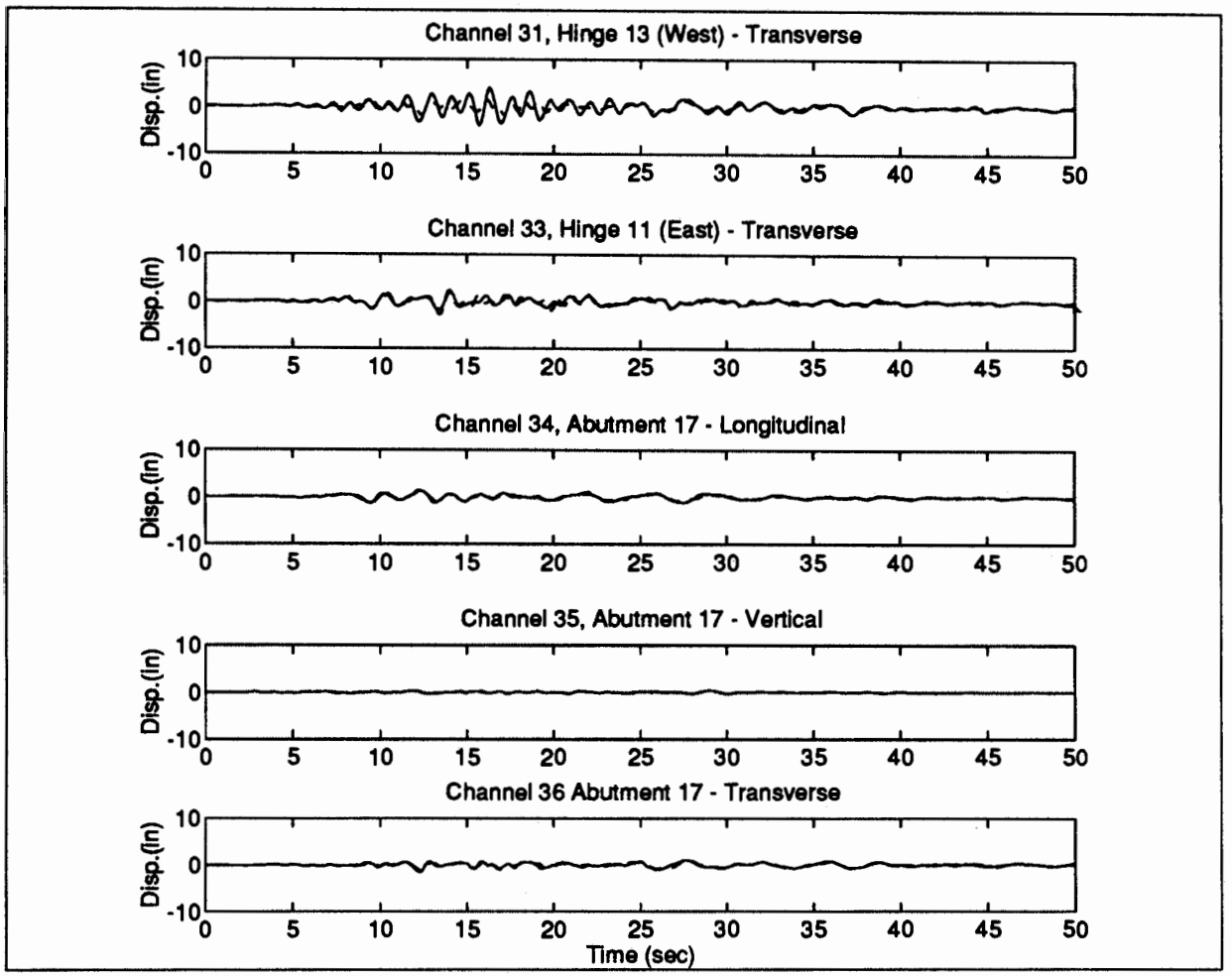

Figure 6.6 Comparison of Recorded Total Displacement (solid line) with Computed Total Displacement (dashed line) for Big Bear Earthquake (continued from previous page).

Relative Displacements

Since the forces in the columns depend on the relative displacement of the top of the column with respect to the displacement of the footing, Figs. 6.7 and 6.8 show the relative displacement near the top of Bent 3 (channels 7 and 10) and Bent 8 (channels 18 and 19) as determined from the recorded response and computed from the models. The recorded displacements are the same as those used to generate the trajectories in Figs. 5.2 and 5.3. The model represents the relative displacements well, with the exception of an under estimate of the peaks for the transverse motion at Bent 8 (channel 19) in the Landers earthquake.

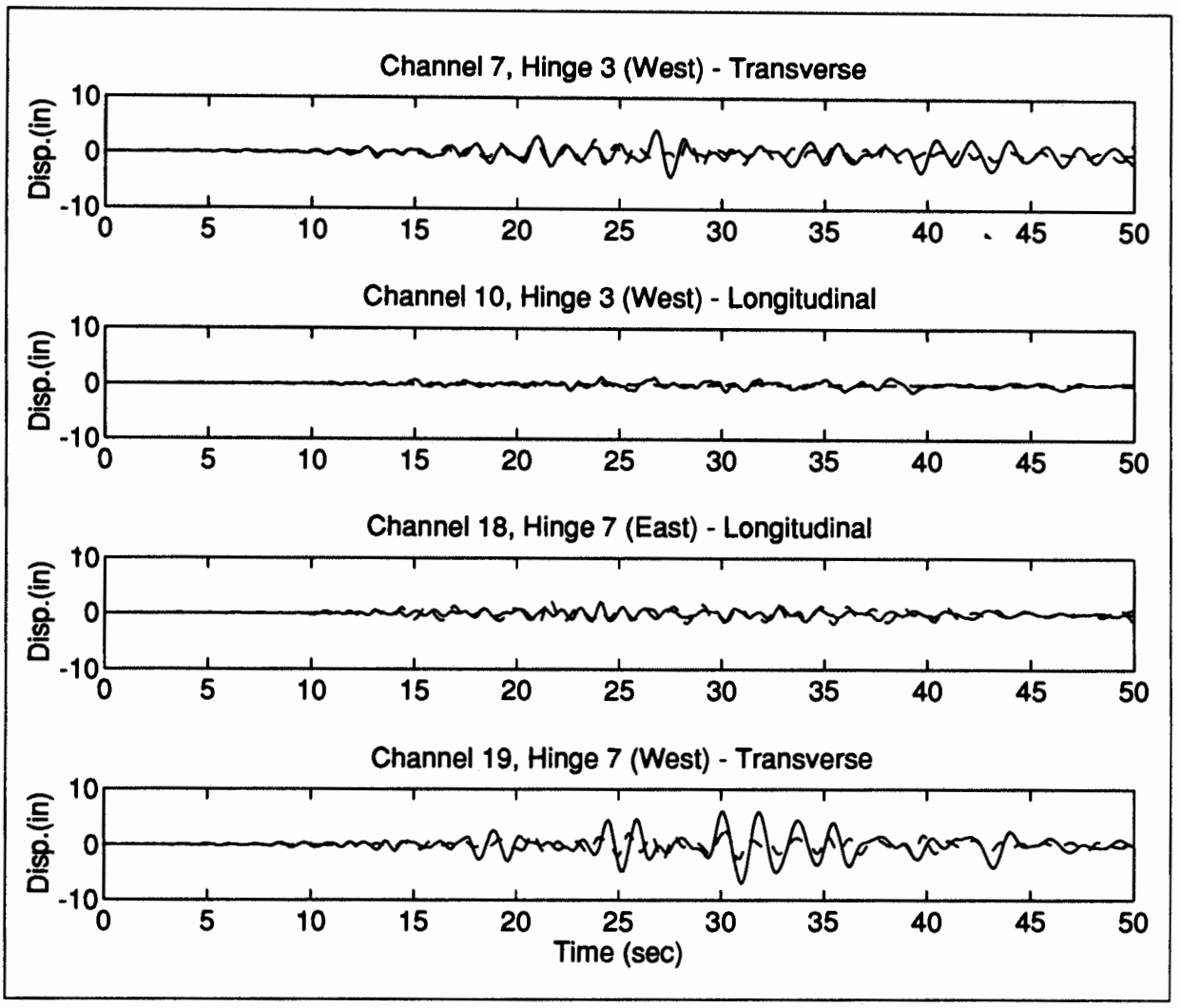

Figure 6.7 Relative Displacement of Deck Relative to Pile Cap in Landers Earthquake (solid–recorded, dashed–model).

6.5 Response of Intermediate Hinges

The response of the intermediate hinges is contained in the displacements plotted in Figs. 6.5 and 6.6, but the scale makes the effects of the hinges difficult to see. To investigate the ability of the model to capture the response of the hinges, Figs. 6.9 and 6.10 show the relative longitudinal of Hinges 7 and 11. The relative longitudinal displacement, velocity, and acceleration across the hinge are plotted for each earthquake for time segments that include significant hinge motion.

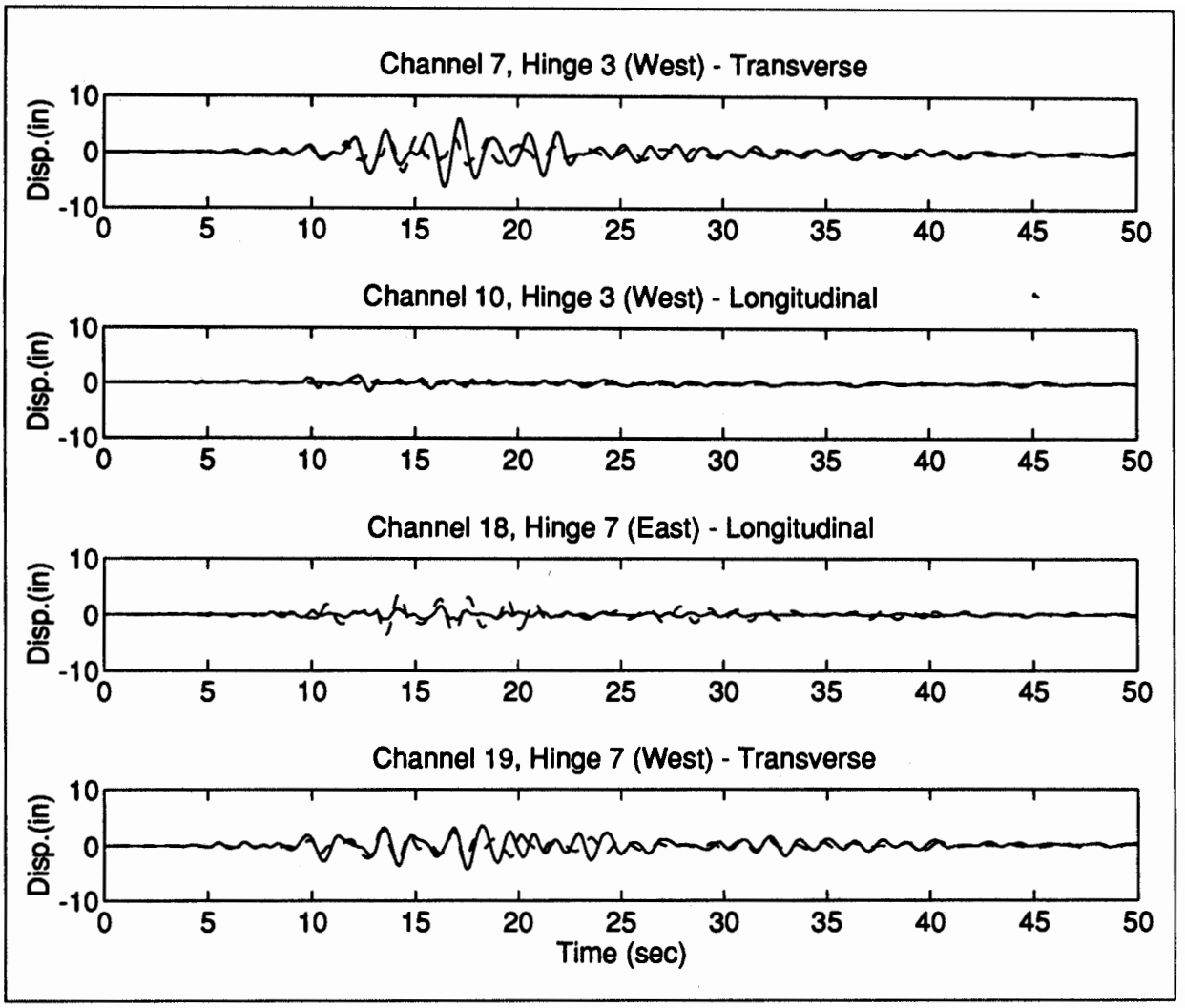

Figure 6.8 Relative Displacement of Deck Relative to Pile Cap in Big Bear Earthquake (solid–recorded, dashed–model).

Considering the Landers earthquake, Fig 6.9 shows that for Hinge 7 the model slightly overestimates the hinge opening and there is a considerable phase shift compared with the recorded response in the time window 23 to 27 seconds. The recorded relative velocity has sharp negative peaks at just past 24.5 and 25.5 seconds immediately prior to the hinge pounding closed at these two times. The corresponding acceleration has a doublet pulse characteristic of pounding (Malhotra, Huang et al., 1994).

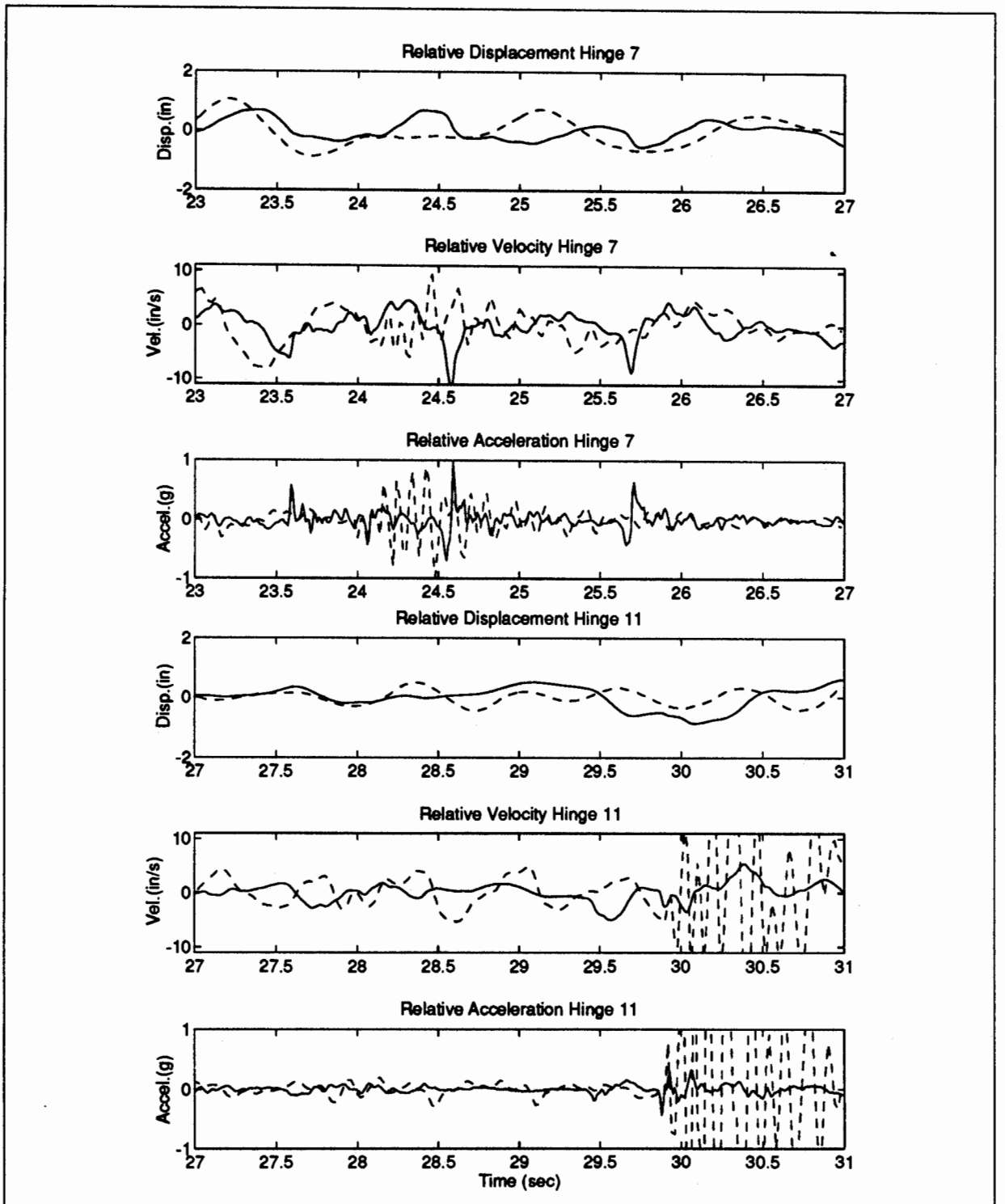

Figure 6.9 Relative Longitudinal Hinge Motion in Landers Earthquake (solid–recorded, dashed–model).

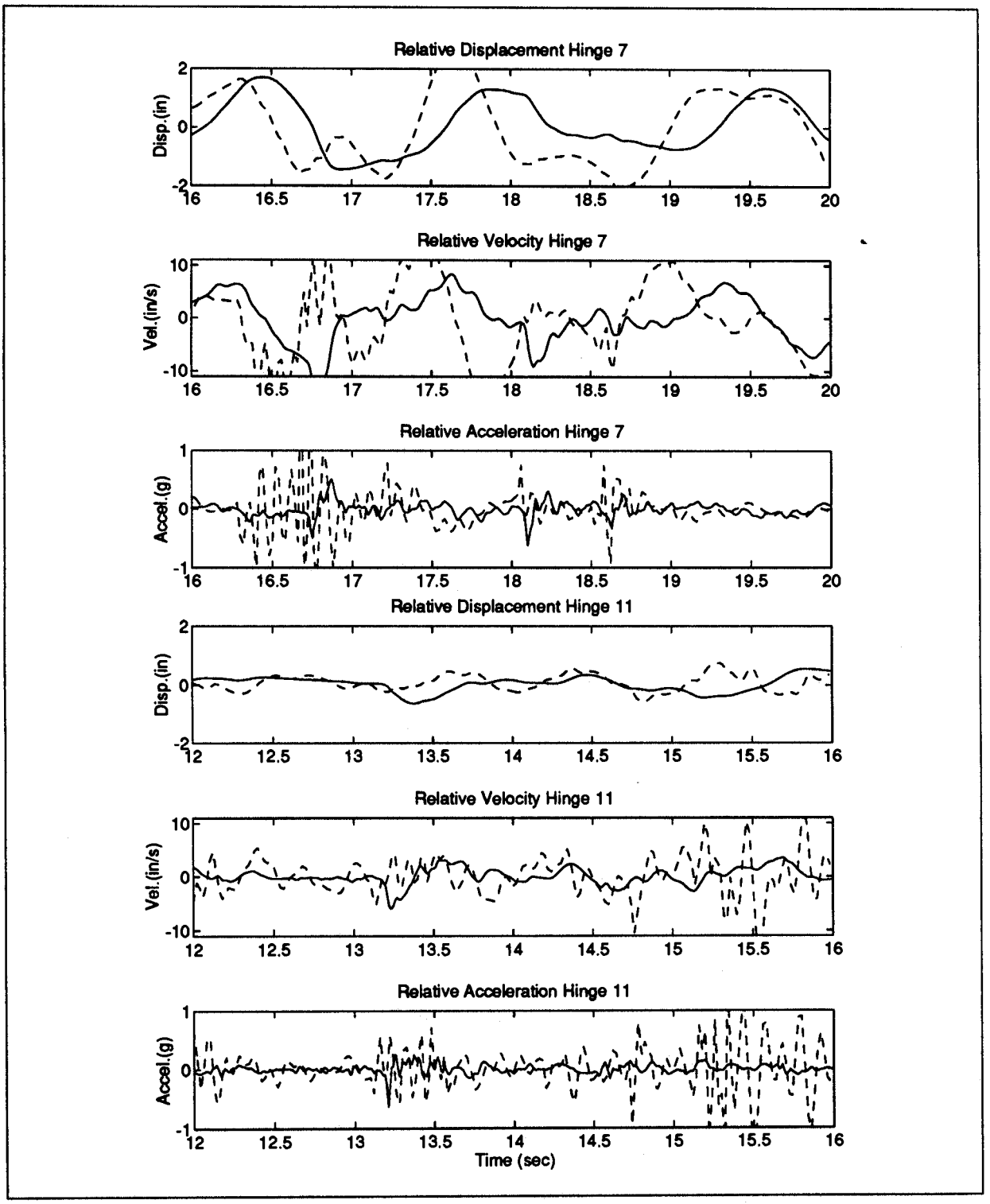

Figure 6.10 Relative Longitudinal Hinge Motion in Big Bear Earthquake (solid–recorded, dashed–model).

Although the nonlinear hinge model represents the overall characteristics of the relative hinge displacement, the model does not provide accurate velocity or acceleration of the hinge. Both show high frequency oscillations that may be caused by lack of energy dissipation in the hinge model. The comparison is somewhat better for Hinge 11, although the relative motion is less than at Hinge 7. The model for Big Bear predicts the hinge opening better than the Landers model, as shown in Fig. 6.10.

The maximum hinge opening and closing displacements from the model are listed in Tables 6.5 and 6.6. For the Landers earthquake, the model over–predicts the maximum opening at Hinges 7 and 11. Hinges 3 and 7 close in the model with 10 to 20 percent penetration more the specified 1.5 inch initial gap. Hinges 9, 11 and 13 do not close in the model, and the opening is also small. The model for the Big Bear earthquake over predicts the opening and closing of Hinge 7, as shown in Table 6.6. The model shows that only Hinges 3 and 7 close with the assumed initial hinge opening of 1.5 in. From the nonlinear model, the maximum restrainer cable stress in the Landers earthquake is 97 ksi at Hinge 3, which is less than the yield stress of 175 ksi. The maximum restrainer cable stress at Hinge 7 is 68 ksi. The restrainer cables at the other hinges are stressed much less. The tension model overestimates the hinge opening and the restrainer stress, with the latter having a maximum of 142 ksi.

Table 6.5. Maximum Longitudinal Hinge Displacements for Landers Earthquake

		Hinge Opening Displacement (in)		Hinge Closing Displacement (in)	
Hinge	Side	Model	Recorded	Model	Recorded
Hinge 3	In	2.88		1.66	
	Out	2.28		1.56	
Hinge 7	In	2.04	1.41	1.57	1.03
	Out	1.69		1.57	
Hinge 9	In	0.54		0.56	
	Out	0.55		0.59	
Hinge 11	In	0.84	0.67	0.96	0.86
	Out	1.20		1.32	
Hinge 13	In	1.21		1.25	
	Out	1.38		1.20	

Table 6.6. Maximum Longitudinal Hinge Displacements for Big Bear Earthquake

		Hinge Opening Displacement (in)		Hinge Closing Displacement (in)	
Hinge	Side	Model	Recorded	Model	Recorded
Hinge 3	In	2.64		1.68	
	Out	2.52		1.68	
Hinge 7	In	2.46	1.70	1.56	1.44
	Out	2.47		1.56	
Hinge 9	In	0.60		0.64	
	Out	0.60		0.77	
Hinge 11	In	0.78	0.56	0.73	0.63
	Out	1.32		1.32	
Hinge 13	In	1.52		1.32	
	Out	1.32		1.30	

6.6 Column Forces

With the calibrated models of the Connector, the maximum forces in the columns can be computed. Figures 6.11 to 6.14 show the maximum shear force and maximum bending moment at the base of each column due to dead load and earthquake response. The forces are computed for three models: (i) the nonlinear model with the hinge opening and closing; (ii) the linear compression model; and (iii) the linear tension model. The longitudinal shear force and moment are due to weak axis bending of the columns in the longitudinal (tangential) direction. The transverse shear force and moment are due to strong axis bending of the columns in the transverse (radial) direction.

Considering the longitudinal shear and moments in the columns for the Landers earthquake in Fig. 6.11, the compression model provides larger forces than the tension model for the short columns, particularly at the end frames. The tension model gives larger forces than the compression model for the taller columns. However, the two linear models do not provide an upper bound on the forces for all columns. The nonlinear model produces larger transverse forces for the Bents 4 to 7 due to pounding at Hinge 7. Other than these two columns, the nonlinear model gives forces that are less than the forces from the tension and compression models.

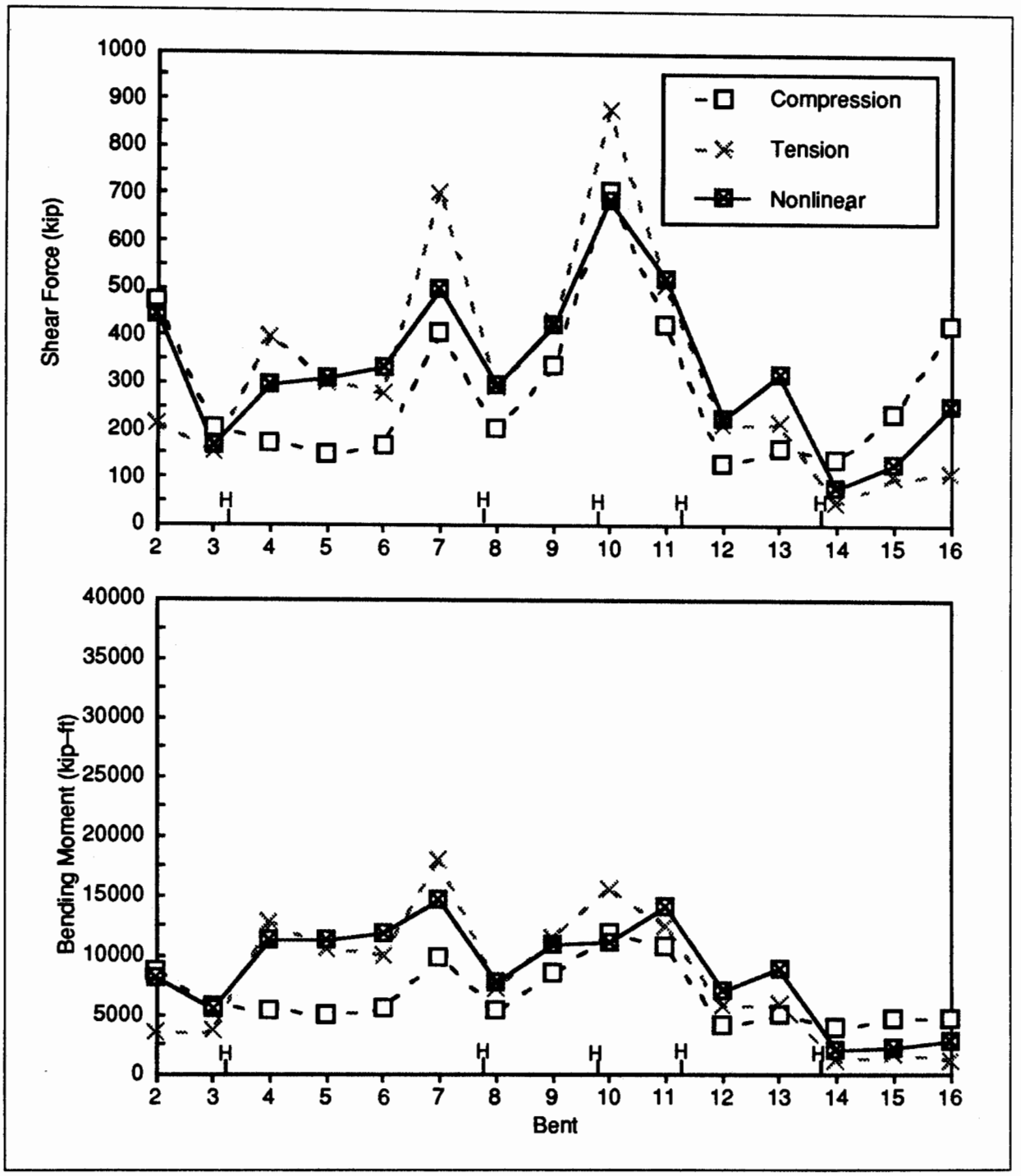

Figure 6.11 Longitudinal Forces in Columns for Landers Earthquake Computed from Three Models.

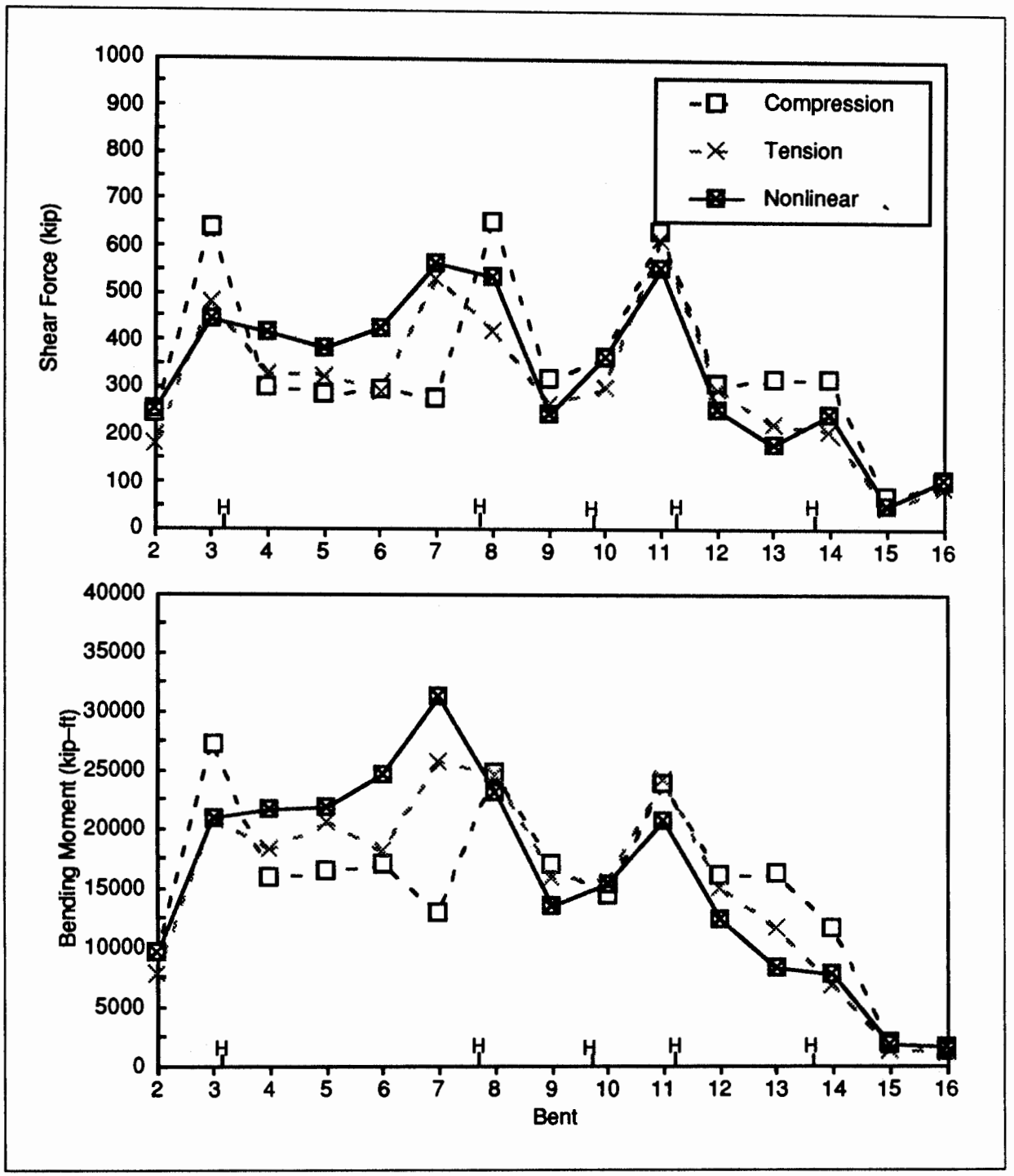

Figure 6.12 Transverse Forces in Columns for Landers Earthquake Computed from Three Models.

The forces predicted by the model in the Big Bear earthquake (Figs. 6.13 and 6.14) show similar trends as the forces in Landers. The tension and compression models bound the forces very well except for the frame H3–H7, in which the nonlinear model gives moments about 30 percent greater than the moments from the tension model. The increase in forces compared with the tension model is due to the pounding at Hinges 3 and 7.

To compare the computed forces in the columns with the strength of the columns, the moment–curvature relationship for each column is computed using a concrete strength of 4000 psi, steel yield stress of 66 ksi, the static axial force, and neglecting the effect of the steel jacket except for confinement. The bending moments in the columns during the Landers earthquake are less than the idealized yield moments for most of the columns. For the longitudinal direction, the maximum moment at Bent 9 is 59 percent of the idealized yield moment. For the transverse direction, Bent 8 is the most heavily loaded at 77 percent of the idealized moment, although the moment–curvature analysis indicates that the outer layer of steel has yielded. Six other bents are loaded from 50 to 70 percent of the idealized flexural strength in the transverse direction.

From the moment–curvature relationships it is possible to determine the effective stiffness of the columns in the transverse direction neglecting the effective of the steel jacket. The effective stiffness varies between 1.10 times the gross moment of inertia for the heavily reinforced columns in Bents 4 to 6, down to a factor of 0.38 for Bents 12 and 13. The transformed stiffness can be considerably larger. The effective stiffness in the longitudinal direction is similar. This compares with the fitted factors of 1.05 and 0.85 from the models, assuming the steel jacket increases the stiffness 10 to 15 percent.

6.7 Response to Larger Earthquake

The ground motion at the Connector site had peak ground accelerations less than 0.10 g in the Landers and Big Bear earthquakes. To investigate what the response of the bridge would be in a larger earthquake, the Landers free–field ground motion is multiplied by a factor of four. The scaled free–field ground motion has a peak acceleration of 0.35 g. This scaled ground motion is typical of a design earthquake ground motion as given by the ARS spectrum.

Figures 6.15 and 6.16 shows the maximum bending moments in the columns for the Connector subjected to the amplified ground motion. The nonlinear effect of hinge behavior can be seen by comparing the forces with the results for unscaled Landers in Figs. 6.11 and 6.12. For example, closing at Hinge 13 with the amplified ground motion provides additional load on the last frame increasing the longitudinal forces in Bents 14 to 16 as compared with the values predicted by the

compression model (Fig. 6.15). In contrast, the smaller response to unscaled Landers does not close Hinge 13, so the forces in the end frame are similar to the values for the tension model (Fig. 6.11). Similar trends are noted at the first frame, although the effect on maximum moment is not as large. Other than the end frames, the two linear models provide an upper bound (or close to it) on forces in the columns.

Table 6.7 lists the maximum hinge opening for the scaled ground motion from the nonlinear model with cable restrainers at the hinges. The maximum opening is 8.68 in. at Hinge 3, which is much less than the seat width of 30 in., so hinge unseating cannot occur although the elastomeric bearing pads would be damaged. The maximum stress in the restrainer cables is 359 ksi, which is greater than the yield stress of 175 ksi since the inelastic yielding of the cables is not represented in the model. The tension model predicts a cable stress of 555 ksi at that hinge, and greatly overestimates the cables stresses at the other hinges.

To investigate the effect of the cable restrainers on the response of the Connector to the scaled Landers earthquake, the maximum moments in the columns are plotted in Fig. 6.17 for the bridge with and without cable restrainers. The restrainers have a small effect on the forces, except for an increase of transverse moment at Bents 4 and 5 because of transfer of longitudinal forces across Hinge 3 and an increase at Bent 11 because of restraint of frame H9–H11. When cable restrainers are absent, the hinges open about 30 percent more, as shown in Table 6.6.

Table 6.7. Maximum Longitudinal Hinge Displacement for Landers Earthquake Scaled by Four

Hinge	Side	Hinge Opening Displacement (in)	
		With Restrainers	No Restrainers
Hinge 3	In	8.68	9.06
	Out	7.36	7.69
Hinge 7	In	4.76	6.68
	Out	4.50	7.20
Hinge 9	In	1.31	1.50
	Out	1.46	1.54
Hinge 11	In	2.54	3.55
	Out	5.00	6.20
Hinge 13	In	4.64	4.94
	Out	3.37	4.82

Figure 6.17 also plots the idealized yield moment of the columns in each direction. In the longitudinal direction the largest overstrength ratio is 2.92 for Bent 9. In the transverse direction the largest overstrength ratio is 3.28 for Bent 3 and four other bents have ratios greater than 2.5. For the amplified ground motion, the overstrength ratios indicate that there would be moderate yielding in most of the columns with weak axis plastic hinging.

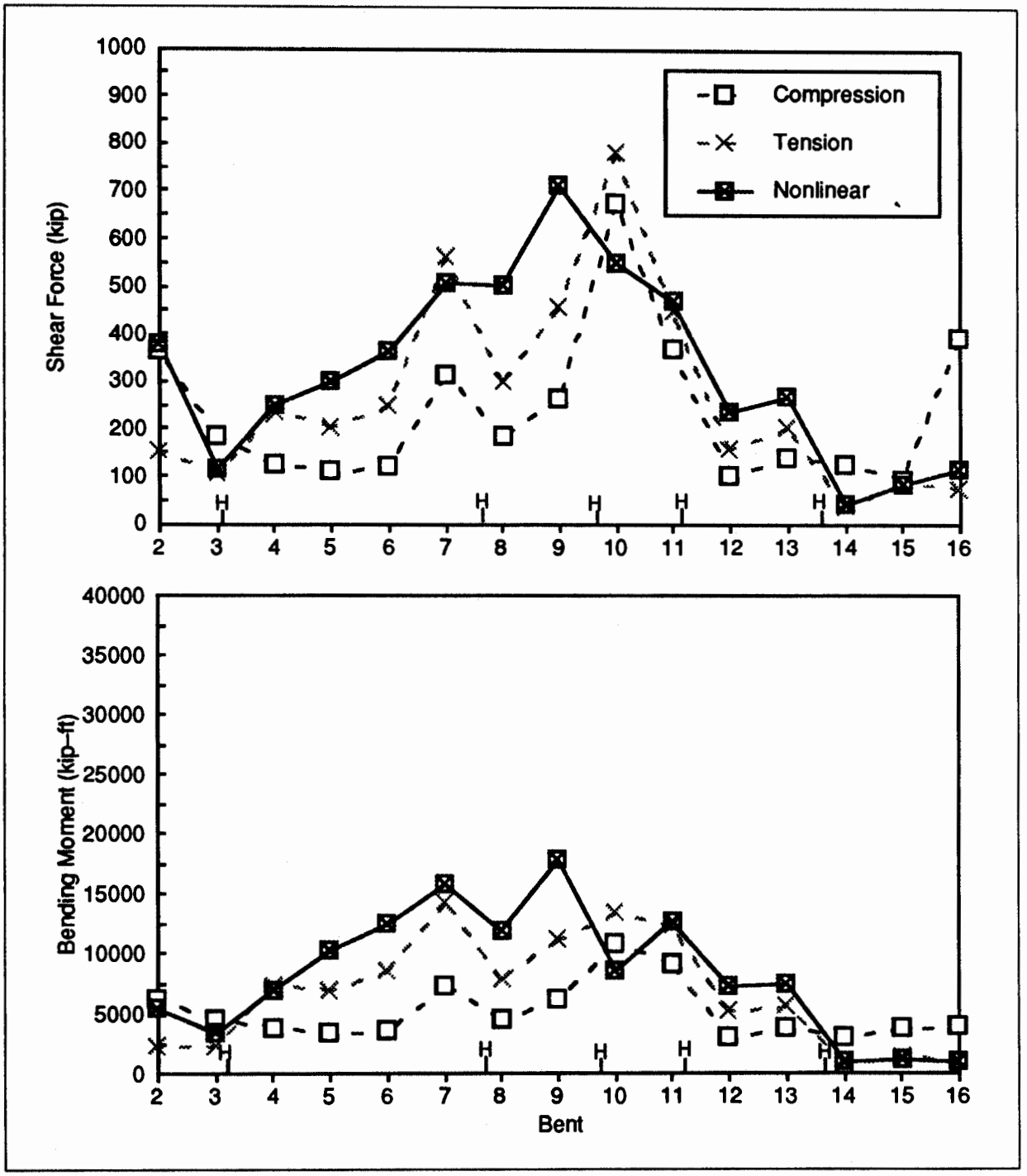

Figure 6.13 Longitudinal Forces in Columns for Big Bear Earthquake Computed from Three Models.

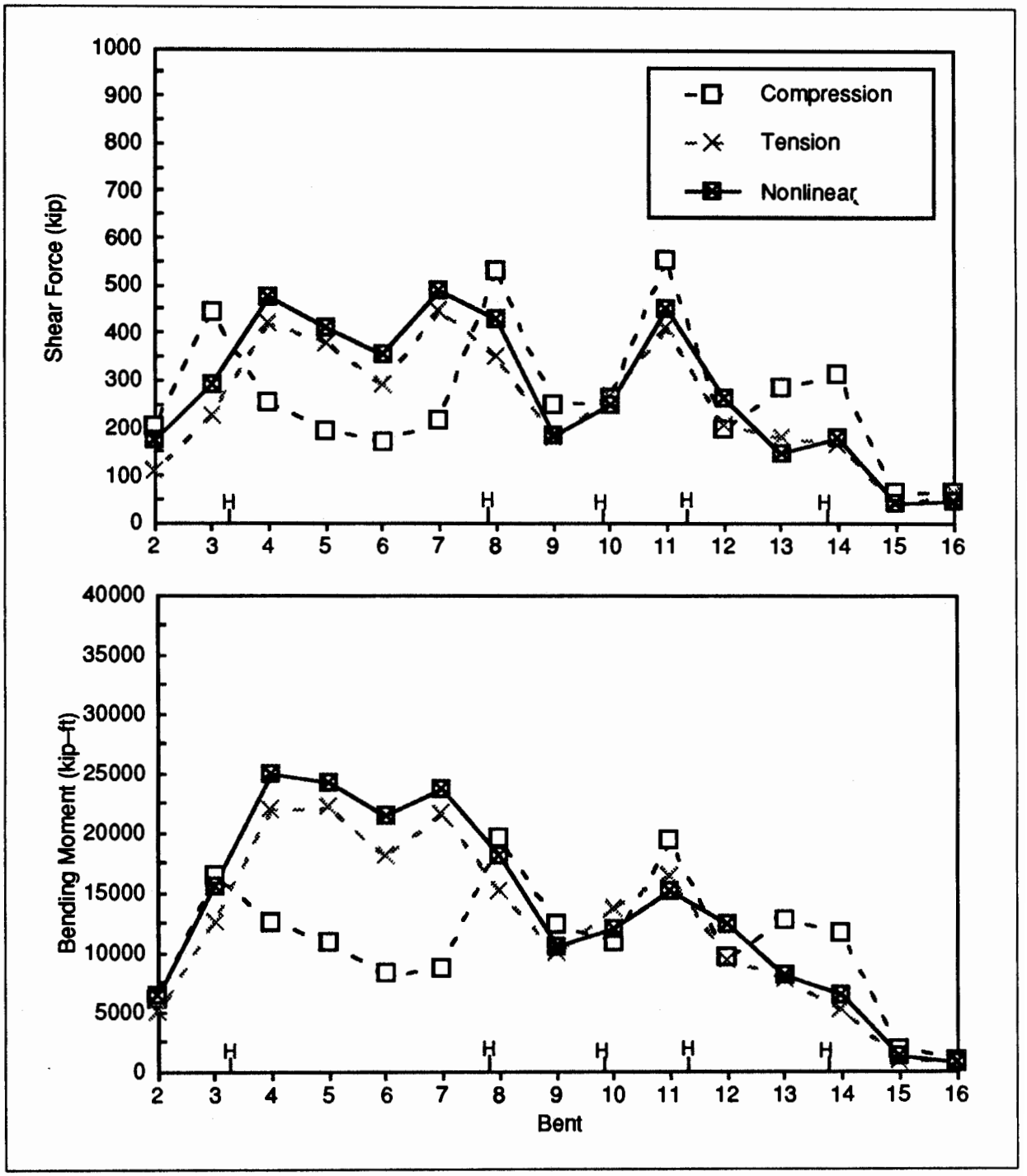

Figure 6.14 Transverse Forces in Columns for Big Bear Earthquake Computed from Three Models.

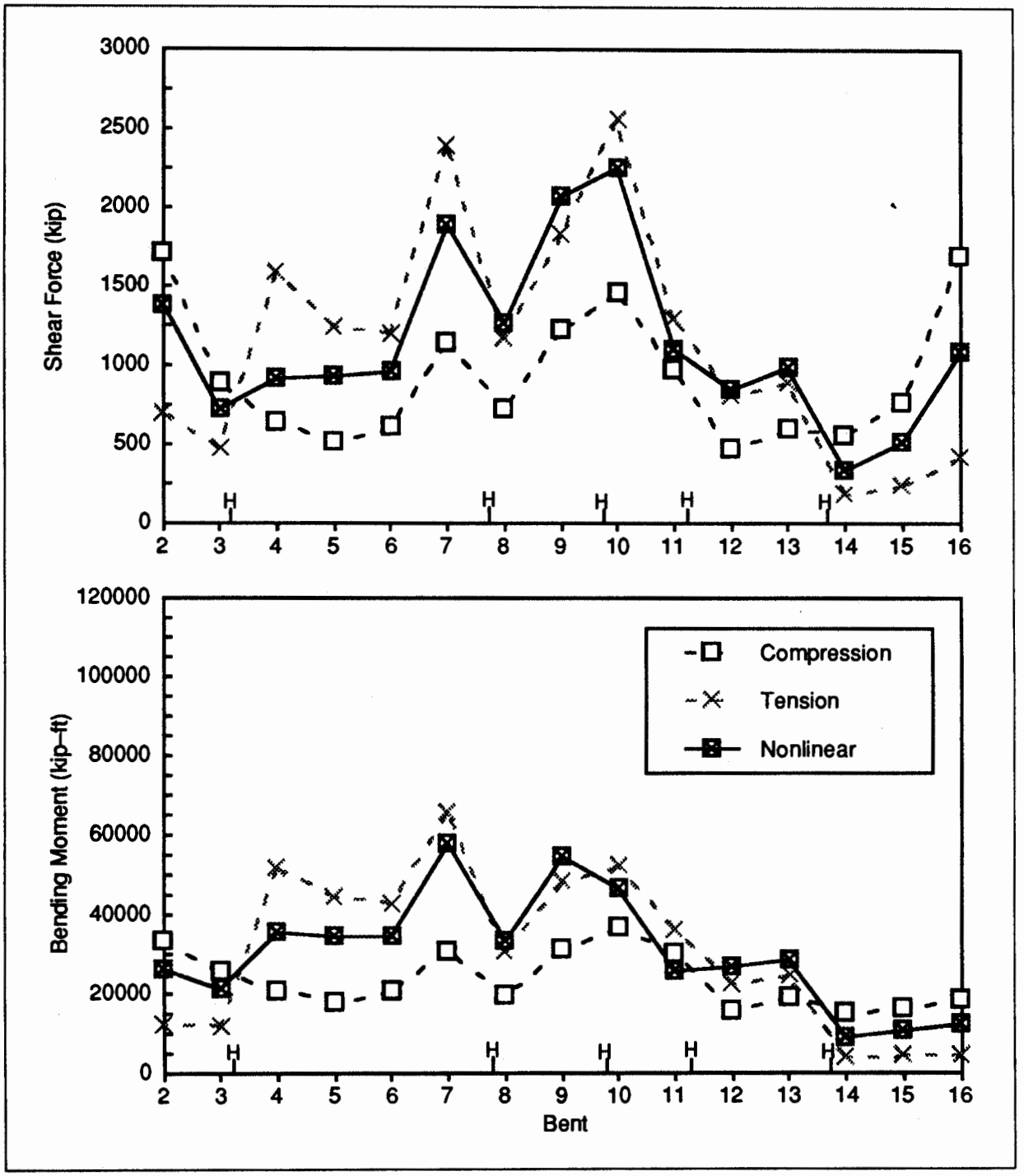

Figure 6.15 Longitudinal Forces in Columns for Landers Earthquake, Scaled by Four, Computed from Three Models.

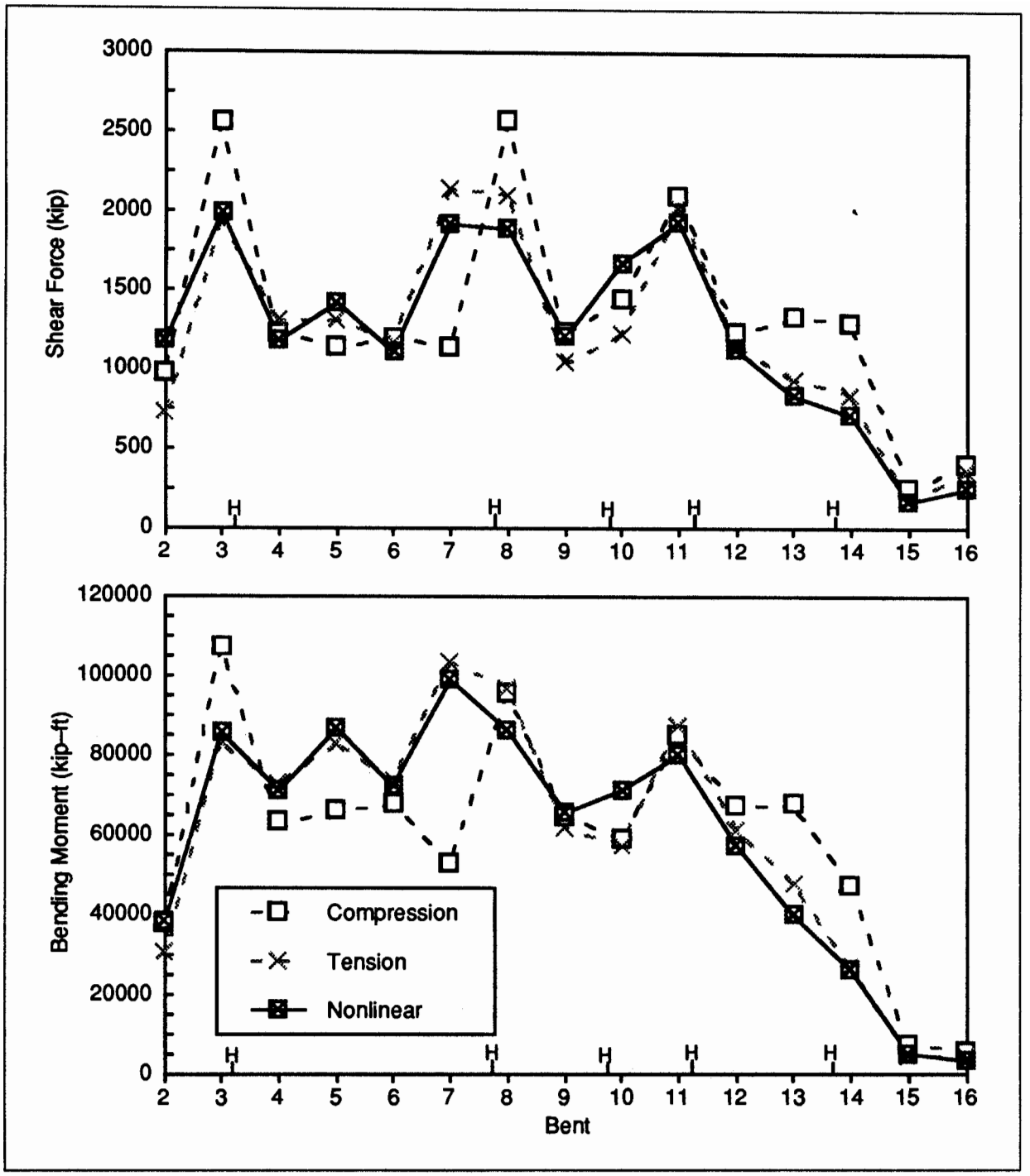

Figure 6.16 Transverse Forces in Columns for Landers Earthquake, Scaled by Four, Computed from Three Models.

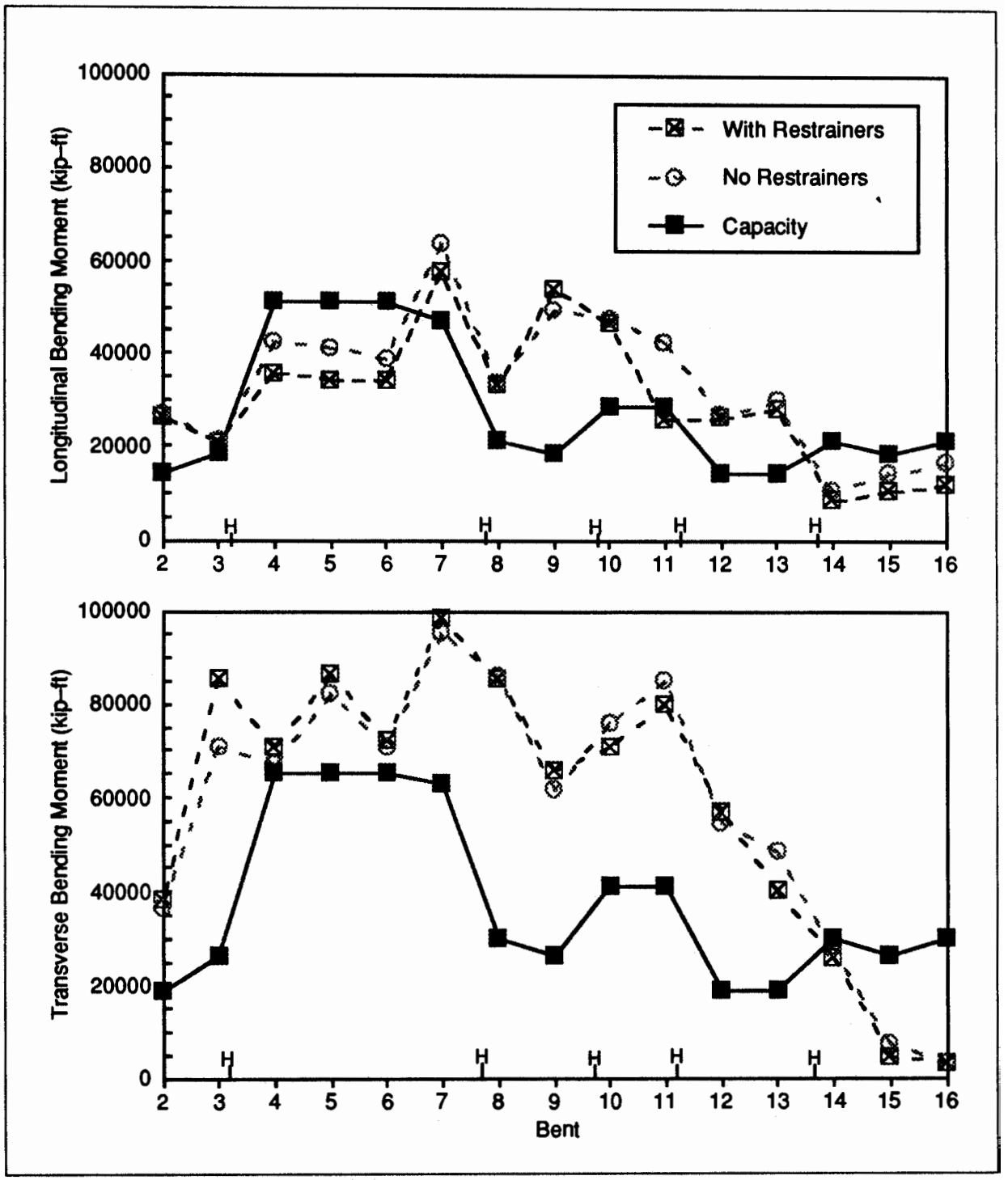

Figure 6.17 Effect of Cable Restrainers on Bending Moments in Columns for Landers Earthquake Scaled by Four.

Chapter 7

CONCLUSIONS AND RECOMMENDATIONS

The strong motion of the Northwest Connector in the 1992 Landers and Big Bear earthquakes was recorded by an instrumentation network. Although the peak ground acceleration at the site for both earthquakes was approximately 0.10 g, much less than the level of ground motion expected in a major earthquake, the strong motion data provides important information about the earthquake response of this typical curved freeway bridge.

The objectives of this study have been to:

- evaluate the importance of non–uniform support motion on the response of the bridge;
- determine the vibration properties of the bridge;
- determine efficacy of typical modeling and dynamic analysis techniques used in the design of bridges to predict the response recorded in the earthquakes;
- examine role of the intermediate hinges on the earthquake response of the bridge.

This chapter summarizes the major findings and conclusions related to these objectives, and it provides recommendations for improving the modeling and earthquake analysis of bridges.

7.1 Summary of Earthquake Response

Importance of Non–uniform Support Motion

The input motion at the supports of a bridge can vary because of incoherence, wave passage, site response, and soil–structure interaction effects. For the Northwest Connector, the input motion was fairly uniform in the two earthquakes.

The maximum relative displacement between the abutments is 3.04 inches and 2.58 inches for the Landers and Big Bear earthquakes, respectively. These relative support displacements are small for a 2540 ft long bridge; they can be easily accommodated as pseudo–static displacements, primarily at the hinges. The displacement histories for the free–field motion, and input motion at four supports are very similar.

The coherency functions for the support motion show that for frequencies less than 2 Hz, the input motion is fairly coherent. It may be concluded that the spatial variation of the input motion is not significant within the range of important vibration frequencies for the Connector.

Characteristics of Recorded Earthquake Response

The earthquake response of the Connector is predominantly transverse. There are two reasons: the input motion is stronger in the transverse direction than the longitudinal direction, and the important vibration modes of the bridge involve transverse motion. Bent 8 near the center of the bridge is the most heavily instrumented bent. The maximum transverse deformation of the column is 4.76 in. for Landers (drift=0.86%), and 2.98 in. for Big Bear (drift=0.54%). Assuming single curvature, these displacements are less than the drift at yield of 6.10 inches.

The pile cap rotation is not negligible; it produces an additional displacement of 0.63 in. at the top of the column in Landers and 0.47 in. in Big Bear. The rotational flexibility of the foundation contributes 13 percent of the transverse displacement of the deck in Landers and 16 percent in Big Bear.

Response of Intermediate Hinges

The strong motion records show the effects of pounding as evidenced by large acceleration spikes for instruments near the five intermediate hinges. Using the processed displacement records, Hinge 7 has the largest opening: 1.41 in. in Landers and 1.70 in. in Big Bear. Hinge 7 closes at most about 1/2–inch during the first 25 seconds of the Landers earthquake. Later the maximum closing displacement is about one inch, indicating that polystyrene filler material (nominally 2 in. thick) in the hinge crushed during the strong motion response. The opening at Hinge 11 is less than the opening of Hinge 7, and the maximum closing displacement is 0.86 in. Several of the closing excursions show the high frequency oscillation associated with pounding.

Hinge 7 opens more in the Big Bear earthquake than in Landers. The maximum closing displacement is nearly 1.5 in., indicating accumulated crushing of filler in the hinge in the second earthquake. The response of Hinge 11 is similar for the two earthquakes.

In the transverse direction, the relative displacement at a hinge is constrained by a shear key. From the processed displacements at the five intermediate hinges, the following observations can be conjectured. During the early parts of the Landers earthquake, when the motion is small, the keys limit the transverse displacement to the nominal gap in some hinges (such as Hinge 3); and friction and perhaps excess filler or other material nearly eliminate all transverse displacement in the other hinges (such as Hinge 7). As the motion increases, local crushing of concrete at the key allows larger transverse displacements. When the Big Bear earthquake occurs, the shear keys have been "loosened-up" by the earlier Landers earthquake, exhibiting more relative transverse displacement. The shear keys are effective in limiting the relative displacement to a maximum of 0.61 in. compared with a transverse displacement of nearby Bent 8 of over 5 in. The maximum relative transverse displacements, however, are greater than the nominal 1/4-inch gap, indicating the shear keys likely suffered minor local damage.

From the processed vertical displacement records for Hinge 7, it appears that slight lift-off and pounding occurred on the inside edge of the Hinge 7, with rotation about the outside edge. Caltrans personnel noted possible settlement at the hinges after the earthquakes.

Vibration Properties of the Bridge

Spectral analysis and parametric identification techniques (using digital filters) were used to identify the vibration periods of the Connector from the earthquake records. The most significant finding is the difference in the fundamental mode period of the Connector in the Landers and Big Bear earthquakes. The fundamental period lengthens from 1.56 sec in Landers to 1.75 sec in Big Bear. The change in period implies a 25 percent reduction in the stiffness of the bridge. Although there is little change in the second mode, the periods of the third and fourth mode are longer in the Big Bear earthquake. The other noticeable difference between the two earthquakes is that the damping ratio increases in the first and third mode, although it decreases in the second mode.

The lengthening of the vibration periods and generally increased damping may indicate that the bridge "softened" in the Landers earthquake. Since the forces in the columns were less than the yield strength, it is unlikely that the softening was due to structural damage although flexural cracking of the columns may have occurred. A more likely explanation is that the soil and pile foundations loosened in the Landers earthquake due to compaction and/or gapping of soil surrounding the piles. This soil behavior provided a larger flexibility in the Big Bear earthquake. Another possible explanation is that the crushing of filler material in the hinges during the Landers earthquake reduced the interaction between adjacent frames in the Big Bear earthquake (as evidenced by larger longitudinal hinge opening), producing a more

flexible bridge. Once the processed records from the 1994 Northridge earthquake are available (CSMIP, 1994), it would be interesting to examine the vibration properties for comparison with the properties from the two 1992 earthquakes.

7.2 Summary of Modeling Assumptions and Response Correlation

The approach in this study was to use modeling and dynamic analysis procedures typically used for bridge design. Since the structural components of the Connector did not experience inelastic deformation in the earthquakes, it is appropriate to use linear elastic models for the components. The opening and closing of the intermediate hinges, however, is nonlinear and that behavior is represented in the model. Although the behavior of the foundation and soils is nonlinear, as evidenced by the change in vibration properties of the bridge in the two earthquakes, the foundations are modeled as linearized springs.

Modeling Assumptions

The following summarizes the major assumptions in the modeling of the Connector:

- The elastic modulus for concrete was based on the design strength, increased by 20 percent for overstrength.
- For the conventionally reinforced spans, the moments of inertia are the gross sections multiplied by 0.75 to account for cracking. There is no reduction from the gross section for the prestressed spans. Section properties near the bent cap are reduced based on the effective width of the bent cap.
- Each span of the box girder is modeled by four or five elements. The torsional mass moment of inertia is included along with the translational inertia.
- The hinges are modeled with nonlinear compression–only and tension–only elements to allow relative longitudinal displacement, but relative transverse displacement is constrained.
- Each column is modeled by three elements. The gross moments of inertia are increased by 10 or 15 percent to account for the steel jackets. The modified moments of inertia are reduced to match the fundamental vibration period of the model with the lowest identified period from the earthquake response, as described below.
- The pile foundations are modeled by translational and rotational springs. The translational spring stiffness is based on a lateral stiffness of 65 kip/in per pile for the firm sandy soils at the site. The rotational stiffness coefficient is 4×10^7

kip–ft for Landers and $2x10^7$ kip–ft for Big Bear, based on the recorded pile cap rotation of Bent 8 in the two earthquakes.

- The abutments are modeled by longitudinal and transverse springs following standard Caltrans guidelines.

- Based on the identified damping ratios, 3 percent damping for all modes is used for modeling the response of the Connector in the Landers earthquake and 5 percent for all modes in the Big Bear earthquake.

The modified gross moments of inertia for the columns were scaled to match the vibration periods of the Connector in the two earthquakes. For the Landers model, the modification factor is 1.05; for the Big Bear earthquake the factor is 0.85. The reduction in stiffness of the columns between the two earthquakes, along with the reduced rotational stiffness for the pile foundations, accounts for the lengthening the vibration periods identified from the recorded motion.

Response Comparison

The free–field ground motion is assumed as uniform earthquake input to the model. With these assumptions, the comparison between the model motion and recorded motion is good in many aspects, but deficient in other aspects. The following summarizes the response comparison

- The horizontal and vertical translation of the supports are well represented by the model. This indicates that the assumptions for the free–field input motion and support springs are adequate.

- Much of the transverse response is captured in the model, although there are some differences. For channel 7, near Bent 3, the model has many of the peaks in the recorded response and the phase comparison is good, particularly for Landers. However some of the recorded peaks are under–estimated by the model.

- The phasing in channel 11 for the Big Bear earthquake is not particularly good. This may indicate that the Big Bear model does not represent the transverse modes of the span well, or nonlinear response changes the characteristics of the bridge or foundation during the earthquake in a manner not captured by the model.

- The longitudinal response is very well represented in the model for both earthquakes.

- The vertical response of the bridge in the two earthquakes is captured very well by the model.

The model's ability to represent the opening and closing of hinges was examined in detail. The major observations are:

- The model overestimates the 1.41 in. opening of Hinge 7 in the Landers (it gives 1.92 in.). The opening of Hinge 11 is represented well for Landers. The model for Big Bear also overestimates hinge opening displacements, but not as much as for Landers.

- Although the nonlinear hinge model represents the overall characteristics of the relative hinge displacement, the model does not provided accurate velocity or acceleration of the hinge. Both show high frequency oscillations that may be caused by lack of energy dissipation in the hinge model.

- Based on the assumption of 0.5 in. slack, the models show that the restrainers cable develop stresses less than one–half the yield stress in the two earthquakes.

7.3 Forces in the Columns and Effectiveness of Restrainers

Using the models, the forces in the columns were computed for the two earthquakes. The forces show the nonlinear effects of hinge opening and closing. The tension and compression models typically used in design do not always provide an upper bound on the forces in the columns, since the linear models cannot include the effects of frames pounding against each other. The maximum forces in the columns in the earthquakes were less than the idealized flexural strength. The most heavily loaded column was Bent 9 in the Landers earthquake, with a maximum bending moment that was 73 percent of the idealized flexural strength, although the moment was enough to cause yielding in some longitudinal reinforcement.

To examine the response of the Connector in a larger earthquake, the model was subjected to the Landers free–field ground motion scaled by a factor of four. Although the tension and compression models do not provide an upper bound on the bending moments in two of the columns, the bounds are close enough for design purposes. The maximum moments are approximately 3.25 times the flexural capacity, an acceptable value for this level of earthquake ground motion.

With the scaled Landers ground motion, the maximum opening displacement is 8.68 in. at Hinge 3, which is much less than the seat width of 30 in., so unseating cannot occur. The maximum stress in the linear model of the restrainer cable is 359 ksi, indicating that the cable will yield. The tension model greatly overestimates the restrainer stresses and forces.

The restrainers have a small effect on the response of the Connector to the scaled Landers earthquake. The lack of restrainers slightly increases the opening at some hinges, but in fact reduces the opening at other hinges because of changes in out–of–phase motion.

7.4 Recommendations

Strong Motion Instrumentation

The number and quality of the digital strong motion instruments is an improvement over the earlier instrumented bridges which had a small number of accelerometers with film recorders. However, a few improvements in the strong motion instrumentation can be suggested.

Since the issue of non–uniform motion is poorly understood, additional information about the free–field ground motion at the site would be helpful. It would be desirable to have at least two free–field instruments separated by a distance equal to the bridge length to allow characterization of the coherence at the site. Timing between all instruments, free–field and structure, is essential. More reliable timing mechanisms should be implemented in the field.

The processing of strong motion acceleration records makes it impossible to determine permanent offset displacements of the hinges. It may be possible to retain the long period signals in the processing to estimate the offset after an earthquake. This type of processing should be investigated.

The issue of hinge displacements may be better addressed with the development of rugged displacement measuring devices for hinges instead of relying on accelerometers. The measurement of hinge displacements at both edges (or sides) of hinges would help improve the understanding of hinge kinematics during an earthquake.

Finally for data utilization studies, more information about the structure and soil should be collected at instrumented bridges. In particular, concrete core samples to determine properties of the materials is necessary. A more thorough investigation for the profile and properties of the soil. The type of information collected from typical geotechnical investigation at a bridge site is not sufficient for accurate modeling beyond an approximate site response and soil–structure interaction analysis.

Modeling Guidelines

For the two earthquakes with peak ground acceleration less than 0.10 g, the elastic models of the foundations, columns, and superstructure, and the nonlinear

models of the intermediate hinges provide an adequate representation of the bridge response for the purpose of design. The response is sensitive to the assumption of the column stiffness, which is dependent on the level of motion and perhaps history.

Certainly more experimental data is needed to provide a priori estimates of column stiffness. In lieu of the lack of data it is prudent to base design decisions on a range of reasonable assumptions for column stiffness instead of a single value. Similar comments apply to foundation stiffness and locations for the point of fixity for columns.

Although the simple hinge model used in this study appears to capture the overall effect of hinge opening and closing, the hinge model is clearly inadequate for the high frequency response near the hinge caused by pounding. Improved methods for modeling hinges in bridges for practical analysis should be developed.

Implications for Bridge Design

The tension and compression models provide an upper bound on forces for many columns but not all, since they do not represent the nonlinear dynamics of hinge pounding. Based on this study, however, the tension and compression models capture the overall response of the Connector accurately enough to make design decisions. A further aspect that must be considered though is that once a column yields, pounding of adjacent frames may substantially increase the ductility demands of the yielded columns.

The nonlinear hinge models with elastic models for the remainder of the structure have several advantages over the linear models. The nonlinear models provide reasonable estimates of hinge opening and restrainer forces. Further, the nonlinear models can indicate transfer of forces by pounding, and isolation of frames by hinge opening. It is recommended that this type of modeling be considered for evaluating bridges in which hinge opening is judged to be an important effect. Such does not appear to be the case for the Colton connector.

Further Research

The study has illuminated many aspects of earthquake response of connector bridges and the ability of models to represent the strong motion response. The following areas could benefit from further research:

- improved methods of system identification for nonlinear systems to identify opening and closing of hinges and changes in stiffness;
- better modeling of columns, particularly with steel jacket retrofits, calibrated against experimental test data;

- improved models of intermediate hinges that provide information about damage and energy dissipation, and can represent the velocity and acceleration of the hinges more accurately.

More strong motion data from the Northwest Connector and other bridges will provide more information about whether the conclusions of this study are specific to the case studied or can be generalized. It is believed, however, that the conclusions of this study are generally applicable to other connector bridges.

Chapter 8

REFERENCES

Abrahamson, N. (1988). "Empirical Models of Spatial Coherency of Strong Motion Records," Second Workshop on Strong Motion Arrays, Taipei, Taiwan, pp. 65–92.

Abrahamson, N. A. (1985). "Estimation of Seismic Wave Coherency and Rupture Velocity Using the SMART–1 Strong Motion Array Recordings," *Report No. UCB/EERC–85/02*, Earthquake Engineering Research Center, University of California at Berkeley.

ACI (1989). *Building Code Requirements for Reinforced Concrete*, American Concrete Institute, Detroit, MI.

Astrom, K. J. and B. Wittenmark (1990). *Computer–Controled Systems*, Prentice–Hall, Englewood Cliffs, NJ.

Beck, J. L. (1978). "Determining Models of Structures from Earthquake Records," *Report No. EERL 78–01*, Earthquake Engineering Research Laboratory, California Institute of Technology.

Beck, J. L. and L. S. Katafygiotis (1992). "Probabilistic System Identification and Health Monitoring of Structures," Tenth World Conference on Earthquake Engineering, Vol. 7, Madrid, Spain, pp. 3721–3726.

Bollo, M., S. A. Mahin, et al. (1990). "Observations and Implications of Tests on the Cypress Street Viaduct Test Structure," *Report No. UCB/EERC–90/21*, Earthquake Engineering Research Center, University of California at Berkeley.

Caltrans (1990). "Bridge Design Specifications Manual," California Department of Transportation.

CDMG (1977). "Special Studies Zones, San Bernardino South Quadrangle," Sacramento, CA, California Division of Mines and Geology.

Chen, S. S., J. B. Mander, et al. (1993). "Structural Modeling Implications from Snap–Back Tests on a Slab–on–Girder Bridge," Ninth U.S.–Japan Bridge Engineering Workshop, Tsukuba Science City, Japan.

Clough, R. W. and J. Penzien (1993). *Dynamics of Structures*, Second Edition, McGraw–Hill, New York.

CSMIP (1994). "Strong Motion Records from the Northridge, California Earthquake of January 17, 1994," *Report No. OSMS 94–07*, Office of Strong Motion Studies, Division of Mines and Geology.

Darragh, R., T. Cao, et al. (1993). "Processed CSMIP Strong–Motion Records from the Landers and Big Bear, California, Earthquakes of 28 June 1992 — San Bernardino, I10/215 Interchange," *Report No. OSMS 93–08*, Office of Strong Motion Studies, Division of Mines and Geology.

Darragh, R. B., T. Q. Cao, et al. (1993). "Strong Motion Data from the Large California Earthquakes of 1992," SMIP 93, Sacramento, CA, pp. 13–26.

Doser, D. I. (1992). "Historic Earthquakes (1918 to 1923) and an Assessment of Source Parameters Along the San Jacinto Fault System," *Bulletin of the Seismological Society of America*, Vol. 82, No. 4, pp. 1786–1801.

Douglas, B. M., E. A. Maragakis, et al. (1990). "Analytical Studies of the Static and Dynamic Response of the the Meloland Overcrossing," Fourth U.S. National Conference on Earthquake Engineering, Vol. 1, Palm Springs, CA, pp. 997–992.

Douglas, B. M., G. Norris, et al. (1984). "Behavior of the Meloland Road Overcrossing During the 1979 Imperial Valley Earthquake," Seismic Research for Highway Bridges (U.S.–Japan Program), Pittsburgh, PA, pp. 339–366.

Fenves, G. L. (1992). "Earthquake Analysis and Response of Multi–span Bridges and Viaduct Structures," Seismic Design and Retrofit of Bridges, Berkeley, CA,

Fenves, G. L., F. C. Filippou, et al. (1992). "Response of the Dumbarton Bridge in the Loma Prieta Earthquake," *Report No. UCB/EERC–92/02*, Earthquake Engineering Research Center, University of California at Berkeley.

Gardner–Morse, M. G. and D. R. Huston (1993). "Modal Identification of Cable–Stayed Pedistrian Bridge," *Journal of Structural Engineering*, ASCE, Vol. 119, No. 11, pp. 3384–3404.

Gates, J. H. and M. J. Smith (1984). "Results of Ambient Vibration Testing of Bridges," Eighth World Conference on Earthquake Engineering, Vol. VI, San Francisco, CA, pp. 873–880.

Goel, R. K. and A. K. Chopra (1994). "Seismic Response Study of the US 101/Painter Street Overpass Using Strong Motion Records," SMIP 94 Seminar, Los Angeles, pp. 75–88.

Hao, H. (1989). "Effects of Spatial Variation of Ground Motions on Large Multiply-Supported Structures," *Report No. UCB/EERC–89/06*, Earthquake Engineering Research Center, University of California at Berkeley.

Hjelmstad, K. D., S. L. Wood, et al. (1992). "Mutual Residual Energy Method for Parameter Estimation of Structures," *Journal of Structural Engineering*, ASCE, Vol. 119, No. 1, pp. 223–242.

Hogue, T. D., A. E. Aktan, et al. (1991). "Localized Identification of Constructed Facilities," *Journal of Structural Engineering*, ASCE, Vol. 117, No. 1, pp. 128–148.

Imbsen, R. A., R. V. Nutt, et al. (1978). "Seismic Response of Bridges–Case Studies," *Report No. UCB/EERC–78/14*, Earthquake Engineering Research Center, University of California at Berkeley.

Jackura, K. A. (1991). "Study of Liquefaction Potential at the I–10/I–215 Interchange in San Bernardion County," California Department of Transportation.

Kanamori, H., H. K. Thio, et al. (1992). "Initial Investigation of the Landers, California, Earthquake of 28 June 1992 Using TERRAscope," *Geophysical Research Letters*, Vol. 19, No. 22, pp. 2267–2270.

Katafygiotis, L. S. (1991). "Treatment of Model Uncertanties in Structural Dynamics," *Report No. EERL 91–01*, Earthquake Engineering Research Laboratory, California Institute of Technology.

Kim, W. and A. H. Ang (1992). "Damage Assessment of Existing Bridge Structures with System Identification," Tenth World Conference on Earthquake Engineering, Vol. 8, Madrid, Spain, pp. 4887–4891.

Knott, J. R. and A. F. Goldschmidt (1991). "Engineering Geology Report, Route 215/10 Interchange, San Bernardino County, CA," California Department of Transportation, Engineering Geology Branch–South.

Kubo, T. and J. Penzien (1977). "Characteristics of Three–Dimensional Ground Motions Along Principal Axes: San Fernando Earthquake," Sixth World Conference on Earthquake Engineering, New Delhi.

Ljung, L. (1987). *System Identification*, Prentice–Hall, Englewood Cliffs, NJ.

Malhotra, P. K., M. J. Huang, et al. (1994). "Interaction at Separation Joints of the I10/215 Bridge During Earthquakes," SMIP 94 Seminar, Los Angeles, CA, pp. 49–59.

Maroney, B., K. Romstad, et al. (1990). "Interpretation of Rio Dell Freeway Response During Six Recorded Earthquake Events," Fourth U.S. National Conference on Earthquake Engineering, Vol. 1, Palm Springs, CA, pp. 1007–1016.

McCallen, D. B. (1992). "Response Studies of the Dumbarton Bridge," Lawerence Livermore National Laboratory.

McCallen, D. B. (1993). "Nonlinear Study of Painter Street Overcrossing," Lawerence Livermore National Laboratory.

Mitchell, L. D. (1982). "Improved Methods for the Fast Fourier Transform (FFT) Calculation of the Frequency Response Function," *Journal of Machine Design*, ASME, Vol. 104, pp. 277–279.

Moehle, J. P. (1994). "Preliminary Report on the Seismological and Engineering Aspects of the January 17, 1994 Northridge Earthquake," *Report No. UCB/EERC–94/01*, Earthquake Engineering Research Center, University of California at Berkeley.

Oppenheim, A. V. and R. W. Schafer (1989). *Discrete–Time Signal Processing*, Prentice–Hall, Englewood Cliffs, NJ.

Pandit, S. M. (1991). *Modal and Spectrum Analysis*, John Wiley, New York, NY.

Prakash, S. and H. Sharma (1990). *Pile Foundations in Engineering Practice*, John Wiley, New York, NY.

Priestley, M. J. N., F. Seible, et al. (1992). "Seismic Retrofit of Bridge Columns Using Steel Jackets," Tenth World Conference on Earthquake Engineering, Vol. 9, Madrid, Spain, pp. 5285–5290.

Priestley, M. J. N., F. Seible, et al. (1994). "The Northridge Earthquake of January 17, 1994: Damage Analysis of Selected Freeway Bridges," *Report No. SSRP–94/06*, Structural Systems Research Project, AMES, University of California, San Diego.

Raghavendrachar, M. and A. E. Aktan (1992). "Flexibility by Multireference Impact Testing for Bridge Diagnostics," *Journal of Structural Engineering*, ASCE, Vol. 118, No. 8, pp. 2166–2203.

Richardson, J. A. and B. M. Douglas (1993). "Results from Field Testing a Curved Box Girder Bridge using Simulated Earthquake Loads," *Earthquake Engineering and Structural Dynamics*, Vol. 22, No. 10, pp. 905–922.

Roberts, J. E. (1991). "Research Based Seismic Design and Retrofit of California Bridges," First Annual Seismic Research Workshop, Sacramento, CA, pp. 1–10.

Safak, E. (1991). "Identification of Linear Structures Using Discrete–Time Filters," *Journal of Structural Engineering*, ASCE, Vol. 117, No. 10, pp. 3064–3085.

Salane, H. J. and J. Baldwin J.W. (1990). "Identification of Modal Properties of Bridges," *Journal of Structural Engineering*, ASCE, Vol. 116, No. 7, pp. 2008–2021.

Sharp, R. V. (1972). "Map showing recently active breaks along the San Jacinto fault zone between the San Bernardino area and Borrego Valley, California," U.S. Geological Survey Miscellaneous Geological Investigations.

Sieh, K., C. Cheatum, et al. (1973). "Geological Investigations of Portions of the San Jacinto Fault Zone, San Bernardino Valley, California," *Geological Investigations of the San Jacinto Fault Zone*, University of California, Riverside, Riverside, CA.

Sieh, K., L. Jones, et al. (1993). "Near–field Investigations of the Landers Earthquake Sequence, April to July 1992," *Science*, Vol. 260, April 9, pp. 171–176.

Sweet, J. and K. B. Morrill (1992). "Nonlinear Soil–Structure Interaction Simulation of the Painter Street Overcrossing," Second Annual Caltrans Seismic Research Workshop, Sacramento, CA.

Tseng, W. S., M.S. Yang, et al. (1992). "Seismic Performance Investigation of the Hayward BART Elevated Section," *Report No. CSMIP/92–02*, International Civil Engineering Consultants, Inc.

USGS (1992). "The 1992 Landers Earthquake and Surface Faulting," *Earthquakes & Volcanoes*, Vol. 23, No. 5, pp. 209–218.

Werner, S. D., J. L. Beck, et al. (1987). "Seismic Response Evaluation of Meloland Road Overpass Using 1979 Imperial Valley Earthquake Records," *Earthquake Engineering and Structural Dynamics*, Vol. 15, pp. 249–274.

Werner, S. D., C. B. Crouse, et al. (1993). "Model Identification and Seismic Analysis of Meloland Road Overcrossing," Report to California Department of Transportation, Dames & Moore.

Wesnousky, S. G., C. S. Prentice, et al. (1991). "An Offset Holocene Stream Channel and the Rate of Slip Along the Northern Reach of the San Jacinto Fault Zone,

San Bernardino Valley, California," *Geological Society of America Bulletin,*, Vol. 103, No. 5, pp. 700–709.

Williams, D. and W. G. Godden (1976). "Experimental Model Studies on Seismic Response of High Curved Overcrossings," *Report No. UCB/EERC–76/18*, Earthquake Engineering Research Center, University of California at Berkeley.

Wilson, E. L. (1992). "SADSAP: Static and Dynamic Structural Analysis Programs," Structural Analysis Programs, Inc.

Wilson, E. L., M. I. Suharward, et al. (1994). "Static and Dynamic Analysis of Structures with a Limited Number of Nonlinear Elements," Advances in Earthquake Engineering Practice, Berkeley, CA.

Wilson, J. C. (1984). "Analysis of the Observed Earthquake Response of a Multiple Span Bridge," *Report No. EERL 84–01*, Earthquake Engineering Research Laboratory, California Institute of Technology.

Wilson, J. C. and B. S. Tan (1990). "Bridge Abutments: Assessing Their Influence on Earthquake Response of Meloland Road Overpass," *Journal of Engineering Mechanics*, ASCE, Vol. 116, No. 8, pp. 1838–1856.

Yashinksy, M., L. Maulchin, et al. (1992). "Performance of Bridges During the Landers and Big Bear Earthquakes, Post–Earthquake Investigation Team Report," Division of Structures, California Department of Transportation.

LIST OF CSMIP DATA UTILIZATION REPORTS

California Department of Conservation
Division of Mines and Geology
Office of Strong Motion Studies
California Strong Motion Instrumentation Program (CSMIP)

The California Strong Motion Instrumentation Program (CSMIP) publishes data utilization reports as part of the Data Interpretation Project. These reports were prepared by investigators funded by CSMIP. Results obtained by the investigators were summarized in the papers included in the proceedings of the annual seminar. These reports and seminar proceedings are available from CSMIP at nominal cost. Requests for the reports, seminar proceedings and/or for additional information should be addressed to: Data Interpretation Project Manager, Office of Strong Motion Studies, Division of Mines and Geology, California Department of Conservation, 801 K Street, MS 13-35, Sacramento, California 95814-3531. Phone: (916)322-3105

CSMIP/92-01 **"Evaluation of Soil-Structure Interaction in Buildings during Earthquakes,"** by G. Fenves and G. Serino, June 1992, 57 pp.

CSMIP/92-02 **"Seismic Performance Investigation of the Hayward BART Elevated Section,"** by W. Tseng, M. Yang and J. Penzien, September 1992, 61 pp.

CSMIP/93-01 **"Influence of Critical Moho Reflections on Strong Motion Attenuation in California,"** by P. Somerville, N. Smith and D. Dreger, December 1993, 84 pp.

CSMIP/93-02 **"Investigation of the Response of Puddingstone Dam in the Whittier Narrows Earthquake of October 1, 1987,"** by J. Bray, R. Seed and R. Boulanger, December 1993, 60 pp.

CSMIP/93-03 **"Investigation of the Response of Cogswell Dam in the Whittier Narrows Earthquake of October 1, 1987,"** by R. Boulanger, R. Seed and J. Bray, December 1993, 53 pp.

CSMIP/94-01 **"Torsional Response Characteristics of Regular Buildings under Different Seismic Excitation Levels,"** by H. Sedarat, S. Gupta, and S. Werner, January 1994, 43 pp.

CSMIP/94-02 **"Degradation of Plywood Roof Diaphragms under Multiple Earthquake Loading,"** by J. Bouwkamp, R. Hamburger and J. Gillengerten, February 1994, 32 pp.

CSMIP/94-03 **"Analysis of the Recorded Response of Lexington Dam during Various Levels of Ground Shaking,"** by F. Makdisi, C. Chang, Z. Wang and C. Mok, March 1994, 60 pp.

LIST OF CSMIP DATA UTILIZATION REPORTS (continued)

CSMIP/94-04 **"Correlation between Recorded Building Data and Non-Structural Damage during the Loma Prieta Earthquake of October 17, 1989,"** by S. Rihal, April 1994, 65 pp.

CSMIP/94-05 **"Simulation of the Recorded Response of Unreinforced Masonry (URM) Infill Buildings,"** by J. Kariotis, J. Guh, G. Hart and J. Hill, October 1994, 149 pp.

CSMIP/95-01 **"Seismic Response Study of the Hwy 101/Painter Street Overpass Near Eureka Using Strong-Motion Records,"** by R. Goel and A. Chopra, March 1995, 70 pp.

CSMIP/95-02 **"Evaluation of the Response of I-10/215 Interchange Bridge Near San Bernardino in the 1992 Landers and Big Bear Earthquakes,"** by G. Fenves and R. Desroches, March 1995, 132 pp.

SMIP89 "SMIP89 Seminar on Seismological and Engineering Implications on Recent Strong-motion Data," Preprints, Sacramento, California, May 9, 1989

SMIP90 "SMIP90 Seminar on Seismological and Engineering Implications on Recent Strong-motion Data," Preprints, Sacramento, California, June 8, 1990

SMIP91 "SMIP91 Seminar on Seismological and Engineering Implications on Recent Strong-motion Data," Preprints, Sacramento, California, May 30, 1991

SMIP92 "SMIP92 Seminar on Seismological and Engineering Implications on Recent Strong-motion Data," Proceedings, Sacramento, California, May 21, 1992

SMIP93 "SMIP93 Seminar on Seismological and Engineering Implications on Recent Strong-motion Data," Proceedings, Sacramento, California, May 20, 1993, 114 pp.

SMIP94 "SMIP94 Seminar on Seismological and Engineering Implications on Recent Strong-motion Data," Proceedings, Los Angeles, California, May 26, 1994, 120 pp.